INTERPRETING SEDIMENT GEOCHEMICAL RECORDS FROM A MINERALOGICAL PERSPECTIVE:

A QUANTITATIVE METHOD FOR RECONSTRUCTING HISTORICAL ENVIRONMENTAL CHANGES IN CHINA

Thesis submitted in accordance with the requirements of the University of Liverpool for the degree of Doctor in Philosophy

by Ningning Li

December 2009

“ Copyright © and Moral Rights for this thesis and any accompanying data (where applicable) are retained by the author and/or other copyright owners. A copy can be downloaded for personal non-commercial research or study, without prior permission or charge. This thesis and the accompanying data cannot be reproduced or quoted extensively from without first obtaining permission in writing from the copyright holder/s. The content of the thesis and accompanying research data (where applicable) must not be changed in any way or sold commercially in any format or medium without the formal permission of the copyright holder/s. When referring to this thesis and any accompanying data, full bibliographic details must be given, e.g. Thesis: Author (Year of Submission) "Full thesis title", University of Liverpool, name of the University Faculty or School or Department, PhD Thesis, pagination.”

Interpreting sediment geochemical records from a mineralogical perspective: a quantitative method for reconstructing historical environmental changes in China

Abstract

Ningning Li

Geochemistry is increasingly important in reconstructing historical environmental changes and linking it with current climate conditions. Previous studies have attempted to use various climate proxies as independent tools for quantifying past environmental or climate conditions. However, most of them lack detailed and comprehensive geochemical data and are not fully quantitative. In addition, results from bulk geochemical analysis (element concentrations and their ratios) are not directly correlated to environmental/climate changes, but minerals are. Therefore, historical environmental changes can be quantified if the mineralogy of the corresponding sediment is known and can be obtained as quantitative data. This thesis is to present a newly developed numerical model, the mineral dissolution model, for converting geochemical records from sediments into quantitative mineralogical data and linking these data with relevant environmental/climate events.

Two different sites, the Chinese Loess Plateau and the Chaohu Lake from China, have been selected for this study. Attempts are given to examine the applicability of the model to different sites with different climate conditions; and to discuss the reliability of the model for reconstructing palaeoclimate change by comparing with other methods.

New detailed and comprehensive geochemical data have been provided for quantitative mineralogical analysis. The rainfall rates for the Chinese Loess Plateau and the mineral compositions of the Chaohu Lake sediments were estimated by the model and presented in this thesis. The results indicate that quantitative mineralogical analysis can be used as an independent proxy for historical environmental study and can avoid site-specific factors; and that the mineral dissolution model is a useful tool for reconstructing palaeoclimate changes, although refinements are needed for some parameters.

Contents

Acknowledgements

Many people have contributed to help me with this thesis, including my family, friends, supervisors and colleagues. First of all, special thanks should be given to my supervisors John Boyle and Jan Bloemendal, for their support, encouragement and patience during the last four years. Thanks to John Dearing, who was a former member of my supervision panel, for his great help and support on the data of the lake project, e.g. sampling, radiocarbon dates and magnetic measurements, although he forgot the samples were dated under his financial support and by the company recommended by himself. A big thank you to all the technicians and I have been working with – Bob Jude, Irene Cooper, Hilda Hull, Alan Henderson, Bob Hunt, Steven Crowley and Carmel Pinnington, for their technical support and advice. Another thank you to all the academic staff and colleagues in the department, for their challenge (or harassment?) and creativity in academic discussion, languages, humour and alcohol.

A big thank you should be also given to Frank Oldfield, for his help in interpreting magnetic data and defining the age model for the lake. I would also like to thank Richard Jones for his advice in radiocarbon dating and his great laboratory work on pollen and charcoal data. Magnetic susceptibility records for the loess sections is provided by Eleanor Parker, Xiuming Liu and Jan B.; magnetic measurements and pollen analysis on the alluvial core were undertaken by Xuerong Dai and his colleagues. They are also much appreciated. Special thanks also go to Quaternary Research Association and Royal Geographical Society (RGS-IBG) for their financial support on the XRD measurements on my loess samples.

Finally, I would like to thank my parents and grandparents for their support emotionally and financially, although they preferred the title 'climatologist' rather than 'geographer'. And to all my best friends, Linjing, Lin, Tao, Mengqi, Lu, Fan, Miao, Zhixiong, Trevor, Sandy and Kabir, for their regular greetings specially designed for me: 'why you haven't graduated yet?'

Abbreviations

CBD	Citrate-bicaronate-diothionite Method
CL	Chaohu Lake
CLP	Chinese Loess Plateau
DOC	Dissolved Organic Carbon
DRS	Diffuse Reflectance Spectroscopy
EDX	Energy Dispersive X-ray
FD	Frequency-dependent Susceptibility
GCM	Global Climate Model
IRM	Isothermal Remanent Magnetisation
MAP	Mean Annual Precipitation
MAT	Mean Annual Temperature
MS	Magnetic Susceptibility
QMA	Quantitative Mineralogical Analysis
SEM	Scanning Electronic Microscope
TEM	Transmission Electron Microscopy
TN	Total Nitrogen
TOC	Total Organic Carbon
REE	Rare Earth Elements
XRD	X-ray Diffraction
XRF	X-ray Fluorescence

List of Tables

List of Figures

Chapter 1 Introduction

1.1 Introduction

It is recognised that palaeoclimate change study has been an important role to play for current climate change studies and future climate forecast (e.g. An, 2000; Dearing et al., 2006). Many studies have been conducted to reconstruct palaeoclimate/environmental change using different methods, including environmental magnetism (e.g. Thompson and Oldfield, 1986; Evans and Heller, 2001; Bloemendal and Liu, 2005), geochemistry (e.g. Gallet et al., 1996; Wan et al., 2003; Jahn et al., 2001; Boyle, 2007), grain size (e.g. Zheng et al., 1991; Derbyshire et al., 1997; Ding et al., 2002) and palynology (e.g. Wang et al., 2008). However, no method is perfect. The difficulty in distinguishing between magnetite and maghaemite in sediments complicates the interpretation of the magnetic susceptibility records. The indirect link between element ratios and the contemporary environment and the variation in mineral groups limit the determination of the relationship between mineral and weathering. The same particle size distribution can be attributed to different climate and environment scenarios. Pollen and charcoal analyses sometimes could be site-specific and plausible when compared to the chronology. In addition, most of these methods are qualitative or semi-quantitative.

Therefore, this thesis is to provide a new approach to quantitatively reconstructing historical environmental change by combining quantitative mineralogical analysis with the geochemical records of sediments from different sites.

Two different landforms in China – Chinese Loess Plateau (CLP, central North China) and Chaohu Lake (East China) are selected for this study. Attempts are given (1) to quantify the mineral-weathering relationship along with the climate change in CLP within last 0.5 million years, and then to estimate the palaeo-precipitation rates in this area; and (2) to investigate the environmental change and the evolution of

Chaohu Lake during middle to late Holocene using geochemical proxies. Previous studies at both sites have shown significant progress (e.g. Maher et al., 1994; Chen et al., 2005; Jia et al., 2006; Wang et al., 2008), but lack detailed and comprehensive geochemical and mineralogical analyses. Thus, it is expected to provide new evidence based on geochemical/mineralogical data.

1.2 Aims and objectives

The aims of this study are:

- To provide a new approach to quantitative geochemistry, interpreting patterns in terms of mineralogy and assess its sensitivity and applicability to historical environment studies by comparing with other methods.
- To create a numerical model based on a mineral depletion predictive model (Boyle, 2008) and ALLOGEN, a computerized model developed by Boyle (2007), to estimate the palaeo-precipitation rates and examine the model's reliability by comparing with the rainfall-susceptibility climo-function model proposed by Maher et al. (1994).

As stated above, two sites in China have been selected for this study. There are sub-objectives for each site.

(1) For the Chinese Loess Plateau site:

- To undertake comprehensive and detailed mineralogical analysis from three loess sections on a latitudinal and climate gradient. This is expected to yield a better understanding of the composition and origin of loess minerals, their temporal and spatial changes in concentration and structure, and their correlation with weathering history and climate change.
- To examine the mineral-weathering relationship and reconstruct the palaeo-rainfall rates quantitatively using a mineral dissolution model. This model is part of the weathering rate predictive model proposed by Boyle (2008) but it was not designed for loess mineralogical study and must be optimised for

Chinese loess. It will represent an entirely new approach to loess mineralogical study.

(2) For the Chaohu Lake site:

- To calculate the mineral compositions of the lake sediment using quantitative geochemistry and then to decipher the environmental change and the evolution of Chaohu Lake through the interpretation of the mineral data and the records of other environmental proxies.
- To attempt to distinguish the effects of human activities and environmental changes on the lake by using relevant records.

Chapter 2 Literature Review

According to previous studies, several methods have been widely accepted for palaeoclimate reconstruction from sedimentary archives, such as magnetic susceptibility, geochemistry, micromorphology, grain size analysis and pollen analysis. These methods have also been used in this study. Therefore, a brief view has been given on these approaches, especially on their application to loess and/or lake sediments. In addition, previous studies have also carried out on mineral-weathering relationship within Chinese loess, the environmental change around the Chaohu Lake and the application of quantitative mineralogical analysis.

2.1 Methods for palaeoclimate reconstruction used in this study

2.1.1 Magnetic properties

The application of environmental magnetic techniques (Thompson and Oldfield, 1986) represents one of the earliest attempts to extract palaeoenvironmental information from Chinese loess (e.g. Heller and Liu, 1982). Historically, Liu's study (1975; cited in Liu, 1985) showed that the magnetic susceptibility of palaeosols is higher than that in loess at Heimugou on the Chinese Loess Plateau. After that, An et al. (1977) used magnetic susceptibility at low fields to distinguish loess and palaeosol. Since then, this approach has become increasingly important for obtaining high-resolution records from loess/palaeosol sequences in China (e.g. Liu, 1985; Kukla et al., 1988; Heller and Liu, 1994). One of the first and most significant findings was that high and low values of magnetic susceptibility correspond to palaeosols and loess, respectively. Furthermore it was shown that the alternating loess-palaeosol sequences in the extensive central Chinese Loess Plateau recorded at least 56 soil-forming intervals and the major interglacial soils in the last 2.6 Ma (Heller and Liu, 1982; Liu, 1985; Kukla et al., 1988; Rutter et al., 1990; Guo et al., 1996a), almost all of them characterised by increased magnetic susceptibility values.

This implied an alternating glacial-interglacial pattern of Quaternary climate, which matched the record from other archives, such as the deep-sea sediment record. Researchers (e.g. Heller and Liu, 1984; Cao, 1997; Florindo et al., 1999; Kemp et al., 2001) studying the loess-palaeosol sequences have undertaken some comparisons between magnetic susceptibility and marine oxygen isotope records, which generally show a good agreement between these two climate proxies (Figure 2-1), and this clearly underlines the climatic significance of loess magnetic properties.

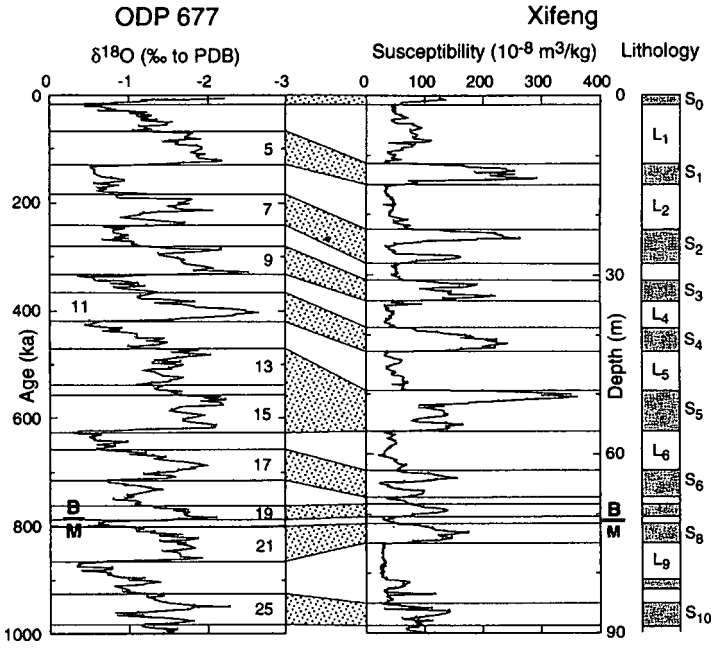

Figure 2-1Correlation of the marine $\delta^{18}O$ record and loess magnetic susceptibility. From: Heller and Evans (1995)

Initially Heller and Liu (1984) suggested that the magnetic susceptibility enhancement of palaeols resulted from carbonate dissolution during warm, humid interglacial weathering conditions. Later, Kukla (1988) suggested a different mechanism, whereby the flux of magnetic minerals from some distant, unknown source was alternately diluted and concentrated by variations in the accumulation rate of the weakly magnetic sediment matrix. Thus susceptibility values were lower during cool, dryer glacial periods when the loess accumulation rate was the most rapid. However, the work of Zhou et al. (1990) and Zheng et al. (1991) showed that

the magnetic mineral assemblages in the palaesols were much finer-grained than in the loess layers, and in addition that they were concentrated in the fine (clay/fine silt) soil particle size fractions. This clearly indicated that the origin of the magnetic enhancement was the pedogenic formation of fine-grained secondary ferrimagnetic minerals (e.g. magnetite, maghemite), a process which had been previously well documented in temperate zone soils (e.g. Tite and Linington, 1975; Mullins, 1977). This accorded with the concept of increasing weathering intensity and soil formation during interglacials. A further development was the suggestion that loess and palaeosol magnetic properties could be used to quantitatively reconstruct past climates on the Chinese loess plateau, specifically the intensity of the East Asian summer monsoon, which delivered the bulk of the precipitation to the area. Maher et al. (1994) and Liu et al. (1995) demonstrated a near-linear relationship between modern precipitation on the loess plateau and the magnetic properties of modern soils, or the early Holocene palaeosol, S0 (e.g. Figure 2-2).

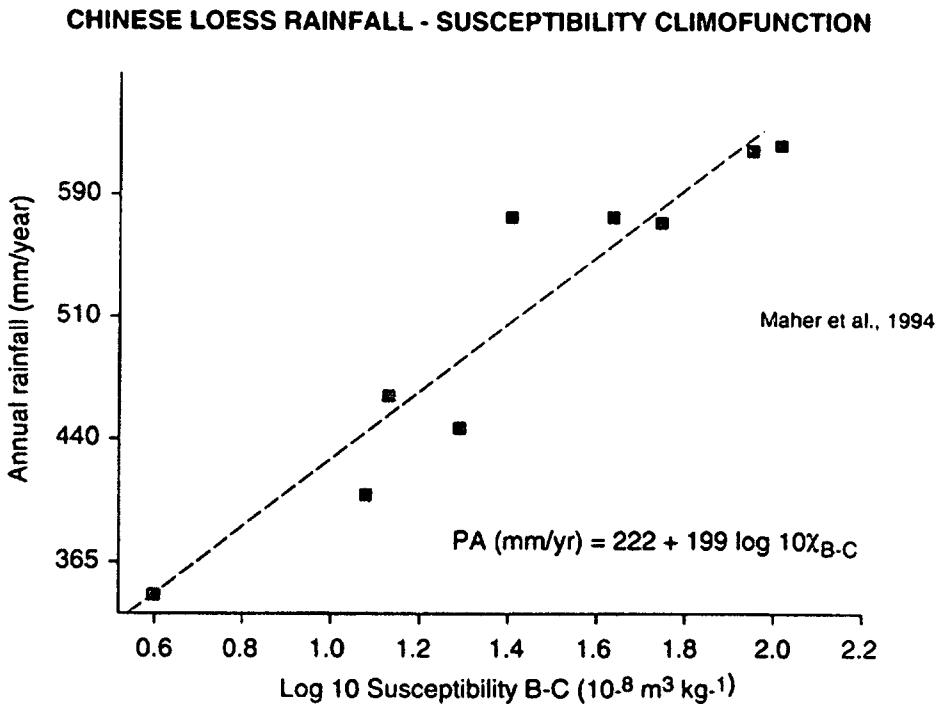

Figure 2-2 B-C horizon magnetic susceptibility versus modern annual rainfall. From: Maher et al. (1994)

Maher et al. (1994) suggested that the increases in monsoonal rainfall during interglacials were particularly enhanced at the westernmost sites, adjacent to the northeastern edge of the Tibetan plateau, while a decline in rainfall during glacial periods was also identified across the whole area, with the greatest reduction in the southeast areas. They also argued that climate change, rather than soil-forming duration, is the key factor in controlling pedogenic susceptibility. One advantage, they suggested, of using magnetic properties is that the reconstructions of palaeoprecipitation based on magnetic susceptibility measurements can be directly compared with palaeorainfall results from GCM. However, they thought that attention should be paid to the limitation of the use of modern annual rainfall data in developing the magnetic climofunction at the contemporary calibration sites, although Maher et al. (1994) argued that the northern hemispheric pattern of rainfall is in good agreement with the their climofunction data, regardless of the discrepancies in the general pattern. Later, Han et al. (1996) obtained another climofunction (Figure 2-3) from 63 sites covering almost the entire Loess Plateau and the regions with loess deposits outside the main Loess Plateau area. This climofunction, obtained using polynomial regression analysis, showed a more complex, non-linear relationship between the magnetic susceptibility of modern surface soils and both mean annual precipitation (MAP) and mean annual temperature (MAT). Han et al. (1996) concluded that linear and logarithmic climofunction coefficients between magnetic susceptibility and climate parameters could lead to an incorrect reconstruction of palaeoprecipitation. However, all of the climofunctions obtained so far imply that in general magnetic susceptibility increases with increasing MAT and/or MAP.

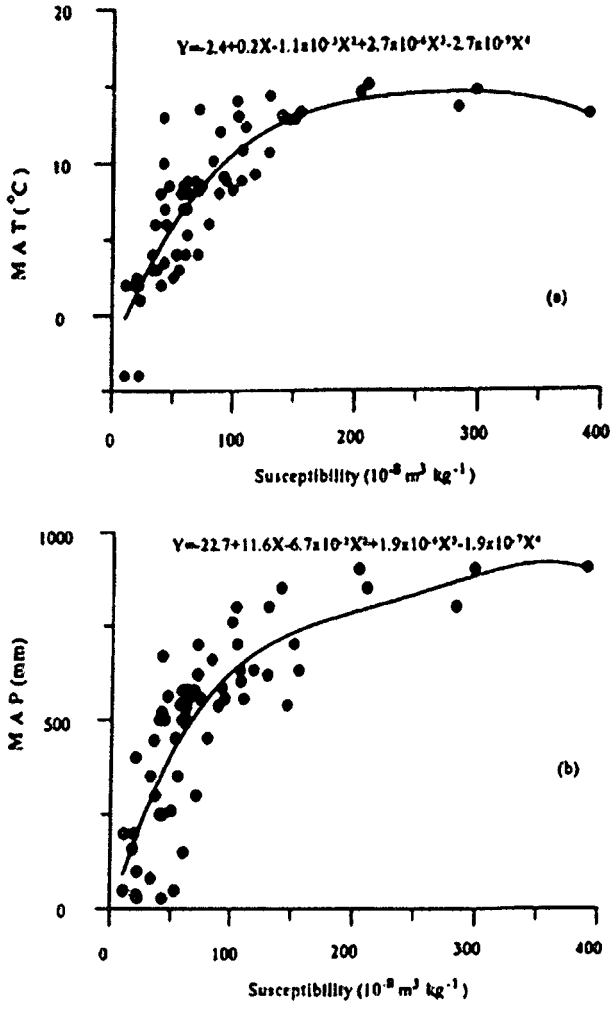

Figure 2-3 Susceptibility Climofunctions developed by Han et al. (1996)

Top: Susceptibility versus mean annual temperature

Bottom: Susceptibility versus mean annual precipitation.

Nevertheless, the actual mechanism of susceptibility enhancement remains debatable. For example, magnetic susceptibility should be enhanced in all of the palaeosols, as is generally observed on the Chinese Loess Plateau. However, in the case of the Weinan and Lantian loess sections, in the southernmost part of the Loess Plateau, this is not the case. In addition, it is widely accepted that S1SS3 corresponds to marine oxygen isotope substage 5e, and formed under the warmest and most humid climatic conditions during the last interglacial. Zhu et al. (2001b), however, pointed out that the magnetic susceptibility values within S1SS3 are much lower than those within S1SS2 and S1SS1 based on the magnetic susceptibility records for the Znojmo section in Czech Republic and for the Weinan section in the Chinese Loess Plateau.

In addition, previous studies focused on the general similarity of magnetic susceptibility records and precipitation curves; however, now some researchers have started to examine the relationship in more detail and in some cases have pointed to the differences between these two data sets. Guo et al. (2001), in particular, have argued that there are complexities in interpreting the magnetic susceptibility records of the loess-palaeosol sequences solely in terms of palaeoprecipitation. In addition, Guo et al. (2001) suggested that there is an increasing gradient in pedogenic intensity from north to south, but within the same spatial trend, no obvious increases can be found in maghemite content and magnetic susceptibility in S8, both of which are commonly used as indicators of pedogenesis. Derbyshire et al. (1997) examined the correlation of magnetic susceptibility and palaeoclimate changes between Luochuan, Beiyuan and Lanzhou on the Chinese Loess Plateau. It is accepted by them that loess-palaeosol sequences in the western parts of the Loess Plateau possibly provide an even higher resolution climatic record than that derived from the main Loess Plateau sites further east. However, Derbyshire et al. (1997) also pointed out some discrepancies between the magnetic susceptibility curves derived from the three sites over very short distances on Gaolan Mountain (near Lanzhou). Later, Maher et al. (1998) also suggested that any causal links between climate and magnetic properties are likely to be site-specific. Thus, although qualitative agreement of magnetic properties between stratigraphic sections at different localities is relatively easy to establish, their relative magnitudes may be different.

Further research was undertaken on the pedogenic process and environment corresponding to palaeoclimate change and palaeoprecipitation, especially in soils containing high or low amounts of magnetic iron oxides. Maher's study (1998) showed that pedogenic ferrimagnets are relatively abundant in well-drained, not very acidic soils (pH ~5.5-7), on weatherable, iron-bearing (but often not iron-rich) substrate, while the rates of magnetic depletion appear to be highest in permanently wet soils, very acidic podsols and in areas with annual rainfall excess of ~2000 mm p.a. Thus, they (op. cit.) concluded that in those soils that favour magnetic

enhancement processes, there is a correlation between the maximum value of the pedogenic susceptibility and the annual rainfall. Similarly, Liu et al. (2003) also suggested that ferrimagnets are produced while the soil moisture is below the critical value, which will also result in a positive correlation between the magnetic susceptibility records and pedogenic intensity. If the soil moisture exceeds the critical value, however, ferrimagnetic dilution occurs and the susceptibility/pedogenesis correlation is negative. If the soil moisture oscillates around the critical value, it is difficult to establish the correlation between magnetic susceptibility and pedogenic enhancement. Thus, the time-averaged soil moisture is the critical parameter that controls pedogenic formation or ferrimagnetic depletion. However, annual rainfall may be an insensitive measure of soil moisture (Derbyshire et al. 1995), so further investigation is required to establish the correlation between the pedogenic susceptibility and contemporary climate change (Maher, 1998; Liu et al., 2003). In addition, Liu et al. (2003) pointed out that further detailed investigation of magnetic susceptibility is needed to clarify relationships between magnetic susceptibility and climate, specifically properties such as Curie temperature, IRM acquisition, and magnetic hysteresis. Different Curie temperatures correspond to different magnetic minerals; and IRM acquisition curves can be used to distinguish between ferrimagnets and haematite. Thus, these techniques may provide some evidence on mechanism and source of any link between magnetic properties (Maher, 1998).

2.1.2 Geochemistry

Geochemical techniques, such as measurement of Rb/Sr ratio, Al_2O_3/CaO ratio and iron oxide state, are also used to reconstruct palaeoclimate on the Loess Plateau. It is agreed that Rb/Sr ratio and Al_2O_3/CaO ratios correspond to pedogenic weathering of soils relative to the so-called 'parental loess' (Ding et al., 2001). Typically, the ratios of Sr/Rb and Al_2O_3/CaO are widely used in reconstructing the climate change of the Loess Plateau in the Pliocene and Pleistocene (Chen et al., 1999a; Ding et al. 2000; Gallet et al., 1996), because the soluble elements Ca and Sr are very sensitive to

climatic changes. In addition, Ding et al. (2001) have attempted to use other chemical components of red clay[1] and applied various geochemical methods, including rare earth elements (REE) patterns, U/Pb, Sr/Rb, Sr/Ba and CaO/Al2O3, etc. They found that "*the eolian loess and red clay materials must have been subject to thorough sedimentary differentiation and moderate chemical weathering in the source area*" (Ding et al., 2001, p. 901); and in comparison with magnetic susceptibility, the ratios of CaO/Al_2O_3, Sr/Rb and Sr/Ba may be more sensitive proxies for reconstructing late Cenozoic climate change. Similarly, Li et al. (2006) have also used the concentrations of Rb and Sr, REE patterns and magnetic susceptibility; however, in this study the samples were sieved into different grain-size classes. From Li et al.'s (op. cit.) study, it is suggested that grain-size sub-population analysis is an effective way of reconstructing the palaeoenvironment; and that the clay mineralogy within loess is sensitive to changes in chemical weathering and its variation can affect the changes in Rb/Sr ratios, but not magnetic susceptibility.

However, proxies of the long-term evolution of East Asian summer monsoon, such as magnetic susceptibility (MS) and Rb/Sr ratio, have their own limitations. Magnetic properties do not clearly show some climate signals that are recorded by other proxies, such as pedological indicators (Guo et al., 1998). Differences can be found between the Rb/Sr ratio records for palaeosols S2, S3, S4 and the morphology of the soils at the same section (Tang et al., 2003). Therefore, several researchers have suggested another proxy, i.e. the CBD (citrate-bicarbonate-dithionite) extractable free Fe_2O_3 (FeD) to total Fe_2O_3 (FeT) ratio in loess sections, which is regarded to be sensitive to the palaeo-weathering intensity of Chinese loess (op. cit.). Compared with magnetic properties and the Rb/Sr ratio, the FeD/FeT ratio is a better indicator of pedogenic processes within loess-palaeosol sequences. In addition, the results of

[1] The red clay is a deposit underlying the loess-palaeosol sequences. There is a prominent boundary between the red clay and the overlying loess-palaeosol sequences. Some researchers believe that red clay extend the history of dust accumulation back to at least ~5-7 Ma.

several studies (e.g., Ding et al., 2001; Guo et al., 1999) show that the FeD to FeT ratio in loess sections clearly shows higher values in palaeosols than in loess horizons, which suggests that the FeD to FeT ratio, by reflecting the proportion of pedogenic iron oxides, is a good proxy indicator of the summer monsoon evolution. However, the FeD to FeT ratio is not a 'perfect' proxy, either. This is because there are some uncertainties in the interpretation of the results of the CBD treatment. For example, it is unclear which iron minerals are being dissolved by the CBD treatment. In particular, it is been questioned whether or not the CBD treatment can selectively dissolve the pedogenic magnetic minerals but leave unaffected the lithogenic magnetic components (cf. Liu et al., 1994).

Another approach for extracting climatic information from loess is the use of stable isotopes and their ratios. One example is ^{10}Be. Gu et al. (1996) have reported the results of ^{10}Be analysis of Chinese loess and red-clay deposits and concluded that ^{10}Be is mainly present in authigenic minerals in palaeosols, but in loess samples the enhancement of ^{10}Be is related to the dust source region. Later, based on this study, Gu et al. (1997) added the measurements of U and Th series, and suggested that most of the weathering in the dust-source regions may have occurred during the interglacials. In addition, Sr isotopic composition of the loess-palaeosol calcites has been measured. Yang et al. (2000) found the ^{87}Sr/^{86}Sr ratio is closely correlated with records of magnetic susceptibility and suggested that the enhancement of this ratio corresponds with increased summer monsoonal precipitation.

Element analysis is useful for palaeoclimate study, but is difficult to obtain an overview of weathering history or environmental change. This is because: 1) element variation is not directly affected by weathering processes or environmental change, but minerals are; 2) it becomes complicated and difficult to interpret the variation when a large number of elements are involved. This makes the procedure of element analysis hard to follow. Therefore, mineralogical analysis is preferred, because the

variation in minerals can directly indicate weathering or pedogenic process, especially when quantitative analysis is required.

2.1.3 Soil micromorphology

The initial implementation of soil micromorphology as an environmental indicator was the analysis of the relationship between the shapes of quartz and calcite grains within the medium-sand fraction and the wind transportation regime (Butzer, 1963). Although it was used in combination with analyses of grain size, geomorphology and sedimentology in order to reconstruct the palaeoclimatic history of the Eurafrican subtropics during the Pleistocene (op. cit.), it was considered as an independent method until some scientists recognized it as a descriptive and diagnostic tool in palaeopedology (e.g. Lowe and Walker, 1997; Kemp, 1985; Catt, 1990; FitzPatrick, 1993). Subsequently, attempts have been made to use micromorphology to describe the characteristics of minerals in loess/palaeosols (Kemp, 1996, 1999; Bronger et al., 1998; Tsatskin et al., 2001; Guo et al., 1996a) and other sediments (e.g. Srivastava, 2001) and their changes during weathering, which could be affected by contemporary climate conditions.

However, there are several drawbacks in using micromorphology: (1) the method is time-consuming and it may be difficult to analyse sufficient samples to characterise the micromorphology of a sedimentary sequence; (2) it is nearly impossible to distinguish all the mineral species within the sample and to give an accurate interpretation, because there could be different processes that contribute to the micromorphological features; and (3) even if some conclusions can be drawn, it is still a qualitative technique. The initial method for micromorphological analysis is to observe thin section samples under an optical microscope, which is qualitative and empirical. After that, scanning electronic microscope (SEM) has been used as an aid for micromorphological analysis (e.g. Holdren et al., 1979); however, it has not been widely used for mineral particle analysis until recently (Pal et al., 2003; Liu et al., 2003; Jeong et al., 2008). According to current techniques, it is possible to undertake

quantitative analysis using SEM with chemical analysis equipment (e.g. energy dispersive X-ray analysis). However, this can only provide qualitative or semi-quantitative element analytical information (Rivière & Myhra, 1998; Pye & Croft, 2004), meaning that the mineral identification still needs to be undertaken based on individual experience and knowledge. Therefore, even with modern techniques, it is still difficult to provide a large amount of quantitative data using this type of approach.

2.1.4 Grain size analysis

Grain size analysis of sediments is a well-established method of providing palaeoenvironmental information (e.g. Syvitski, 1991), and has been extensively applied to Chinese loss. For example, the method has been applied to extracted quartz grains to reconstruct variations in winter monsoon strength during the Pleistocene (e.g. Xiao et al., 1995). Xiao (op. cit.) suggested that medium-diameter quartz grains are a proxy for average winter monsoon wind strength, while the proportion of maximum-diameter grains reflects the maximum wind strength. This study provided a semi-quantitative approach to palaeoclimate reconstruction. Ding et al. (2002) compared the grain size variation of the loess-palaeosol sequences with marine isotope oxygen records, and demonstrated a high-level correlation between them, suggesting that the climate in North China showed a similar cyclicity to that of the high latitude north hemisphere region. However, caution is needed in interpreting grain size records of loess-palaeosol sequences: (1) both regional and local climate events can affect the grain size distribution (Ding et al., 2002), so it is necessary to distinguish these two from each other when reconstructing the climate conditions; (2) the results obtained using the methods are significantly dependent on the sample dispersal methods used, and on the type of analytical instrument (e.g. Parker and Bloemendal, 2005).

The interpretation of the grain size distribution of lake sediments is normally only indirectly related to the climate. It is suggested (Li et al., 2008) that a high proportion

of coarse grains indicates a relatively low lake level. This is also partially supported by He et al. (2005), who suggested that the average grain size in lake sediments decreases because of the increasing lake level during humid periods on long-timescales; while on short-term scales in a given climate condition, instead of the lake level, the precipitation intensity is the major factor affecting the grain size distribution of lake sediment – when the rainfall is intense, more coarse material will be brought into the lake, increasing the average grain size. This could complicate the interpretation of the relationship between the grain size distribution of lake sediments and the corresponding humidity level/lake level, which could be mainly controlled by the climate. However, Huang et al. (2008) argued that only short-term rainfall changes can be reconstructed from grain size analysis, based on the study of Lake Bosten sediments in Xinjiang Province, China. Their observations indicated that the grain size distribution of the lake sediment can only represent flood events and strong precipitation in the surrounding area, but cannot reveal the lake level or wind speed changes, which is related to long-term historical climate change. In contrary, Zhai et al. (2002) found that changes in the intensity of the winter monsoon in North China in the past 8500 years are correlated to the annual laminations of grain size in the Angulinuo lake sediment, which consists of lacustrine and aeolian deposits, and the latter are transported by the winter monsoon. Recent research (Jia et al., 2006; Wang et al., 2008) on Chaohu Lake and its catchment have also shown that the grain size distribution can reflect the mineralogical composition of the samples, revealing the sedimentary environment. However, particle size analysis cannot be directly applied to palaeoclimate reconstruction, because grain size variations could be influenced by both short-term environmental change and long-term climate change; and furthermore, it can be also affected by site-specific factors (Wang et al., 2008).

2.1.5 Pollen analysis

Pollen analysis has long been used for palaeoclimatic reconstruction, for example using the indicator species approach, in which the modern distribution of a species is

strongly related to contemporary climate (e.g. Steven & Schofield, 1973; Betancourt & Devender, 1981; Barnosky, 1984; Lowe & Walker, 1997). By comparing the pollen records with other palaeoclimate proxies, e.g. marine isotope records (Barnosky, 1984) or grain size distribution (Wang et al., 2008), it has been shown that pollen records can reveal alternating warm and cool climate changes as the other proxies do, in spite of various discrepancies. However, the interpretation of pollen data can sometimes be difficult because of narrow geographical distribution and broad ecological tolerance of species (Steven & Schofield, 1973). Modern pollen analysis techniques have been improved by using regional pollen data to reconstructing regional vegetation patterns and applying transfer functions for data calibration (Bartlein et al., 1986; Huntley, 1992; Lowe & Walker, 1997).

2.2 Loess mineralogy

2.2.1 Detrital minerals

'Detrital' is a term used to describe particles of rock derived from pre-existing rock through processes of weathering and erosion. Detrital particles can include lithic fragments (particles of recognisable rock), or of monomineralic fragments (mineral grains). These particles are often transported as clasts through sedimentary processes to depositional sites such as riverbeds, lakes or the ocean thereby forming sedimentary successions. Minerals such as biotite, quartz, albite, and K-feldspars are commonly found to be detrital minerals (Liu, 1985; Guo et al., 1993; Kim et al., 2006) which are of igneous or metamorphic origin and forming under conditions of high temperature and/or high pressure. Goldich (1938) determined the relative stability of the common high-temperature minerals under weathering conditions. Figure 2-4 shows the exogenic stability of various high-temperature minerals, including the minerals mentioned above. This illustration can be interpreted as showing that, for instance, the equilibrium conditions for olivine formation deviate more significantly from the environmental conditions established at or near the earth surface than they do for any other high temperature mineral (Degens, 1965).

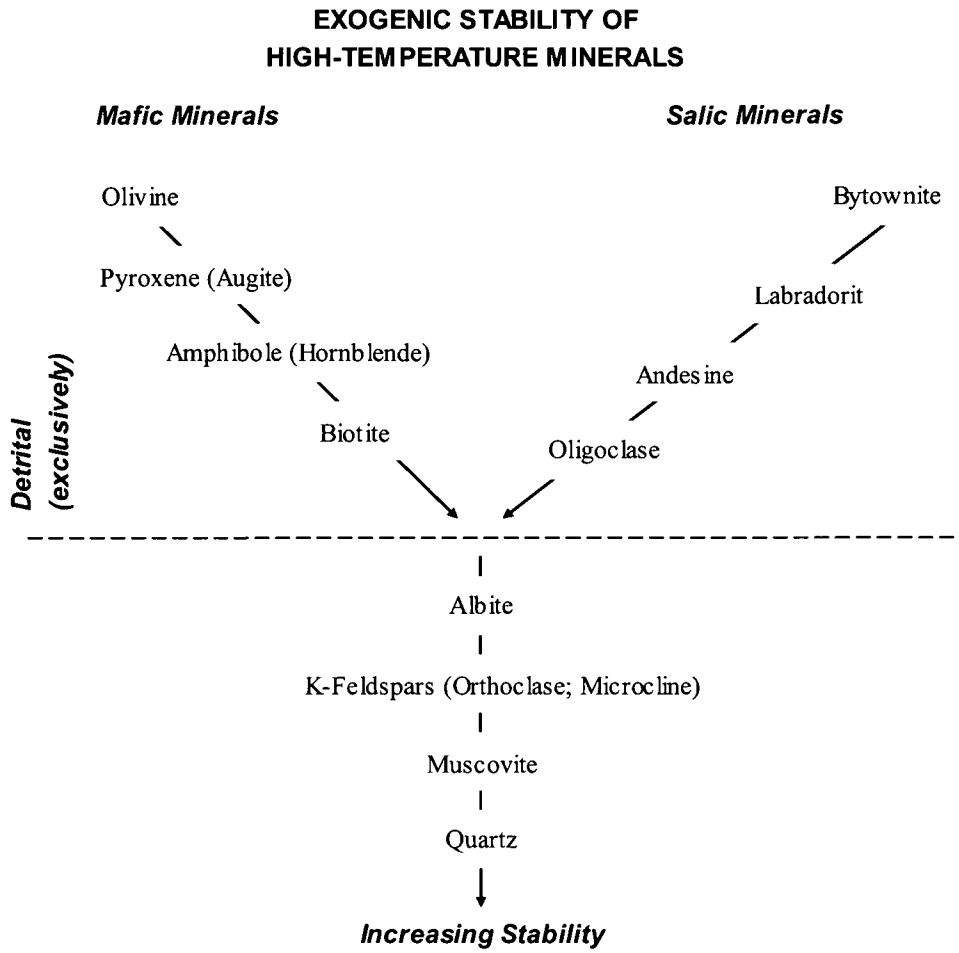

Figure 2-4 Weathering stability series of primary rock-forming minerals (From: Goldich, 1938; cited by Degens, 1965).

In addition, according to previous loess mineralogical studies (Liu 1985; Guo et al., 1993; Chen et al., 2005) and on the basis of the results reported here (Chapter 5, Section 5.2), Chinese loess samples are relatively rich in clay minerals. Some of them may be detrital, because they could have been formed at the source area by partial decomposition of minerals like feldspar. The clay minerals found in loess samples so far are mainly kaolinite, illite and chlorite. Regardless of various clay mineral groups, they are potentially important and valuable for constructing the weathering history and the past precipitation conditions in the Chinese Loess Plateau. Therefore, clay minerals are discussed individually in this review.

2.2.2 Quartz

In the loess scientific literature, some researchers have investigated the grain size distribution and the origin of quartz components in loess, including Chinese loess. It is stated by some scientists that most quartz grains in loess are silt size, which is described as either the range 20-50 μm (Nemecz et al., 2000) or 20-60 μm (Smalley et al., 2005). In addition, it has been ascertained that most quartz constituents in loess-palaeosol sequences of central China are of aeolian (detrital) origin and are resistant to the weathering process, as mentioned above. Thus the quartz in loess sections could be a potential indicator of weathering intensity. Xiao et al. (1995) measured the median and maximum diameters of quartz components in loess and palaeosol materials collected from Luochuan section, in the southern part of Chinese Loess Plateau. The long-term variations in grain size of quartz were compared with the curve of equivalent magnetic susceptibility as a summer monsoon proxy and with the marine oxygen isotope record. Then Xiao et al. (1995) argued that the medium grain size of quartz in loess and palaeosol materials could be used as a reliable proxy for average intensity of winter monsoon under palaeoclimatic conditions, and the maximum grain size of quartz component as a proxy of maximum wind strength. This agrees with other scientists' work (e.g. Lu and An, 1998; An, 2000; Ding et al., 2002). In addition, comparing with the magnetic susceptibility of the bulk samples, Sun et al. (2006) also suggested that the mean grain size of quartz is a more reliable proxy indicator of dust transport dynamics, unaffected by pedogenic modification and can be used to clearly delineate variations of the East Asian palaeomonsoon.

2.2.3 Feldspars

Feldspar is the most abundant mineral group in the lithosphere, occurring in many kinds of sediments and rocks and with various grain sizes. Studies of feldspar weathering have been undertaken in different regions and environments.

In order to test the hypothesis that profiles of a (buried) palaeosol developed on the higher/older terraces of the River Thames in SE England are more weathered than those formed on lower/younger terrace surfaces, Read et al. (1996), based on previous studies, developed a weighted index of feldspar weathering (IFW) using the following simple formula:

$$IFW = \frac{(L \times 1) + (ML \times 2) + (MH \times 4) + (H \times 8)}{n}$$

where L, ML, MH and H represent the numbers of grains of the low, medium-low, medium-high and high weathering class, respectively; n = number of grains.

Their results provided a semi-quantitative support for the hypothesis mentioned above, and indicated that the feldspars in the parent material are generally less weathered than those in the soil. In addition, Read et al. (1996) suggested that this technique (IFW) could also be applied to other regions where chronosequences extend across texturally variable parent materials.

However, because of possible variations in composition and structure of the feldspars, the nature of the parent material samples, soil processes and environments over time, the usefulness of IFW could be questioned. Another more precise and more detailed model was suggested by White et al. (2001) in order to calculate differential rates of feldspar weathering in granite regolith developed on the Panola Granite in Georgia, USA. The results of the model implied that differential feldspar weathering in the low-permeability Panola bedrock environment is more dependent on relative feldspar solubilities than on differences in kinetic reaction rates (White et al., 2001). Nevertheless, this model is site-specific, so its general applicability is unclear.

In addition to the intensity of feldspar weathering, another research area is the mechanism of feldspar weathering. Dultz (2002) has attempted to investigate the effects of parent material and weathering on feldspar content in three soils developed from Pleistocene calcareous till, glacial sand and loess in NW Germany using

different particle size fractions. They used quartz of 2-2000 μm and 2-63 μm fractions as indices to establish the mass balances for feldspar. Thus, the original feldspar content in soil horizons is calculated by comparison with the actual feldspar content using the following equation:

$$\frac{Oringinal\ feldspar\ content\ in\ the\ A\ horizon}{Index(quartz)\ in\ the\ A\ horizon} = \frac{Actual\ feldspar\ content\ in\ the\ C\ horizon}{Index(quartz)\ in\ the\ C\ horizon}$$

It was found that in the 100- to 500- μm sand fraction, there is a lower feldspar content than in coarser or finer fractions, which could mainly result from: (1) physical weathering of feldspars in this sand fraction into silt and clay size and (2) the decomposition of feldspar-containing rock particles of gravel size and aeolian sedimentation. Dultz (2002) argued that the change in feldspar contents has its highest intensity in a soil derived from glacial sand.

Another complexity of feldspar weathering is its possible kinetic change. The observation on Greek albite of Beig and Luttge (2006) indicated that the dissolution rates of albite crystals could be differential because of a kinetic change in dissolution mechanism with deviation from equilibrium conditions. Beig and Luttge (2006) then argued that a mineral sample's reaction history can have a significant impact on its subsequent dissolution rate.

2.2.4 Iron oxides

Iron oxides in Chinese loess mainly include magnetite, hematite, goethite and maghaemite (Liu et al., 2004; Maher, 1998). In the literature, scientists have attempted to identify those iron minerals using optical microscopy, X-ray diffraction, magnetic susceptibility and other methods, and to discuss the formative environments of different iron compounds and the conditions for possible hydration or dehydration. However, their arguments remain controversial.

Ji et al. (2001) have undertaken a study on Chinese loess at Luochuan section based on diffuse reflectance spectroscopy (DRS). They concluded that hematite appears to be concentrated in more weathered palaeosols, while goethite is concentrated in less weathered loess. Torrent et al. (2006) also reach the same conclusion using a different standard for DRS, although in another study Torrent et al. (2007) argued that the results of DRS could vary, depending on different methods and different external standards. The hematite enhancement in palaeosols is probably because the formation of hematite is favoured by high temperatures and dry conditions followed by a short period of limited precipitation (Maher, 1998; Balsam et al., 2004). It is difficult to interpret the environmental significance of goethite in loess, because this mineral can form under a wide range of conditions (Schwertmann and Taylor, 1989; Ji et al., 2001). However, it is said that this hydrated iron oxide is commonly formed as a surface coating on many minerals during weathering and hydrothermal alteration (Krauskopf and Bird, 1995). Therefore, it is difficult to directly use the hematite/goethite ratio for palaeoenvironmental interpretation, although this ratio is very sensitive to environment (Torrent et al., 2007).

Unlike goethite, the environmental conditions favouring the formation of magnetite and maghemite are relatively precise. Liu et al. (2003) suggested that (1) ferrimagnets (including magnetite and maghemite) are produced while the soil moisture is below a critical value, which will also result in a positive correlation between the magnetic susceptibility records and pedogenic intensity; (2) If the soil moisture exceeds the critical value, however, ferrimagnetic dilution occurs and the susceptibility/pedogenesis correlation is negative; and (3) If the soil moisture oscillates around the critical value, it is difficult to establish the correlation between magnetic susceptibility and pedogenic enhancement. Thus, the time-averaged soil moisture is the critical parameter that controls pedogenic formation or ferrimagnetic depletion.

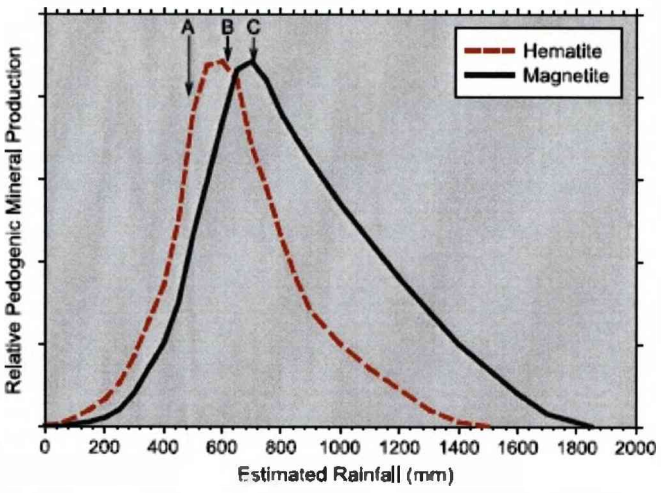

Figure 2-5 A model of rainfall vs. pedogenic production of hematite and ferrimagnets, primarily magnetite. Source: *Balsam et al. (2004). Arrow A indicates conditions typical for the formation of the Wucheng and Lower Lishi loess*[2] *when rainfall was high enough to produce significant amounts of hematite but moderate to low amounts of ferrimagnets and hence low MS values. Arrow B is indicative of conditions during the formation of palaeosol S5 which is usually characterized by the highest magnetic susceptibility values observed within the loess-palaeosol sequence, and by high hematite contnet. Arrow C is typical of loess sections above S5 where MS falls off slightly and hematite and goethite exhibit modest decreases.*

Since the hematite/goethite ratio cannot be directly applied to palaeoenvironmental study (Torrent et al., 2006), it seems better to use the hematite-magnetite (or maghemite) relationships as an indicator of the environment in Chinese loess sections. According to the conceptual model (Figure 2-5) of Balsam et al. (2004), hematite-magnetite relationships can be summarised as follows: (1) hematite can reach a maximum when the temperature is high and the period of soil moisture is too short to produce significant magnetite; (2) as the length of the wet season increases, hematite formation first plateaus, and then decreases rapidly, while magnetite increase and reaches a maximum when the rainfall and temperature are above a certain threshold; and (3) with further increase in rainfall, magnetite concentration

[2] These terms are used to describe the stratigraphy of the Chinese loess. The base of the loess is **Wucheng** loess, containing traces of the Villafranchian Nihewan fauna in the early Pleistocene. Moving upward, elements of Zhoukoudian faunas have been found in the **Lishi** loess of middle Pleistocene age.

decreases although the magnetite/hematite ratio continues to increase. If the soil is saturated with water for long periods, hematite is no longer produced and iron oxides are reductively dissolved.

This model is partly supported by the data of Torrent et al. (2006), who suggested that the hematite is positively correlated with the degree of pedogenesis. However, precautions should be taken for its application. One problem is that the formation of iron oxides in sediments is directly related to soil moisture rather than precipitation. In addition, in some circumstances annual rainfall is not a good indicator of soil moisture, in other words, their relationship could be nonlinear. The other problem is that the thresholds of the rainfall rate (Arrows A, B and C on Figure 2-5) mentioned in the model could be site-specific, because changes in temperature and/or biological processes could also affect the formation of iron oxides, especially during a long-term process.

2.2.5 Calcite and dolomite

In order to understand the weathering processes of calcite and dolomite, it is important to investigate the chemical composition of these carbonates and their relevant chemical reactions with water (H_2O).

Calcite

It is well known that calcium carbonate can be dissolved under acid conditions, where in nature it is commonly in contact with water and carbon dioxide.

$$CaCO_3 + H_2CO_3 \rightarrow Ca^{2+} + 2HCO_3^-$$

When pH values in the solution increase, the reverse reaction could undergo like this:

$$Ca^{2+} + HCO_3^- + OH^- \rightarrow CaCO_3 + H_2O$$

In general, the dissolution of $CaCO_3$ mainly depends on the pH of its environment. In nature, normally this could be interpreted as that when the solubility of CO_2 in water increases, more $CaCO_3$ can be dissolved, while anything that decreases the amount of CO_2 causes $CaCO_3$ to precipitate (Krauskopf and Bird, 1995).

Based on this, it can be concluded that any factor with effect on CO_2 solubility will affect the dissolution process of $CaCO_3$, either directly or indirectly. Therefore, both temperature and pressure are naturally included in these factors. Because of less solubility of CO_2 under high temperatures and low pressures, the dissolution of $CaCO_3$ will increase; while the situation will reverse under low temperatures and high pressures. In addition, some organic activities can accelerate $CaCO_3$ precipitation directly or indirectly; and decay of organic matter makes CO_2 more soluble, resulting in more dissolution of $CaCO_3$ (Krauskopf and Bird, 1995).

An indicator that links calcite with weathering could be the $^{87}Sr/^{86}Sr$ ratio, because the presence of strontium, normally associated with calcite, is sensitive to chemical weathering. Yang et al. (2000) compared the $^{87}Sr/^{86}Sr$ ratio of loess-palaeosol calcite in one loess section in China with its magnetic susceptibility and marine isotope record curves, and found that those three plots were consistent with each other. Yang et al. (2000) therefore suggested that variation in $^{87}Sr/^{86}Sr$ ratio of loess-palaeosol calcites is largely attributed to changes in chemical weathering intensity closely related to palaeoclimate. They further concluded that the Sr isotopic composition of the loess-palaeosol calcites could be a proxy of chemical weathering associated with the East Asian summer monsoon.

Dolomite

Dolomite [$CaMg(CO_3)_2$] has a close connection with calcite in terms of their interactions, which can be described as:

$$CaCO_3\ [\text{calcite}] + Mg^{2+} + 2HCO_3^- \leftrightarrow CaMg(CO_3)_2\ [\text{dolomite}] + H_2CO_3$$

and $2CaCO_3$ [calcite] + $Mg^{2+} \leftrightarrow CaMg(CO_3)_2$ [dolomite] + Ca^{2+}

Bowers et al. (1984) and Krauskopf and Bird (1995) show that dolomite is favoured over calcite by low activity ratios of Ca^{2+} to Mg^{2+} and by an increase in temperature. It could be considered as an intermediate stage during the conversion of calcite to magnesite.

Dolomite is known as a common sedimentary material formed under normal conditions of temperature or pressure, but its origin remains uncertain both in the laboratory and from the observation. Some scientists (Krauskopf and Bird, 1995) suggested that most dolomite is not a primary precipitate but forms rather as a product of slow reactions altering originally deposited calcium carbonate. Evidence from the Chinese Loess Plateau (Liu et al., 2006) shows that the dolomite in loess-palaeosol sequences is detrital in origin and it only exists in the zones where modern rainfall is less than 540mm/yr permitting its preservation. Thus, the weathering of dolomite may be a proxy of palaeoclimate change.

2.2.6 Clay minerals

Since clay minerals are sensitive to environmental changes, especially unstable mixed-layer clay minerals (Li et al., 2006), it can be proposed that they could be potential indicators of loess-palaeosol alternations and the intensity of weathering. For instance, the illite could degrade significantly with increased weathering intensity (Liu, 1985; Ji et al., 1999; Li et al., 2006).

Little work has been done in this area. Kalm et al. (1996) estimated compositions of clay minerals from the loess-palaeosol sequence at Baoji in the southern Chinese Loess Plateau using X-ray diffraction, and suggested a possible history of climate change base on variations in concentrations of clay minerals related to weathering intensity and environmental change. Recently, using the same laboratory method but with a different calculation approach, Gylesjo and Arnold (2006) analysed <2μm diameter minerals in red clay-loess sequences at Lingtai in the central part of the

Chinese Loess Plateau. Compared with the work of Kalm et al. (1996) at Baoji, the changes in clay mineral concentrations at both sites are consistent, and thus Gylesjo and Arnold (2006) concluded that the finding drawn from the Lingtai data are applicable over a broad region. In addition, both studies considered illite as an indicator of weathering intensity and thus East Asian summer monsoon intensity. In addition, Liu (1985) also suggested that in northern Chinese loess, illite crystallinity could be used to distinguish loess and palaeosols, being higher in loess than that in palaeosols. Other scientists (Ji et al., 1999; Li et al., 2008), however, suggested that although some structurally unstable clay minerals such as kaolinite or interstratified illite-smectite can indicate weathering intensity, some structurally stable clay groups such as illite are preferably used as indicators of formation environments of source material and their provenances rather than as proxies of weathering. This is supported by a recent study on illite in loess-palaeosol sequences at Luochuan (Chen et al., 2005), which showed that two types of illites – one with good (higher) crystallinity, the other with poor (lower) crystallinity – are mutually exclusive throughout the section. Their results indicated no obvious relationship between illite crystallinity and loess stratigraphy.

2.2.7 Biotite

Biotite [$K(Mg,Fe^{2+})3AlSi_3O_{10}(OH,F)_2$] is a mineral group including many species. It can be considered as a trioctahedral mica, commonly occurring in soils under conditions where other ferromagnesian minerals are rapidly altered. It can be formed either by intercrystalline exchange reactions, where Fe^{2+}-Mg^{2+} replacement involved, e.g.

$$\underset{\text{garnet}}{Fe_3Al_2Si_3O_{12}} + \underset{\text{biotite (phlogopite)}}{KMg_3AlSi_3O_{10}(OH)_2} \leftrightarrow \underset{\text{garnet}}{Mg_3Al_2Si_3O_{12}} + \underset{\text{biotite (annite)}}{KFe_3AlSi_3O_{10}(OH)_2}$$

or by redox reactions, such as a reaction involving K-feldspar, biotite, and magnetite:

$KAlSi_3O_8 + Fe_3O_4 + H_2O \leftrightarrow KFe_3AlSi_3O_{10}(OH)_2 + \frac{1}{2}O_2$

K-feldspar magnetite biotite (annite)

The weathering of biotite is much more rapid than that of muscovite, a dioctahedral mica (Leonard and Weed, 1970; Kretzschmar et al., 1997). The main initial point of biotite weathering is the replacement of interlayer K^+ by other hydrated cations such as Ca^{2+}, Mg^{2+}, or H^+. Biotite can be weathered in two different ways: (1) edge-weathering. Biotites release their interlayer K^+ from all adjacent interlayers at similar rates, resulting in edge-expansion and formation of a zone of vermiculite surrounding a zone of remnant biotite; and (2) layer-weathering. Some biotites almost completely release the K^+ from some interlayers while other interlayers remain intact, resulting in regularly interstratified biotite-vermiculite (hydrobiotite) or random mixed layer of biotite and vermiculite (Buol and Weed, 1991; Kretzschmar et al., 1997).

In nature, the products of biotite weathering can vary under different chemical environments (Ismail, 1970). In addition, the rate of weathering as well as weathering pathways may also be affected by the chemical structure and grain size of the biotite (Harris et al., 1985; Kretzschmar et al., 1997). Under laboratory conditions, the chemical weathering of biotite follows the pathway biotite → interstratified biotite-vermiculite → vermiculite (Farmer and Wilson, 1970; Kretzschmar et al., 1997; Blum and Erel, 1997). However, under natural conditions in soils of temperature-humid climatic regions, biotite weathering usually follows the pathway biotite →interstratified biotite-vermiculite → vermiculite (→ hydroxyl-Al-interlayered vermiculite, kaolinite, smectite) (Feldman et al., 1991). Under arid and semi-arid regions, the weathering pathway could be biotite → vermiculite → smectite (Ismail, 1970). In addition, compared to feldspar weathering, the rate of biotite weathering is enhanced in the younger soils, and this rate decreases systematically with soil age (Blum and Erel, 1997).

Biotite weathering appears to play an important role in the genesis, mineralogy, chemical properties and physical properties of soils developed from biotite-rich parent rocks. However, the application of biotite weathering in loess sections is questionable, because the small amount of biotite in loess makes the quantification difficult.

2.2.8 Mineral-weathering relationships in loess

Since detrital minerals in Chinese loess are mainly affected by weathering process, it is possible to quantify the relationship between detrital minerals and weathering intensity, which is indicative of the contemporary East Asian Monsoon regime. Therefore, the mineral-weathering relationship is clearly important for palaeoclimate studies on the Chinese Loess Plateau (CLP). During the last fifteen years, this research field has increasingly attracted the attention of geophysicists, geochemists and mineralogists. Initially, Anderson & Hallet (1996) created a numerical model to simulate magnetic susceptibility profiles in loess and to quantify the rates of dust deposition and pedogenic processes. They found that the rates of the two processes have varied dramatically over the last 140 kyr and the Luochuan loess sequence has the best fit with the $\delta^{18}O$ records when driven by the model. However, Maher (1998) emphasized that caution is needed when interpreting magnetic properties of palaeosols as they tend to be more site-specific. Balsam et al. (2004) used both iron oxide mineralogy and magnetic susceptibility and attempted to find the relationship between weathering and the nature of soil magnetic minerals. The ratio of hematite/goethite was found to consistently decrease throughout the Pleistocene, and they suggested that precipitation on the Loess Plateau became less seasonal and/or occurred during times when temperature was lower. Similarly, another mineral magnetic study (Deng et al., 2006) suggested that there is a long-term decrease over the Quaternary period in chemical weathering intensity in both glacial-stage source region and interglacial-stage depositional area, as the relative contributions of both

aeolian and pedogenic hematite have decreased during glacial and interglacial times, respectively.

With regard to other minerals within loess-soil sequences, because of the complexity when interpreting magnetic properties and ratios between iron minerals, researchers have tried to find other approaches to associate with magnetic studies. Kalm et al. (1996) used X-ray Diffraction (XRD) to estimate quantitatively the clay composition within loess. The 'quantitative analysis' in this study means it is based on the relative height of the first-order diffraction peak of each mineral and normalized to 100%. It was suggested that the variation in the concentrations of different clay minerals in different periods is due to contemporary changes in humidity and weathering intensity. This has also been supported by another clay mineralogical study (Gylesjo & Arnold, 2006), which has applied similar but a technically advanced approach to quantitatively analyze the XRD pattern. However, their results also indicated that the changes of clay minerals appeared to be more variable than shown by the earlier study over the same timescale. A recent clay mineralogical study (Li et al., 2008) has used XRD and a wet chemical method as a combination to decipher the impact of monsoon changes on the silicate weathering process. Their results suggested that during last 130 kyr, there are two types of cycles in silicate weathering within loess-palaeosol sequences: the ~23 kyr cycles are correlated with the changes of summer monsoon intensity, while the ~100 kyr glacial-interglacial alternation may correspond to the variation of the winter monsoon. In addition, it is also argued that the enhancement of silicate weathering could be another mechanism relating late Cenozoic tectonic activity to global cooling. The major difficulty or uncertainty is how to distinguish various species within each type of clay minerals and how to analyze them individually and quantitatively. This issue has limited the application of clay mineralogy within loess weathering study. An alternative way may be to measure the concentrations of elements within the loess samples, and relate relevant geochemical proxies to possible weathering or climate contexts. This is because the

measurement of elements using chemical approaches could be more technically straightforward and precise.

Although many methods have been developed to reconstruct climate change within CLP, there are still some major uncertainties: (1) most previous mineralogical studies focus on one or two mineral/mineral groups, and fail to distinguish different sub-species within the same mineral group, e.g. feldspars, clays; (2) most of them are qualitative or semi-quantitative analyses, which limits the application of these analytical tools. Detailed geochemical and mineralogical studies of loess are still rare. Only one article published recently (Jeong et al., 2008) has conducted both quantitative bulk and single particle mineralogical studies using XRD, bulk chemical analysis, electron microprobe, SEM and TEM. They have refined the determination of mineral types and their composition within loess/palaeosols, attempted to ascertain the origin of the minerals, and tried to explain the possible weathering paths and environments at both source and depositional regions. This work indicates that loess mineralogy can be used as a complementary approach associated with other established climatic proxies; and that it can provide a new insight into the source lithology and weathering in the source and depositional areas. However, because only one loess section in the western CLP was selected for loess mineralogical study as far as the upper L2 loess, some important weathering periods older than L2 may have been missed and there needs to be a further systematic comparison among loess sections with similar weathering intensity but from different localities in order to help clarify the regional aeolian process (Jeong et al., 2008).

2.3 Previous studies in Chaohu Lake

Although Chaohu Lake has been studied in relation to eutrophication and environmental pollution for a long time, detailed palaeo-environmental changes for the long record are less well known. A recent study (Dai and Dearing, in preparation) has been conducted on an alluvial core collected from the catchment near the inflow where the biggest river, Hangbu River, draining into the lake. The Holocene records

in magnetic proxies, geochemical/mineralogical properties, grain-size composition and pollen distribution, reveal that the evolution process of the lake and its catchment experienced seven different climatic periods during last 10k years (op. cit.). In addition, it is concluded that changes in sea level and climate are the dominant factors contributing to the evolution of Chaohu Lake. This is also supported by Jia et al. (2006), who proposed three shrinkages of the lake during last c.6000 years, according to the grain size analysis and organic chemical analysis (TOC and TN contents) of the alluvial core collected on the catchment. In addition to the close relationship between the evolution of Chaohu Lake and changes in sea level and Yangtze River during the Holocene, both studies also suggested that human activity is another important factor contributing to the lake shrinkage in the late Holocene.

Another important study in this field was undertaken by Wang et al. (2008), who collected the lake sediment samples from the western part of the Chaohu lake and undertook grain size distribution and pollen analysis. Comparing the results from these three papers, some discrepancies can be found. For example, all the three papers suggested a warm yet generally dry climate period. However, Jia et al. (2006) suggested it was 2239 – 2136 a. BP, and 4860-2170 a. BP by Wang et al. (2008), while Dai and Dearing (in preparation) argued that it was a cooling period although the temperature has slightly gone up during 3150 – 2150 a. BP and the grain size distribution of Chaohu lake sediment has also been affected by the formation of the underwater delta at c. 2150 a.BP.

However, these studies also have similar problems: 1) none of them have provided enough details in radiocarbon dating procedure, i.e. materials/equipment used, laboratory methods, calibration methods, etc., which could make the radiocarbon ages plausible; 2) although historical records in the climate indicators have been obtained, it is not clear yet that there is a simple, linear relationship between these proxies and regional climate/environmental change. In other words, variation in grain size distribution, pollen assemblage, or element ratios does not necessarily only

attribute to the local or regional environmental change; and 3) there are also issues in the research methods themselves, resulting in misinterpretation or even wrong understanding of the data. As mentioned in Section 2.1, drawbacks of using grain size distribution, pollen data or other methods for palaeoclimate reconstruction, can complicate the interpretation of the results. Moreover, these issues can also be the reasons for the discrepancies between the conclusions of the studies on the Chaohu Lake although the site-specific factor can also affect the results and data interpreting.

In addition, although both elemental and XRD analyses have been undertaken on Chaohu lake sediments and its catchment samples, previous studies do not have detailed and comprehensive quantitative mineralogical data, which can indicate the sedimentary environment or deposit process in this area. Lack of these data means more difficulties in relating geochemical database with contemporary environmental conditions.

2.4 Computerised model for quantitative mineralogy and palaeo-precipitation reconstruction

2.4.1 Quantitative mineralogy

Quantifying mineral concentrations in sediments is an important step in reconstructing environmental change from a mineralogical perspective. Initial successful attempt was given to identify mineral species by using infrared spectra and comparing their chemical compositions with those of standards to determine the mineral content (Lyon et al., 1959). However, this can only be applied to those samples without complicated mineral mixture. Along with the development of laboratory techniques and better understanding of mineralogy, electron-probe and electron microscope were used for mineral identification and attempts have also been given to use image analysis to determine the mineral composition quantitatively (Sweatman & Long, 1969; Jones, 1982; Miller et al., 1982; Dilks & Graham, 1985; Petruk, 1988). However, there were many uncertainties due to sample preparation,

equipment performance, and personal knowledge of mineralogy. Additionally, for the microscopy analysis on thin sections, sample heterogeneity could also affect the accuracy of mineral quantification (Ward et al., 1999). Therefore, another approach has been proposed to use X-ray diffraction (XRD) analysis for the mineral content calculation. Some numerical models have been developed (Hill and Howard, 1987; Taylor, 1991; Taylor and Matulis, 1991). The principle is to calculate a series of XRD profiles of the multi-mineral sample based on various possibilities of mineral composition within it, and then to compare these calculated XRD profiles with the observed one by XRD measurement so that the best fit can be found out.

XRD has also been computerised using newly developed software, such as SIROQUANT (Taylor, 1991) and ROCKJOCK (Eberl and Smith, 2009; Uhlik and Eberl, 2006). The SIROQUANT programme is based on the Rietveld technique – using a formula to quantify the intensity of the mineral XRD spectrum and to refine the profile by least-square analysis (Rietveld, 1969, cited by Ward et al., 1999, p.1050). The Microsoft Excel-based ROCKJOCK programme is based on three published methods as described in Eberl's report (2003): *'(1) the matrix flushing technique of Chung (1974), in which integrated intensities of the unknown minerals are compared to that of an internal standard (in the case of RockJock, Al_2O_3, corundum), thereby obviating the need for measuring the mass absorption coefficient for a sample; (2) the whole-pattern fitting routine of Smith and others (1987) for measuring integrated intensities by fitting the sum of pure mineral patterns to that of the measured XRD pattern; and (3) the quantitative method of Srodon and others (2001) for some aspects of sample preparation, and for the method of measuring clay mineral content from non-basal reflections rather than from the more commonly used basal reflections.'*

Normative mineral calculation is another important numerical method for quantitative mineralogy. It is based on the element concentrations from chemical analysis and the chemical composition of reference minerals (Garrels & Mackenzie,

1971; Boyle, 2001), provided that the mineral identification can be determined by complementary observations from thin sections or XRD measurements (Ward et al., 1999). Normative mineral calculation can also be used to test the sensitivity of the quantitative XRD analysis method (op. cit.).

2.4.2 Numerical model for chemical weathering rate estimation

In order to reconstruct the palaeoclimate conditions, i.e. temperature and precipitation rates, it is necessary to estimate the chemical weathering rate from the data of mineral composition. A theoretical model was proposed by Sverdrup and Warfvinge (1988) for the weathering rate of silicate minerals, and showed the correlation of the weathering rate to the exposed surface area of the mineral, the soil moisture saturation and the chemical driving force. This model has been tested by field observation and been proved that the model-calculated weathering rates are in agreement with the observed ones. This concept have been extended and further developed as a computerised model called PROFILE (Warfvinge and Sverdrup, 1992) and it was initially used to calculate the critical load of acidity for forest soils and surface waters at Lake Gårdsjon in southwest Sweden. This model is based on mass balance calculation for different soil layers with three sub-models – soil solution equilibrium sub-model, the weathering rate sub-model and the ion exchanged sub-model. The weathering rate sub-model was developed to use independent and measurable soil properties to obtain the weathering rate. In addition, the difference between this sub-model and the previous model is that the weathering rate here is defined as the release of alkalinity and base cations rather than the dissociation of the silicate structure (op. cit.).

This weathering rate sub-model has also been used as a fundamental concept to build a process model of soil mineral chemical weathering (Boyle, 2007) for a broader application. This new model, named ALLOGEN, has been compared to river flux studies, chronosequences and lake sediment chemical stratigraphy, and performed well. However, further development is needed to correct the calculation of runoff

extremes (op. cit.) and improve its function on hydrological impact and DOC production (Boyle, 2008). Therefore, a newly developed model (Boyle, 2008) was presented for quantifying climate impacts on long-term average surface water acidity.

Another model for weathering rate estimation is created by White and Blum (1995). They attempted to use it to examine the effect of precipitation, runoff and temperature on chemical concentrations and fluxes, and concluded that the model shows a linear relationship between precipitation and weathering rates at any fixed temperature, but it increases exponentially with increasing temperature. This model has been improved later because White and others (1996) found that time needs to be taken into account in calculating mineral weathering rates. The principle of the model is to calculate mineral dissolution rate from mineral loss using a series of formula with parameters such as temperature, precipitation and time.

2.5 Summary

Based on the review on the methods commonly used for palaeoclimate reconstruction, it can be concluded that every method has its drawbacks. Therefore, the mineralogy method has been proposed. Literature research has been undertaken on the application of mineralogy onto loess and lake sediments. It is found that little detailed and comprehensive geochemical/mineralogical data have been provided for Chinese loess and Chaohu lake sediments, and that previous studies lack quantitative geochemical/mineralogical analyses. However, this information is very important for palaeoclimate study. Therefore, in this thesis, attempts will be placed on develop reliable quantitative mineralogical methods for palaeocenvironmental study, based on the detailed geochemical/mineralogical data.

Chapter 3 Study areas & Sampling

3.1 Chinese Loess Plateau

3.1.1 Location and modern climate

The Chinese Loess Plateau (CLP) is located in central-north China between 34 and 45°N, and has a total area of ~380,842 km^2. The Yellow River runs through it. The Plateau has a distinctive topography. There are three types of landform: 1) Mao – a tapered hill, derived from loess deposition in the North Loess Plateau; 2) Liang – ridge-shaped, formed by historical weathering, usually found in the Central Loess Plateau; 3) Yuan – roof-like topography, formed by interbedded loess-palaeosol sequences and present mainly in the South Loess Plateau.

The present climatic conditions of the Loess Plateau are mostly affected by the East Asian monsoon, which consists of two major subsystems – the Indian (or southwest) monsoon and the East Asian (or southeast) monsoon (Ding et al., 2001). The Indian summer monsoon is formed by the interaction of the high atmospheric pressure over the southern subtropical Indian Ocean and the India Low (over the Asian Plateau), while the connection of the Pacific High with the India Low causes the East Asian monsoon. The current climate in the CLP area is characterised by generally low precipitation and relatively arid conditions, but by wetter/warmer conditions in the South CLP and drier/colder conditions in the North CLP (An, 2000). The annual precipitation on the Loess Plateau is normally in the range of 300-600mm, but it can reach 800-1000mm in some areas (CSDB, n.d.). The maximum intensity of rainfall occurs in the summer because of the warm and wet summer monsoon, but it lasts only a short time, usually two months (op. cit.). In contrast, during the winter, it is relatively arid and cold because of the north-westerly winter monsoon mainly derived from the Siberian high-pressure system (An, 2000). Thus, it is evident that the difference between summer and winter on the Loess Plateau is significant. In

addition, the precipitation on the CLP varies considerably on an annual basis. The precipitation in some years can normally be 3 or 4 times, even 30 or 40 times higher than that in some years dominated by dry conditions (CSDB, n.d.).

3.1.2 Formation of loess deposits

Chinese loess is known primarily as a wind-blown Quaternary silt deposit (Heller and Evans, 1995), although it has recently been established that significantly older loess deposits also occur in the area (e.g. Guo et al., 2002). It is characterized as a loess-palaeosol interbedded deposit, with the loess layers corresponding to cooler, drier glacials and the palaeosols to warmer, more humid interglacials. Numerous studies of Chinese loess have been conducted along the climatic gradient from south to north across the Loess Plateau. The thickness of the Quaternary loess increases from southeast to northwest, ranging from 120m in the east to 320m at Lanzhou, on the western Loess Plateau; it even exceeds 500m in some areas (Cao et al., 1997).

The grain size distribution of Chinese loess is typically in the range of 10-50μm, and it is unusual for the loess to be either significantly coarser or significantly finer than this (Heller and Evans, 1995). It is suggested that the grain size distribution in aeolian loess directly reflects the changes of climate and environment. During glacial periods, arid conditions increased the availability of sediment for aeolian transport and the more vigorous atmospheric circulation facilitated the transport of coarser particles. In contrast, during interglacials, more humid conditions promoted the spread of vegetation which enhanced soil stability and reduced sediment availability. Thus, the accumulation of the loess deposits was slower and the grain size distribution of the deposited sediment was correspondingly smaller (Cao et al., 1997). These two phenomena reinforced each other – a high dust deposition rate in glacial times led to relatively unweathered loess, while a lower deposition rate in a warm climate producing more strongly-developed soils during interglacial times (Ding et al., 2002).

3.1.3 Loess stratigraphy

Loess lithology

Several workers have demonstrated a strong correlation during the Quaternary between the magnetic susceptibility of Chinese loess and the marine oxygen isotope record (e.g. Heller and Evans, Fig. 3-1), thereby pointing to a close relationship between global climate state and loess lithology. Palaeosol units labelled as S, correspond to warm and wet periods and to peaks in magnetic susceptibility. Loess units labelled as L are more complicated: those with minima in magnetic susceptibility are considered as unweathered loess, corresponding to cold and dry stages; while those with relatively high values within the loess layer are suggested as weathered loess, corresponding to a relatively warm and wet phase in between cold stages. L and S layers are labelled in a numerical order, respectively. The bigger the number, the older the lithological unit. The sub-layers are also labelled using the L-S system with a numerical order. For example, L1S1 refers to the first (youngest) weathered sub-layer within the loess unit L1; S1L2 refers to the second relatively low-susceptibility sub-layer within the palaeosol unit S1. In addition, L1S1 is also termed the 'Sm' layer (interstadial soil, corresponding to oxygen isotope stage 3), and this term is used subsequently in this thesis.

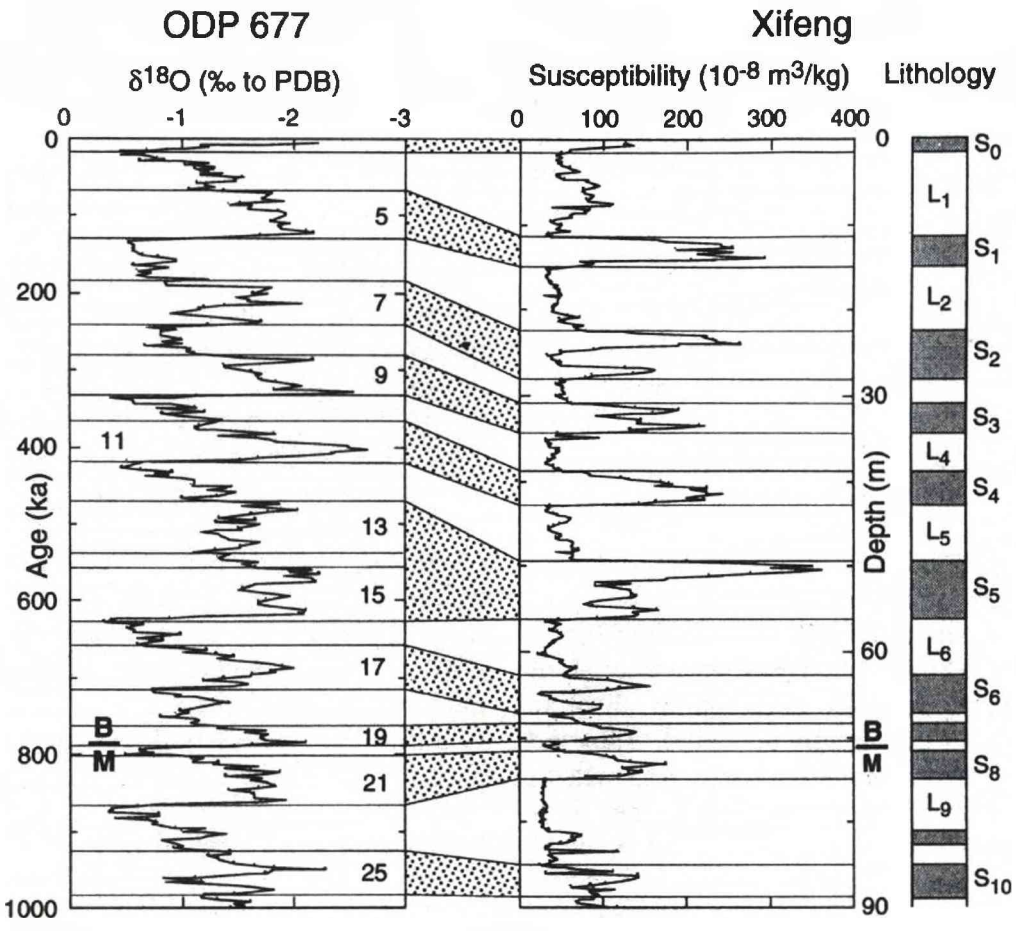

Figure 3-1 Comparison between marine oxygen isotope records and magnetic susceptibility records of samples from the Xifeng loess section. From: *Heller and Evans (1995)*. Warm oxygen isotope stages (1, 5, 7, 9, 13, 15, 17, 19, 21, 25) correspond to peaks in magnetic susceptibility and to palaeosols ('S' layers). Cold stages correspond to susceptibility minima and to weakly weathered loess layers. This demonstrates a close relationship between weathering regime on the Loess Plateau and global climate state.

Loess density

Sun *et al.* (2000) have measured the density of the loess-palaeosol sequences from the Lingtai loess section in Gansu province. They suggested that the dry bulk density in palaeosols is higher than that in loess (Table 3-1). There appears to be a positive relationship between the dry bulk density and the equivalent magnetic susceptibility records, although an increase in the density at the base of some palaeosols and a

decrease in corresponding magnetic susceptibility values have also been noted. This probably implies pedogenic processes lead to the loss of carbonate and downwards movement of clay particles (op. cit.). Comparing the dry bulk density and the equivalent magnetic susceptibility records during glacials, Sun et al. (2000) also suggested that the dry bulk density could be a better proxy indicating the variation in the East Asian Monsoon regime.

Table 3-1 Average value of dry bulk density (g/cm^3) of different loess-palaeosol layers in the Lingtai section. From *Sun et al. (2000)*

Palaeosol (No. of samples)	Density (g/cm^3)	Loess (No. of samples)	Density (g/cm^3)
S0 (9)	2.05	L1 (35)	1.88
S1 (19)	2.07	L2 (29)	1.85
S2 (18)	2.13	L3 (15)	1.88
S3 (10)	2.16	L4 (20)	1.92
S4 (20)	2.18	L5 (14)	1.90
S5 (32)	2.12	L6 (22)	1.89
S6 (6)	2.10	L7 (10)	1.98
S7(14)	2.03	L8 (7)	1.92
S8 (14)	2.09	L9 (38)	1.91

Note: The average values are calculated from the measurement results based on a 20cm resolution.

Duration of pedogenesis

Although it is suggested that magnetic susceptibility records of Chinese loess are positively correlated to the marine oxygen isotope records, which correspond to the alternating glacial-interglacial periods, a recent study (Vidic et al., 2004) argued that the magnetic susceptibility values of palaeosols cannot be directly used for reconstructing palaeo-precipitation rates or the temperature during pedogenic intervals, because their results showed that the magnetic susceptibility enhancement of palaeosols during the past 620 ky depends not only on weathering processes, but also in part on the duration of pedogenesis. Therefore, this factor will also be taken into account for quantitative palaeo-precipitation reconstruction (Table 3-2).

Table 3-2 Age assignments and calculated duration for the Jiaodao loess-palaeosol section. Adapted from *Vidic et al (2004)*

Strat. Layer	Basal age (ky)	Duration (ky) -1	Strat. Layer	Basal age (ky)	Duration (ky) -2	Strat. Layer	Basal age (ky)	Duration (ky) -3
L1L1	n/a	n/a	L1L1	n/a	n/a	L1L1	n/a	n/a
Sm	79	n/a	Sm	71	n/a	Sm	67	n/a
L1L2	n/a	n/a	L1L2	n/a	n/a	L1L2	n/a	n/a
S1	129	50	S1	127	56	S1	129	62
L2	196	67	L2	186	59	L2	193	64
S2	250	54	S2	242	56	S2	243	50
L3	290	40	L3	301	59	L3	279	36
S3	342	52	S3	334	33	S3	334	55
L4	386	44	L4	364	30	L4	369	35
S4	417	31	S4	427	63	S4	418	49
L5	503	86	L5	474	47	L5	452	34
S5	625	122	S5	621	147	S5	620	168

Note: Duration 1 - Age assignments by Heslop et al. (2000)

Duration 2 - Age assignments for correlative marine isotope stages by Bassinot et al. (1994)

Duration 3 - Age obtained by correlation to the ODP 677 planktonic and benthic foraminifera $\delta^{18}O$ record were used to determine the age boundaries for the major isotope events

3.1.4 Weathered loess and palaeosols

From magnetic susceptibility records of the loess-palaeosol sequences, higher values and peaks occur in palaeosols and some weathered loess, corresponding to interglacials or to the shorter-duration interstadials. This normally means a climate with higher temperature and rainfall rate at the period when the weathered loess or palaeosols formed. For example, loess sub-layer L1S1 (Sm) is known as a highly-weathered loess layer from comparison of its magnetic susceptibility values with marine oxygen isotope records. However, it is necessary to obtain evidence from other proxies, e.g. geochemical records, to prove this observation from magnetic susceptibility records. This will be discussed in Chapter 5.

3.1.5 Sampling areas

Three loess sections on a latitudinal and climate gradient were selected for this study: Duanjiapo, Luochuan and Caoxian (Figure 3-2).The Duanjiapo section is located at

34.2°N, 109.2°E (Bloemendal & Liu 2005), in Lantian County on the humid southern edge of the CLP. The present mean annual precipitation (MAP) is ~615mm and the mean annual temperature (MAT) is ~13°C. The thickness of the loess-palaeosol sequence at Duanjiapo section is ~130m, and it overlies a ~30m thick layer of the Pliocene Red Clay Formation. The Luochuan section is located at 35.8°N, 109.4°E in Luochuan County in the central CLP. The present MAP is ~570 mm and the MAT is ~9°C. The loess-palaeosol sequence is typically ~135m thick.

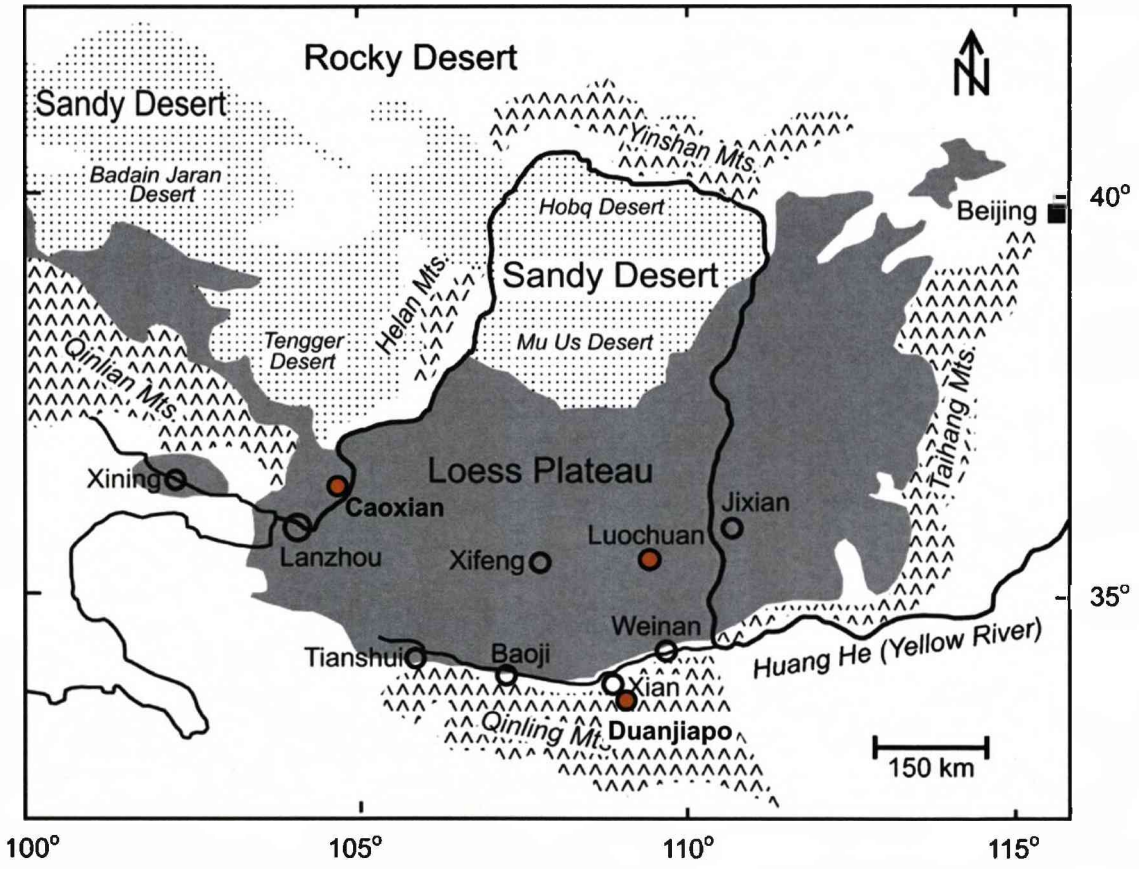

Figure 3-2 Study Area on the Chinese Loess Plateau. Adapted from Jeong et al. (2008)

Unlike these two loess sections, the total sediment sequence at Caoxian, Gansu province (36.6°N, 104.6°E), can be as thick as ~500m (Heslop et al., 1999) and thus the area is characterised by much higher accumulation rate yet with a much lower

degree of pedogenic development, reflecting the significantly greater aridity of this site. The site is >1900m above sea level with a MAT of 5-9°C and a MAP of ~200mm (From: CSDB). Duanjiapo and Luochuan were sampled at a 10 cm interval, and Caoxian at a 2 cm interval. The collected loess-palaeosol samples were bagged, transported back to Liverpool, air-dried, and put into magnetic pots for further analyses. Initial magnetic results from the sections were reported in Bloemendal and Liu (2005) and Parker (1999).

3.2 Chaohu Lake

3.2.1 Location and modern climate

Chaohu, the fifth largest of China's freshwater lakes, is located in the middle of Anhui Province, East China (ca. 117°16′46″–117°51′54″E, 30°43′28″–31°25′28″N). The surface area of the lake is ~800 km^2 and the catchment ~ 13 000 km^2 at ~10m above sea level (Figure 3-3) with a water depth of 3-5 metres. It lies within the Yangtze River lower watershed, which is surrounded by several tributaries. Among these tributaries, Hangbu River is the biggest, originating from Dabie Mountain and delivering over 65% of the total water or silts of the Chao Lake (unpublished data, Dai and Dearing, personal communication).

The area where Chaohu Lake is located has typical subtropical climate features and is mainly affected by the southeast summer monsoon. The mean annual temperature is 16°C and the average monthly temperatures for January and July are 2.8°C and 28.7°C, respectively. The annual mean precipitation is 1000-1157mm; the wet season is normally during June – August; and the annual evapotranspiration is 1653.1mm (http://www.marsh.csdb.cn/survey/anhui.htm, China Marsh and Wetland Database, in Chinese).

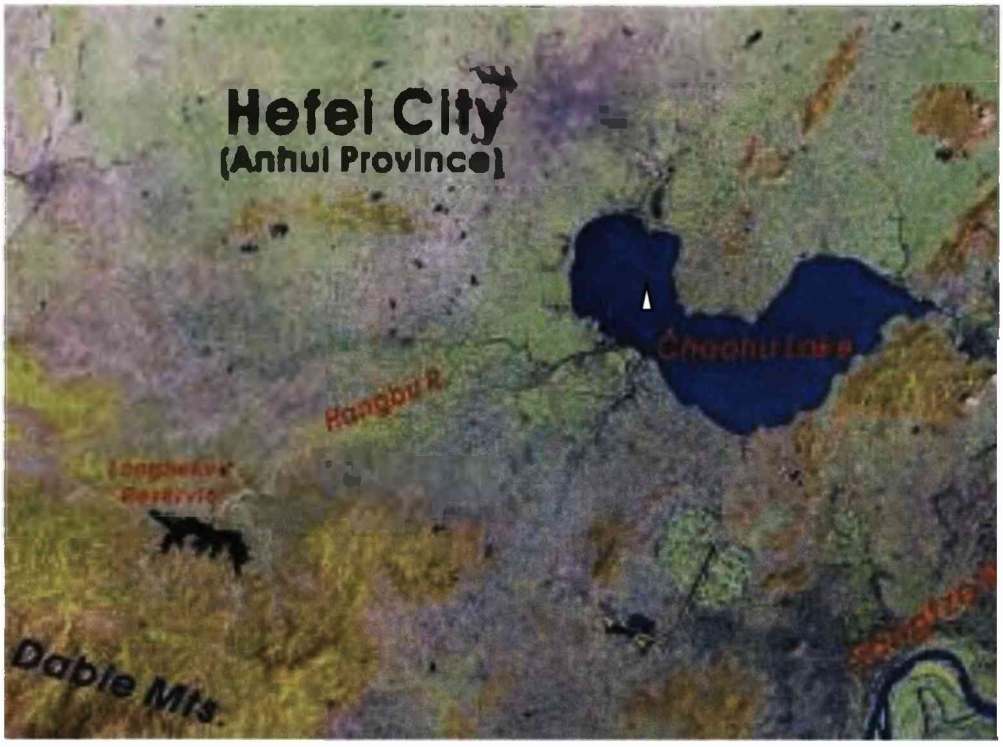

Figure 3-3 Chaohu Lake and its surrounding area. (Dai and Dearing, personal communications). The white triangle point in the lake is the location of the lake sediment core chosen for this study.

3.2.2 Geological and documentary records

Chaohu Lake is considered to be a typical fault-structured lake, evolved on the base of a tectonic basin (Wang et al., 2008). The oldest sediment in the lake was deposited during the early Pleistocene, which is the same epoch when the clayey catchment was formed. This could indicate that the sedimentary structure of Chaohu Lake started in the late Pleistocene (http://www.marsh.csdb.cn/survey/anhui.htm, China Marsh and Wetland Database, in Chinese). It is also stated that Chaohu Lake was formed through the combination of two lakes after a fault occurred – one is Chaohu i.e. the east part of the present Chaohu Lake, the other is Jiaohu Lake i.e. the west part of the present Chaohu Lake (op. cit.). Some geologists (Zhang et al., 1990; Zhu et al., 1998; and Zhu, 2004; cited by Wang et al., 2008, p.154) also suggested that the structural patterns are complex in the study area and the well-developed fault systems controlled the lake formation and its basin-range framework. In addition,

yellow sand or dark-brown greyer silt clay with a fluvial-lacustrine origin mainly comprise the Holocene sediments, spreading along the rivers and lakes near the banks of the Yangtze River (Yang et al., 2000, cited in Wang et al., 2008, p.154).

According to the study of documentary records, the area of Chaohu Lake was about 2000 km^2, and has shrunk by 20% during 760-960 A.D. (Jia et al., 2006). In addition, an underwater historical site of a town in the Han Dynasty has been found and ^{14}C dated as ~2090 B.P., suggesting that the town has been submerged by the lake water after this date (op. cit.).

3.2.3 Sampling

Sediment cores were obtained both from the lake and from the terrestrial catchment (near the main inflow to the lake, core ACN) by East China Normal University, Shanghai, in 2006. Among the cores collected from the lake, the longest one, located in the central part of the western part of the lake (Figure 3-3), has been selected for this study and is named the Lake Core. The lake core is 140.5 cm long, and was sliced into 0.5cm intervals and dried prior to analysis at the Department of Geography, University of Liverpool. The results obtained from this lake sediment core will be compared with those obtained from the 15m long alluvial samples (ACN core) done by East China Normal University, Shanghai, China.

Chapter 4 Methods

4.1 Magnetic measurements

Magnetic measurements for the loess sections from Duanjiapo, Luochuan and Caoxian, and for the lake sediment samples from Chaohu, were already available prior to the commencement of the present study. Briefly, standard techniques were used: magnetic susceptibility was measured with an AGICO KLY-3 Kappabridge; frequency dependent susceptibility was measured with a Bartington Instruments meter and MS2B sensor; anhysteretic remanence was imparted using a DTECH D-2000 A.F. demagnetizer using a 1000mT peak alternating field and a 0.04mT biasing field; and isothermal remanences at various forward and reverse fields were imparted using a Magnetic Measurements pulse magnetizer. All remanences were measured using a Molspin fluxgate spinner magnetometer. The measurements were made in the Environmental Magnetism Laboratory, Department of Geography, University of Liverpool. The results for the loess sections are presented in Bloemendal and Liu (2005); Parker (1999); and Parker and Bloemendal (2005). The results of magnetic measurements of the Chaohu lake sediments are previously unpublished (Dearing, personal communication).

4.2 Dating techniques

4.2.1 Dating of the Chinese loess

Age models used for the Duanjiapo and Luochuan loess samples are described in (Bloemendal & Liu, 2005). Ages of loess samples were obtained by linking the magnetic susceptibility records to the insolation record for 65°N and the marine oxygen isotope record from ODP Site 677 (op. cit.). The derived accumulation rates for the two sites are shown in Chapter 5.

4.2.2 Dating of the Chaohu Lake sediments

Five lake sediments samples have been radiocarbon dated using Accelerator Mass Spectrometry (AMS) method at Beta Analytic Radiocarbon Dating Laboratory, USA. Four bulk samples were used as no suitable macrofossils were found, and the other sample was dated by two different methods, using organic sediment and a macrofossil (a shell-half, probably conch), respectively. 'Acid wash' and 'acid etch' pretreatment methods were applied to organic sediment samples and the shell sample, respectively (See Appendix II). Six AMS radiocarbon dates were calibrated based on the calibration database IntCal04 (Calibration Issue of Radiocarbon, Volume 46, no. 3, 2004), using the cubic spline fit mathematics proposed by Talma and Vogel (1993). Detailed discussion about the radiocarbon ages is undertaken in Chapter 6.

4.3 X-ray fluorescence analyses

4.3.1 Sample preparation and X-ray fluorescence measurements

In order to determine element concentrations for the sediment and soils samples, XRF measurements were undertaken using a Bruker AXS S2 Ranger energy dispersive XRF spectrometer. This instrument can analyse element concentrations by measuring the intensity of the characteristic fluorescent X-rays emitted by the elements inside the sample, after the source X-rays have been directed at the sample. XRF measurements for selected intervals of the Duanjiapo and Luochuan loess-palaeosol sequences were undertaken at a 20cm interval, while for Caoxian measurements were made at 2 cm interval. For the Chaohu sediment samples, measurements were made at a 0.5cm resolution.

All selected samples were ground using a pestle and mortar, packed plastic XRF pots with tightly pulled and smooth cling film at the base, and compressed using a brass plunger. Subsequently, samples were put into the sample chamber and measured in a

helium atmosphere. The results were calibrated using in-house calibration methods using the associated software Spectra EDX.

4.3.2 Correcting the XRF data

The raw XRF data were calibrated using in-house calibration methods created through the associated software Spectra EDX. Because of the discrepancies in results calibrated using different methods, it was necessary to undertake correction of the XRF data before further analysis.

Three calibration methods were used for the loess samples: *General test, Soil & sediment*, and *Sediment*. The main difference between them is in the use of different standards. In order to calibrate the raw data, various samples with known chemical compositions have been used as standards. According to the location where the samples in question were collected, different combinations of these standards were used to form different calibration methods, which were stored and processed using the quantitative analysis software. It is believed that the standard setting of the *Sediment* method is the one closest to the characteristics of Chinese loess, but it could not be applied to all the raw XRF data because of some systemic problems of the software. Therefore, 10 randomly selected samples were re-measured and calibrated using the *Sediment* method. Comparing the element concentrations of the ten samples derived from the three calibration methods, results obtained using *General test* and *Soil & sediment* methods were corrected using the regression lines of *General test-Sediment* and *Soil & sediment-Sediment,* respectively. Afterwards, scatter plots for each element were obtained using these two sets of corrected results (Figure 4-1). They show a high degree of similarity between the two sets of corrected results for the major elements, i.e. Si, Al, Ti, Ca, K, Fe, Mn, Cl, and some trace elements, namely Ni, Rb, Sr, Zn and Zr. Concentrations of Mg, Na, S, As, Ba, Cu, Ga and Y calibrated by *General test* have a positive relationship yet less similarity with those by *Soil & sediment*. Plots for other elements (P, Br, Co, Cr Nb, Pb and V) are more scattered or have negative regression lines. This means that either the XRF

spectrometer cannot measure these elements precisely or the calibration method is not suitable for calibrating these particular elements. In order to undertake the next step of calculation – mineral estimation - it is necessary to use positive values for those elements involved in the mineral calculation, including all the major elements and some trace elements, i.e. Ba, Rb, Sr, Zn and Zr. Therefore, I have used the *Soil & sediment* calibrated results, where positive values can be found for all the elements mentioned.

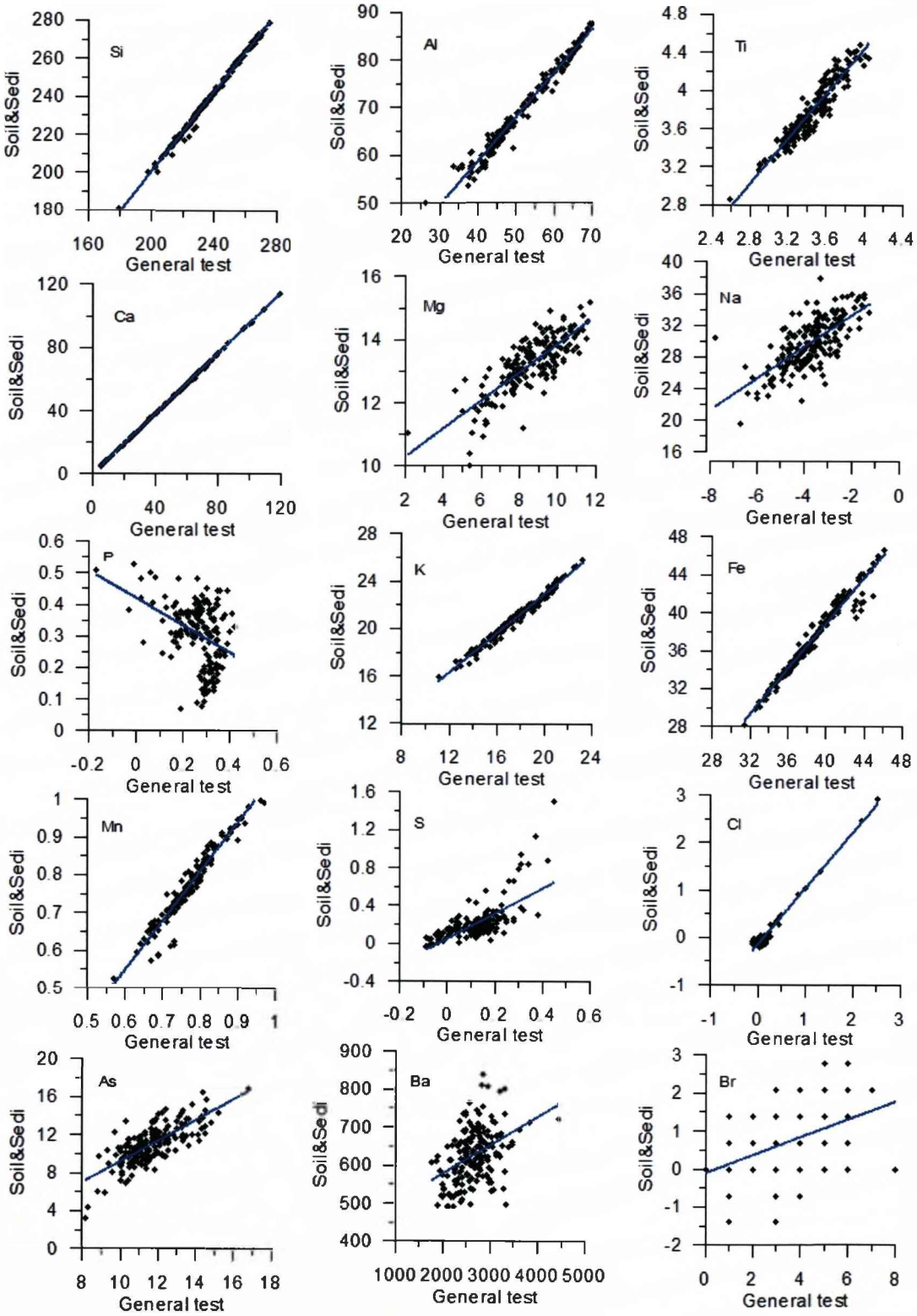

Figure 4-1 Scatter plots for corrected element concentrations derived by XRF calibration methods *General test* and *Soil&sediment*. Unit mg/g is used for Si, Al, Ti, Ca, Mg, Na, P, K, Fe, Mn, S and Cl; for other elements unit ppm is used.

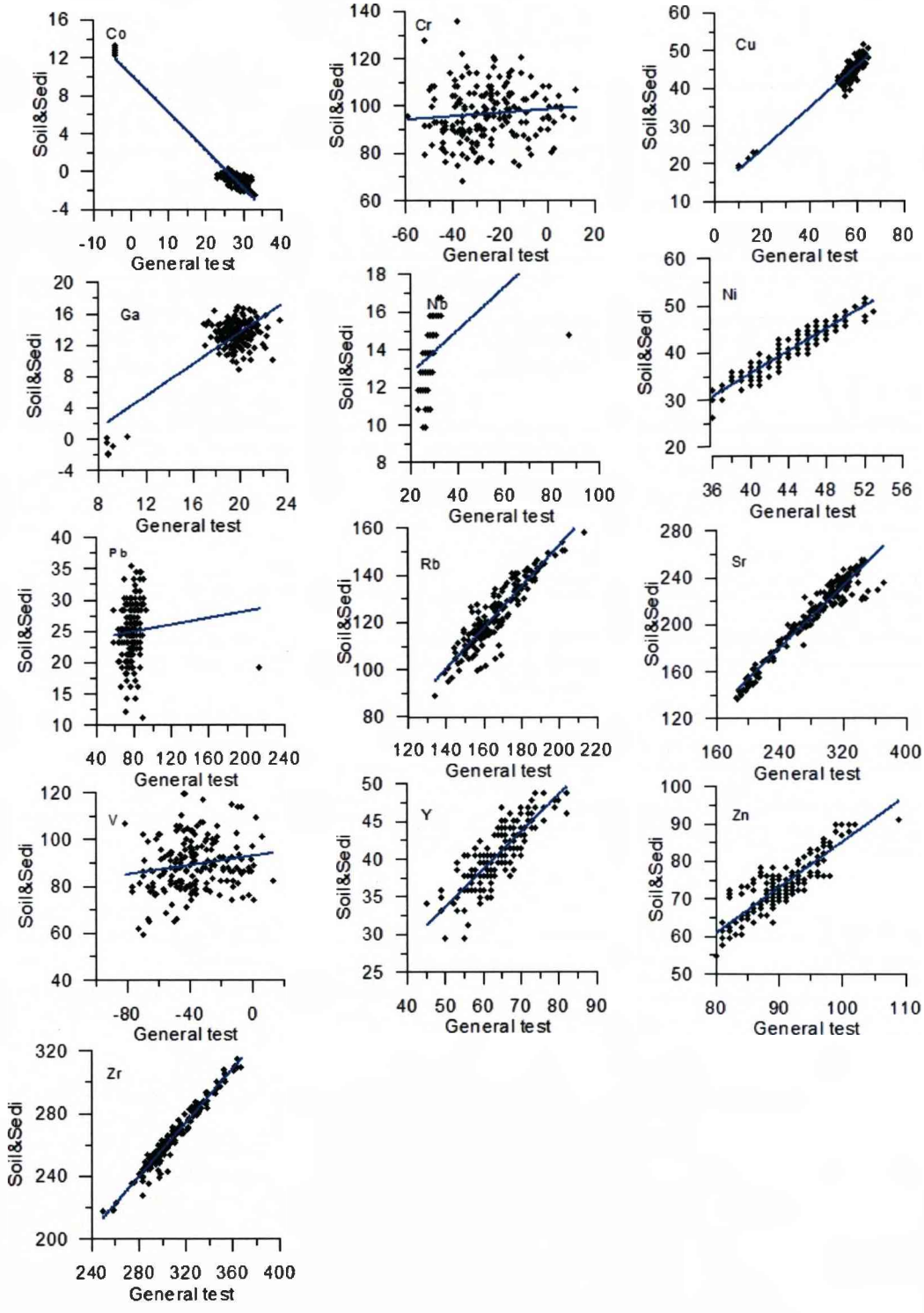

Figure 4-1 continued.

4.4 X-ray diffraction analyses (for the Chinese loess)

4.4.1 Rationale of sample selection

According to the low-frequency susceptibility records of the Duanjiapo and Luochuan sections (Figure 4-2), it is not suitable to choose relatively 'over-developed' palaeosols for XRD and SEM analyses, if general loess mineralogy is to be established. This is because these palaeosol units, especially palaeosol S5, could have developed from both weathering and intense in-situ pedogenic processes, which included complete decalcification and mechanical translocation of fine particles (Han et al., 1998). This complex of pedogenesis could complicate the identification of some minerals, e.g. calcite and clay minerals. Therefore, within the L1-S5 loess-palaeosol sequences, the best developed palaeosol S5 was omitted for mineral qualification analysis, and instead 'typical' (in terms of their degree of pedogenic development) palaeosol units S1, S4 and weathered loess unit Sm (L1S1) were selected. In addition, in order to compare the difference in mineral composition between loess and palaeosols, pristine loess units L2 and L5 were also selected. For the Caoxian loess section, the equivalent L1 and S1 units were selected for comparison. Therefore, 15 loess and palaeosol samples from three loess sections were selected for XRD and SEM analysis (Table 4-1). The locations of the samples in terms of the magnetic susceptibility stratigraphy are shown in Figure **4-2**.

Table 4-1 Samples selected from three loess section

Duanjiapo			
Sample	**Depth (m)**	**Age (ky BP)**	**Unit**
J63	3.20	42	Sm
A61	5.00	113	S1
A101	7.00	152	L2
D97	20.10	407	S4
D133	21.90	425	L5
Luochuan			
Sample	**Depth (m)**	**Age (ky BP)**	**Unit**
A113	5.7	58.0	Sm
A175	8.8	91.3	S1
A237	11.9	149.8	L2
B249	27.5	408.0	S4
B299	30.0	424.5	L5
Caoxian			
Sample	**Depth (m)**	**Age (ky BP)**	**Unit**
CX2448	23.48	n/a	Sm
CX3674	35.74	n/a	L1L2
CX3892	37.92	n/a	S1S1
CX4288	41.88	n/a	S1L2
CX-4192	40.92	n/a	S1S2

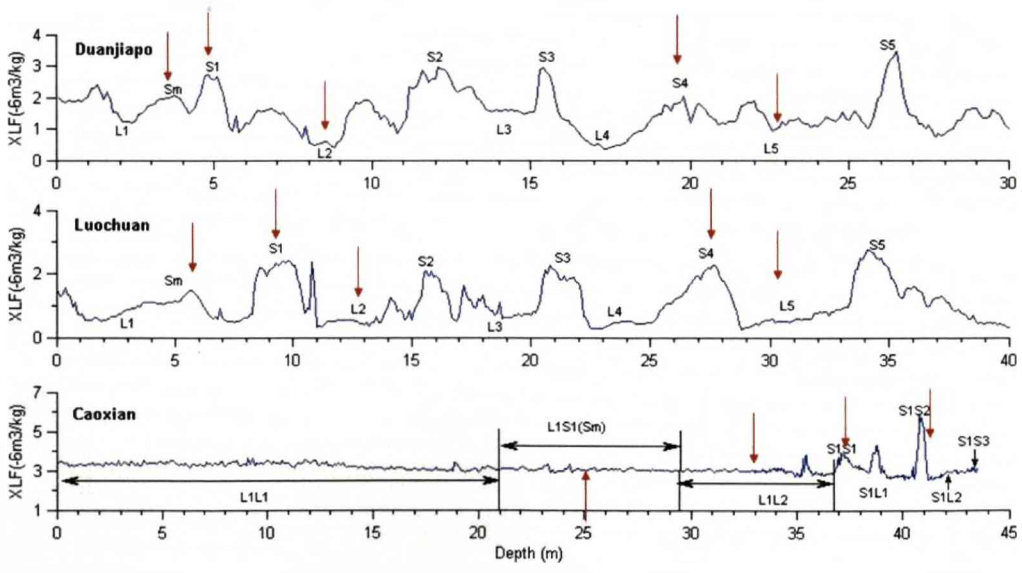

Figure 4-2 Locations of the samples used for XRD and SEM analysis, in relation to the magnetic susceptibility stratigraphy of the three loess sections.

4.4.2 Organic content measurement

Before undertaking XRD and XRF measurements, it is necessary to measure the organic content in the loess and palaeosol samples, because high organic content could reduce the accuracy of the results. However, if weight-loss-ignition (LOI) was used to estimate the organic matter content, errors can be very large for XRD measurements if the sample contains: 1) low organic matter; 2) a significant amount of clay minerals (particularly smectite and kaolinite); or 3) dolomite and/or siderite. Therefore, a wet chemical method (the Walkley-Black method) was used to estimate the organic carbon, and hence the total organic matter content. The method is described in Appendix II. Thirteen loess/palaeosol samples were selected for analysis. The concentrations of organic matters in selected samples are shown below (Table 4-2).

Table 4-2 Mean organic content (%) in loess and palaeosol samples from the three loess sections

Sample	Lithological Unit	% Organic content (mean of analyses)
Duanjiapo		
J63	Sm	0.34
A61	S1	0.26
A101	L2	0.18
D97	S4	0.09
D133	L5	0.08
Luochuan		
A113	Sm	0.30
A171	S1	0.19
A237	L2	0.10
B249	S4	0.14
B299	L5	0.14
Caoxian		
CX2448	Sm	0.13
CX3892	S1	0.16
CX4288	S1	0.12

4.4.3 Sample preparation for XRD analyses

It can be seen in Table 4-2 that the organic content in both loess and palaeosols is sufficiently low as to be regarded as zero for the purpose of the XRF and XRD measurements. Therefore it was possible to measure the loess samples directly using

the X-ray Diffractometer without the removal of organic matter. X-ray powder diffraction analysis was undertaken using a GBC EMMA X-ray diffractometer. Three grams of each sample were crushed using an agate mortar, transferred to a plastic container whereupon agate beads and 15ml of water were added. The samples were then placed in a micronising mill for a few minutes, followed by freeze-drying. Subsequently the powdered samples were mounted in the sample holder and finally X-rayed from 5° to 65° 2θ with a counting rate of 0.02° 2θ step per 2 seconds using Cu K-alpha tube anode and a scintillation counter. Qualitative analysis of the XRD spectra was made using Windows-based Traces software (Version 6, XRD DiffTech software, GBC, Australia, 2003, Part No. 01-0930-00).

4.4.4 Quantification of XRD results

Quantitative analysis of the XRD data was undertaken using an Excel-based model, RockJock Version 5 (developed by Eberl, 2006). The principle of this model is to compare the integrated XRD intensities of individual minerals in complex mixtures to the intensities of an internal standard (Eberl, 2003). These mineral standards have been already measured by the U.S. Geological Survey (USGS) using a Siemens D-500 X-ray diffractometer with the following experimental setup for the X-ray beam: X-ray tube (Cu), 1 degree slit, soller slits, 1 degree slit, sample, 1 degree slit, no filter, 0.05 degree slit, graphite monochromator, 0.6 degree slit, scintillation detector (Ibid: p16).

Subsequently, estimation was made of the possible minerals which could contribute to the most similar overall spectra pattern, i.e. overall XRD spectra intensities. However, there are many combinations of minerals which could generate the same XRD spectrum, so it is still necessary for qualitative identification of the loess mineral types prior to the quantitative stage. Therefore, scanning electron microscopy with energy dispersive X-ray analysis was used for the mineral type identification. In addition, the sensitivity of RockJock V5 was tested by comparing the element

concentrations calculated by XRD quantification with those measured by XRF spectrometer (See Chapter 5).

4.5 Scanning Electron Microscope and Energy Dispersive X-ray analysis (for the Chinese loess)

Detailed petrographical analysis of individual particles was done using a Philips XL30 SEM with an EDX Analyser, at the Department of Earth Sciences, University of Liverpool. Due to limitations of time, budget and availability of the SEM machine, five loose powder samples and four thin section samples were analysed by SEM. Because the similarity of the chemical analysis results between the loose powder samples and thin section samples, only SEM images of the thin section samples were shown in Chapter 5.

4.5.1 Sample preparation

Loose powder samples

A very small amount (less than 1 gram) of the loose powder sample was used and evenly spread on the central area of a glass slide, which has then been placed on a small plate-shaped sample holder (1cm diameter). Subsequently the sample was placed in a coating machine (EMI TECH K950X) for about 12 minutes. After vacuumising, centrifugation and evaporation in the machine, the samples have a C-Pd coating.

Thin section samples

About 1g of each powdered sample was sent to the Geosciences Department, University of Birmingham, for polished thin section treatment. Then each thin section sample was dyed by carbon ink, and put into the coating machine (EMI TECH K950X) for 4 minutes. After vaccuumising, centrifugation and evaporation in the machine, the samples are carbon-coated. However, differing from the coating

procedure for loose powder samples, the evaporation was done twice in order to obtain a reasonably thick carbon layer.

4.5.2 Energy Dispersive X-ray analysis (EDXA)

Secondary and backscattered electron images were obtained by SEM and the chemical composition of specific grains was determined using EDX analysis. All the EDXA spectra were obtained using the associated program and analysed with the reference spectra patterns published online by Microanalytical Laboratory, Earth and Planetary Sciences, McGill University, Canada (URL: http://www.eps.mcgill.ca/~lang/EDSSPEC/edshome.html) and Bausch & Lomb Nanolab Scanning Electron Microscope, Earth Sciences Department, Simon Fraser University, Canada (URL: http://www.sfu.ca/~marshall/sem/mineral.htm).

In addition, because of the differences in sample preparation, one should bear in mind that:

a) For loose powder samples: 1) The spectrum will have higher peaks in Au, C and Pd because of the coating technique; and 2) The data cannot be used for quantitative analysis, because the specimen is not a polished sample. There could be different angles when spotting using the EDX microprobe, which will affect the number of electrons collected by the collector. This means there may be many analytical uncertainties.

b) For thin section samples: 1) The spectrum will have higher peaks in C because of the coating; and 2) Even if the highest resolution is chosen, there still could be some overlaps in the spectrum because of the chemical properties of certain elements.

4.6 Pollen and charcoal analysis (for the Chaohu Lake sediment samples)

Pollen and charcoal analyses were conducted by Dr. Richard Jones at the University of Exeter, Department of Geography. Fifty samples were selected for pollen and

charcoal analyses with 31 samples at 2cm intervals from the top of the lake sediment core to a depth of 60cm, and the other 19 samples were selected from depths below 60cm according to their positions in relation to maxima and minima in the magnetic susceptibility record. In addition, pollen analyses were made at East China Normal University, Shanghai, on samples at 15cm interval from the alluvial core.

4.7 Mineral estimation

4.7.1 Normative Mineral Calculation

X-ray fluorescence spectrometer can be used to estimate the concentrations of most of the elements within the lake sediment samples. A straightforward way to interpret these data is to compare the variation in element concentrations and their ratios against depth. For example, the Rb/Sr ratio within loess-palaeosol sequences can reflect the weathering intensity (Chen et al., 1999b); Zr concentration can be an indicator of coarse material (Deer et al., 1966); and the Mg concentration can sometimes be considered as an indicator of the clay mineral component within the sediment.

However, as mentioned in Chapter 2, Section 2.1.2, it is difficult to obtain an overview of weathering history or environmental change by element analysis. Therefore, mineralogical analysis is preferred here, because the variation in minerals can directly indicate weathering or pedogenic process, especially when quantitative analysis is required.

Normative mineral calculation (Garrels & Mackenzie, 1971; Boyle, 2001) is used to calculate the concentration of minerals from the element concentration data. This method is based on the principle that the molar concentration (moles/100g) of the mineral can be calculated from its oxide molar concentrations using chemical analysis data of the mineral.

As an example, the following steps were used for the Chinese loess samples:

1. Qualitative identification of mineral types. According to the SEM with EDX analysis and XRD quantification, the mineral assemblage in these samples includes zircon, apatite, potassic feldspar, biotite, Na-Ca plagioclase (NCP), illite, chlorite, iron oxides (in the form of FeOOH), titanium oxides (TiO_2), calcite, kaolinite and quartz.
2. All the major elements should be included in the calculation. Recalculate the element concentrations as wt% oxides. Sum the oxides and normalize the sum to 100%.
3. Divide each oxide by its molecular weight to get the molar concentration in moles/100g.
4. Choose reference minerals for these mineral types and find out the chemical analysis data for these reference minerals (e.g. Deer et al., 1966). The oxides in the reference minerals are also converted into moles/100g, as in step 3.

Consequently, molar concentration of the mineral will be calculated using the reference minerals. Idealized minerals are used unless some trace elements are needed for the calculation. Zircon ($ZrSiO_4$); Apatite ($Ca_5(PO_4)_3$); K-feldspar (Deer et al., 1966, p300 no.10); Biotite (Ibid: p199 no. 7); Na-Ca Plagioclase (Ibid: p325 no. 8, $CaAl_2Si_2O_8$); Illite (Ibid: 1966, p251 no. 3); Chlorite (Ibid: p235 no.8); Calcite ($CaCO_3$); Kaolinite ($Al_4[Si_4O_{10}](OH)_8$); Quartz (SiO_2); Ti Oxides (TiO_2); Fe oxyhydroxide (FeOOH).

Distribution of the oxides to the minerals follows this sequence. After each step the total concentration of each oxide is subtracted by the concentration of the same oxide within the mineral of that step.

1. ZrO_2 = Zircon
2. $PO_{2.5} = 3 \times$ Apatite
3. BaO = 0.0283 × K-feldspar

4. $SrO = 0.013 \times$ Biotite
5. Remaining $RbO_{0.5} = 0.0014 \times$ Na-Ca Plagioclase
6. Remaining $KO_{0.5} = 0.7 \times$ Illite
7. Remaining $MgO = 3.681 \times$ Chlorite
8. Remaining $FeO_{1.5}$ (total) = Fe oxyhydroxide
9. Remaining TiO_2 = Ti oxides
10. Remaining CaO = Calcite
11. Remaining $AlO_{1.5} = 8 \times$ Kaolinite
12. Remaining SiO_2 = Quartz

Finally multiply the sum for each mineral by its molecular weight to obtain the wt% concentration (zircon: 179.22; apatite: 502.3; K-feldspar: 273.77; biotite: 925.51; Na-Ca plagioclase: 317.86; illite: 389.34; chlorite: 1207.2; Fe oxyhydroxide: 88.85; Ti oxide: 79.88; calcite: 100; kaolinite: 516.32; quartz: 60.08).

However, some uncertainties can affect the stability of the procedure. The reference mineral chemical compositions are selected empirically. This could significantly affect the mineral estimation, especially for those minerals calculated through their minor oxides concentrations, which can vary in association with different mineral provenances. Furthermore, it is sometimes unclear which element should be chosen for the estimation of a certain mineral. This is because (1) many common elements are abundant in more than one mineral, so they cannot be selected for the quantification of some specific minerals; (2) sometimes more than one trace element can be used for the mineralogical quantification, which makes the elements selection procedure more complicated. Therefore, other methods have also been attempted.

4.7.2 Matrix Calculation

The method was initially presented by Davis (1973) based on the principle of matrix multiplication. Three datasets, i.e. mineral concentrations against depth, mineral compositions against mineral types and oxides concentrations in each sample against

depth, can be regarded as three matrices [X], [A] and [B]. Their interrelation is as follows:

$$\text{depth}_{\text{Min conc}}[X] \bullet_{\text{min type}} \text{depth}_{\text{oxides conc in minerals}}[A] = \text{depth}_{\text{oxides conc in samples}}[B]$$

$$so [X]=[B]\bullet[A]^{-1} \quad \textbf{(4-1)}$$

Where [A] refers to reference mineral chemical analysis; [B] refers to oxides concentrations in samples, which are calculated from element concentrations against depth; $[A]^{-1}$ refers to the inverse of matrix [A].

Therefore, mineralogical quantification can be undertaken by multiplying matrix [B] with the inverse of matrix [A].

The drawback of matrix calculation is that, same as the normative mineral calculation approach, it is also unclear for the procedure of choosing reference minerals, which could cause possible systemic errors through the mathematical analysis.

4.7.3 Quantification of XRD Results

The Excel-based program RockJock (developed by Eberl, 2006) was used for mineralogical quantification of the XRD data obtained from 14 loess and palaeosol samples (Section 4.4). The results were modified or adjusted by comparison with microscopy observations. In addition, the sensitivity of the RockJock model was also tested using XRF results. This is discussed in details in Chapter 5, Section 5.3.1.

4.7.4 Comparison of the three methods

Since none of the three methods for mineral estimation are perfect, it is necessary to compare them so that the best solution can be found. All five samples measured by XRD were selected for the comparison. Mineral concentrations obtained by

normative mineral calculation (Model 1) and matrix multiplication (Model 2) from these five samples are compared with the equivalent XRD quantified mineralogy, respectively (Figure 4-3).

In order to do this, the variation of mineral abundance needs to be narrowed down, because (1) the uncertainty of chemical compositions in some mineral species (e.g. feldspar, biotite, etc.) can complicate the calculation procedure, because it sometimes can be difficult to decide the mineral groups which a particular mineral is from. For example, illite-smectite could be either in illite group or smectite group; and (2) some of the minor minerals (e.g. rutile, apatite, etc.) are present in very low concentrations and will not significantly affect the overall results of mineral quantification. Therefore, mineral groups in loess have been simplified as follows: quartz, potassic feldspar, calcite, chlorite, mica (mainly including biotite and illite) and plagioclase (including albite).

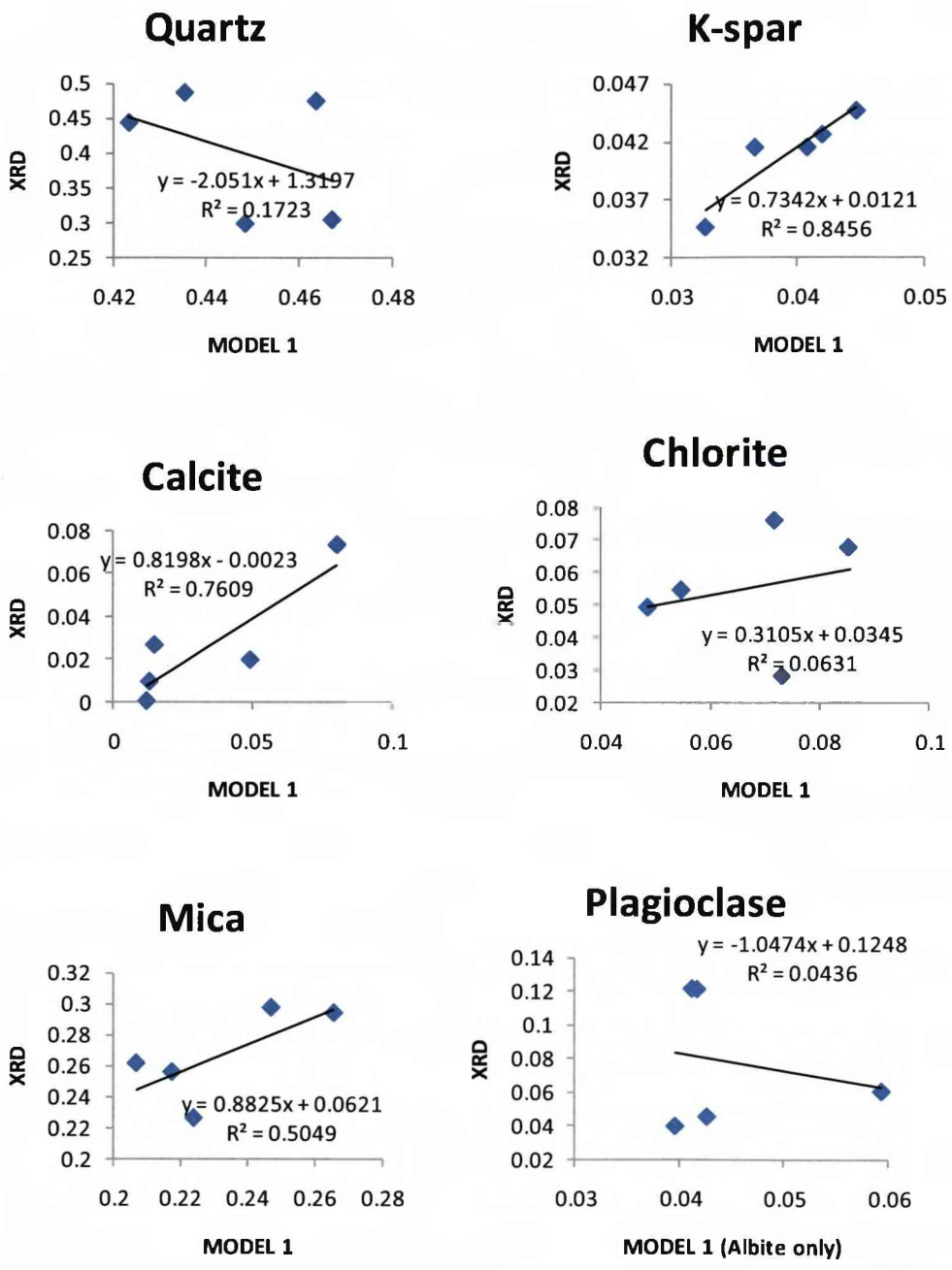

Figure 4-3 Comparison between results for Model 1, Model 2 and XRD quantification on six mineral groups. See text for full explanation.

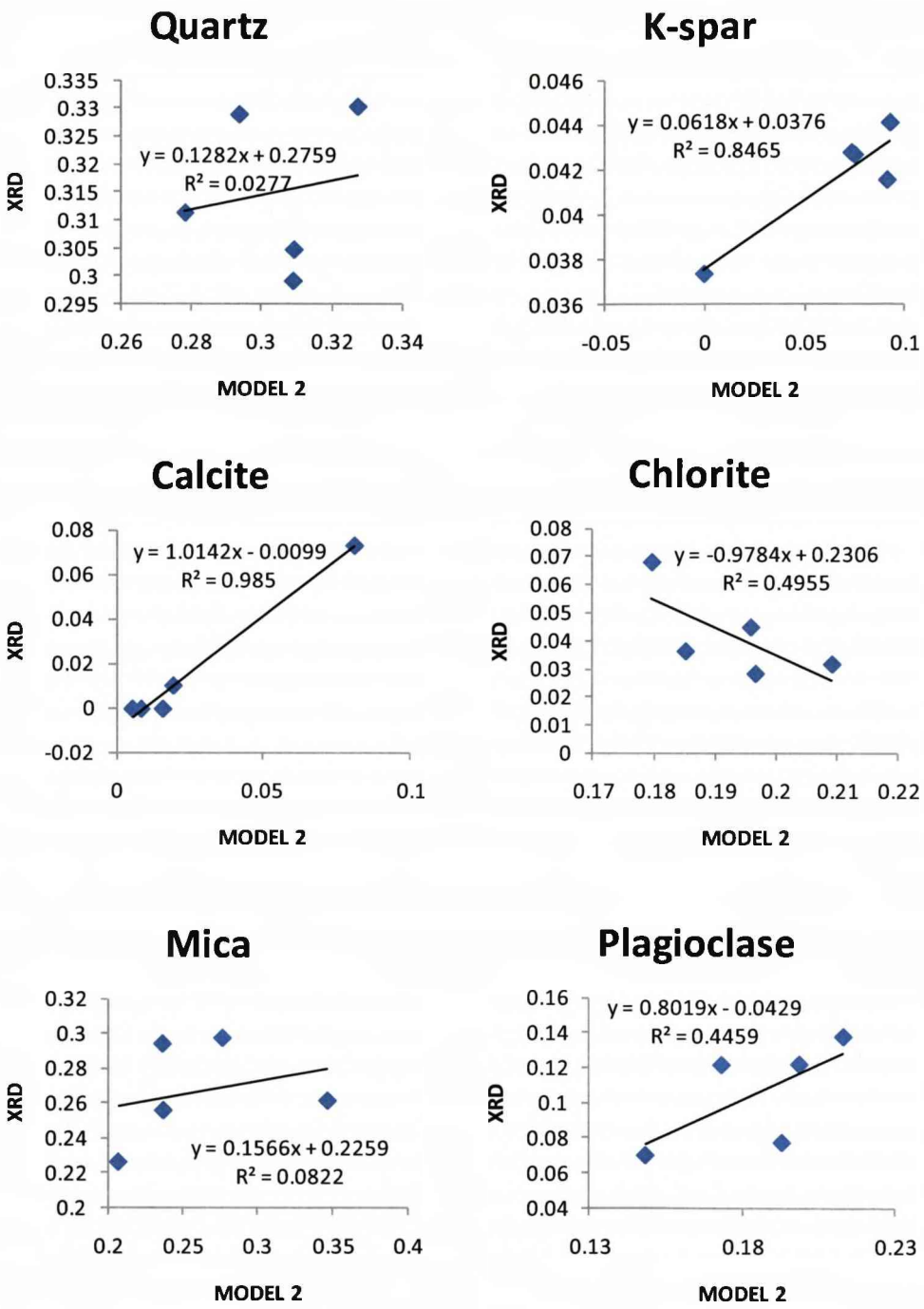

Figure 4-3 Continued

Comparisons have focused on four mineral groups: K-spar, calcite, chlorite and plagioclase, which can be used for runoff estimation. It appears that Model 1 shows the greatest agreement with the XRD quantification results. Thus, results by Model 1 have been modified for runoff estimation using the regression lines.

4.8 The reconstruction of palaeo-precipitation (for the Chinese loess deposits)

4.8.1 Mineral loss

Calculation of mineral loss after weathering

In order to calculate the mineral loss (kg/m^2) during weathering process, it is necessary to obtain data for mineral concentrations (weight %) and soil amount (kg/m^2) before and after weathering. Mineral concentrations after weathering are considered as the mineral concentrations estimated in the previous step (Section 4.7). The soil amount for each weathering interval can be calculated by multiplying the loess/palaeosol density by the depth of the interval. The loess densities used for this calculation (Table 4-3) were obtained from a study of the Lingtai section (Sun et al., 2000). Errors could be found when the data are used for the soil amount at Duanjiapo, Luochuan and Caoxian sections, which are lithologically different from the Lingtai section.

Table 4-3 Average value of dry bulk density (g/cm^3) for different loess-palaeosol layers in the Lingtai section. From: Sun et al. (2000).

Palaeosol (No. of samples)	Density (g/cm^3)	Loess (No. of samples)	Density (g/cm^3)
S0 (9)	2.05	L1 (35)	1.88
S1 (19)	2.07	L2 (29)	1.85
S2 (18)	2.13	L3 (15)	1.88
S3 (10)	2.16	L4 (20)	1.92
S4 (20)	2.18	L5 (14)	1.9
S5 (32)	2.12	L6 (22)	1.89
S6 (6)	2.1	L7 (10)	1.98
S7(14)	2.03	L8 (7)	1.92
S8 (14)	2.09	L9 (38)	1.91

Since mineral concentrations against depth, lithological units and their density are known, it is possible to calculate the mineral loss during weathering. In a certain area

within certain weathered interval, the amount loss of mineral X is calculated as follows:

$$Mineral\ loss = X_p - X_w$$

where X_p refers to mineral amount (kg/m^2) before weathering during this interval and X_w refers to mineral amount (kg/m^2) after weathering during this interval. They can be expressed as follows:

$$X_p = C_{x,p} \times M_p$$

$$X_w = C_{x,w} \times M_w$$

where $C_{x,p}$ – concentration of mineral X before weathering (%);

M_p – soil amount before weathering (kg/m^2);

$C_{x,w}$ – concentration of mineral X after weathering (%); and

M_w – soil amount after weathering (kg/m^2).

$C_{x,w}$ is considered as the mineral concentration calculated by normative mineral estimation. M_w is calculated based on the density records (kg/m^3) of loess and palaeosols obtained by Sun et al. (2000, Table **4-3**):

$$M_w = \rho_w \times d$$

where ρ_w is the density of the soil after weathering, d is the depth (m) of weathered soil during a certain period of weathering. Therefore, mineral amount after weathering can be calculated.

Definition of parent material

Assuming pre-weathering soil is the parent material in the source area and its mineral composition remains the same, theoretically, concentration of mineral X before

weathering ($C_{x,p}$) can be determined if the parent material is defined. However, it is difficult to figure out the mineral composition of parented material. Therefore, soil before weathering is considered as the least weathered loess unit in the loess-palaeosol sequences, where samples have the highest CaO and lowest ZrO_2 or TiO_2 contents, because CaO is regarded as most sensitive to weathering while ZrO_2 and TiO_2 are the least sensitive. This has been described in details in Chapter 4.

The soil amount before weathering is defined in the following principle. Since ZrO_2 and TiO_2 are considered to be the most resistant oxides to weathering (Deer et al., 1966), changes in their amounts (kg/m^2) before and after weathering are normalised to zero. In other words, the amount of ZrO_2 and TiO_2 remains the same during weathering, which can be expressed as:

$$\boldsymbol{C_{Ti,p} \times M_p = C_{Ti,w} \times M_w} \quad (4\text{-}2)$$

or

$$\boldsymbol{C_{Zr,p} \times M_p = C_{Zr,w} \times M_w} \quad (4\text{-}3)$$

where $C_{Ti,\,p}$ and $C_{Zr,\,p}$ are the TiO_2 and ZrO_2 concentrations (weight %) prior to weathering; $C_{Ti,\,w}$ and $C_{Zr,\,w}$ are the concentrations (weight %) of TiO_2 and ZrO_2 concentrations after weathering, respectively; and M_p and M_w are the soil (loess or palaeosol) amount (kg/m^2) before and after weathering, respectively. Therefore, soil amount before weathering (M_p) can be obtained in the following equations:

$$M_p = \frac{C_{Ti,w} \times M_w}{C_{Ti,p}}$$

or

$$M_p = \frac{C_{Zr,w} \times M_w}{C_{Zr,p}}$$

Since there is no available data for $C_{Ti,p}$ or $C_{Zr,p}$ in parent material, loess samples with the highest CaO concentration (since this is considered to be one of the least stable oxides during weathering) and highest TiO_2 or ZrO_2 concentration are selected to represent the parent material prior to the weathering process.

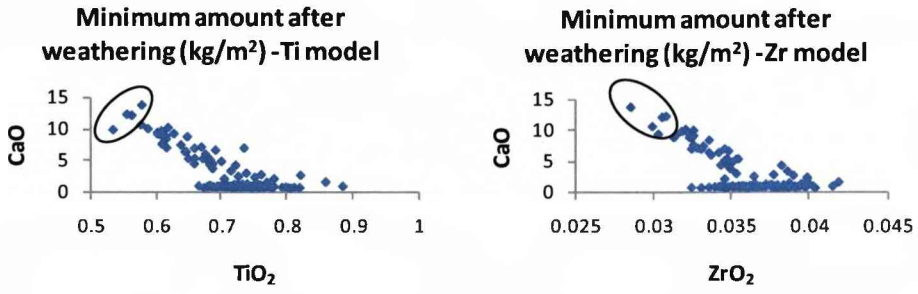

Figure 4-4 Mineral amount (kg/m^2) after weathering at Duanjiapo loess section in this study

Four samples highlighted in Figure 4-4 were selected for the determination of the initial composition of the parental material in each model. The concentrations of the minerals TiO_2 and ZrO_2 in these four samples have been averaged as the mineral compositions and TiO_2 (or ZrO_2) concentrations in the parent soil. Therefore, the pre-weathering mineral amount (kg/m^2) can be estimated by the multiplying the average mineral concentrations (weight %) and pre-weathering soil amount (kg/m^2), which can be estimated from equation (4-2) or (4-3).

Calculation of the alkalinity flux

Since the mineral amounts before and after weathering have been obtained, the amount of mineral loss (kg/m^2) in each sample can be calculated by subtraction. This is an important step for calculating the alkalinity flux (meq/m^2 per yr), i.e. the loss of some alkali cations (e.g. Na^+, Ca^{2+}, Mg^{2+}, K^+) during weathering, which is one of the parameters in the runoff calculation.

In order to compute the alkalinity flux, the following steps are undertaken:

1. Sum the amount of mineral loss in each loess or palaeosol layer, which is believed to represent an individual glacial or interglacial event.
2. Estimate the duration of each event, and calculate the mineral loss per year in each layer, i.e. mineral weathering rate:

$$Mineral\ weathering\ rate = \frac{Total\ mineral\ loss}{Duration}$$

   The duration is estimated by averaging the equivalent results published in different papers (Table 4-4).
3. Convert the amount of mineral loss per year ($kg/m^2/yr$) into equivalent loss of the per year ($meq/m^2/yr$). Firstly, multiply the mineral loss per year ($kg/m^2/yr$) by 1000 to convert the unit into $g/m^2/yr$. Secondly, convert the mass of mineral loss ($g/m^2/yr$) into mineral loss in mole ($mM/m^2/yr$) by dividing the former by the atomic weight of the mineral (chemical formula of each mineral was used). Finally, multiply the mineral loss in mole ($mM/m^2/yr$) by the number of positrons of the alkali cation(s) in each mole of the mineral. Thus, the positron loss ($meq/m^2/yr$) is obtained.
4. The loss of alkali cations is presented by positron loss in milli-equivalent/m^2 per year, i.e. the alkalinity flux.

Table 4-4 Ages of loess/palaeosols shown in differnt studies. Adapted from Vidic et al. (2004).

Strat. Layer	Basal age (ky)	Duration (ky) -1	Strat. Layer	Basal age (ky)	Duration (ky) -2	Strat. Layer	Basal age (ky)	Duration (ky) -3	Strat. Layer	Basal age (ky)	Duration (ky) -4	Average Duration (ky)
L1 L1	38.6		L1			L1			L1			
Sm	72	33.4	Sm	79		Sm	71		Sm	67		
S1	128.9	56.9	S1	129	50	S1	127	56	S1	129	62	56.23
L2	193.9	65	L2	196	67	L2	186	59	L2	193	64	63.75
S2	248	54.1	S2	250	54	S2	242	56	S2	243	50	53.53
L3	288	40	L3	290	40	L3	301	59	L3	279	36	43.75
S3	339	51	S3	342	52	S3	334	33	S3	334	55	47.75
L4	388	49	L4	386	44	L4	364	30	L4	369	35	39.5
S4	419	31	S4	417	31	S4	427	63	S4	418	49	43.5
L5	494	75	L5	503	86	L5	474	47	L5	452	34	60.5
S5	622.8	128.8	S5	625	122	S5	621	147	S5	620	168	141.5

Notes: Duration 1 – Age obtained for the Luochuan section in this study

Duration 2 - Age assignments by Heslop et al. (2000)

Duration 3 - Age assignments for correlative marine isotope stages by Bassinot et al. (1994)

Duration 4 - Age obtained by correlation to the ODP 677 planktonic and benthic foraminifera $\delta 18O$ record were used to determine the age boundaries for the major isotope events.

4.8.2 Runoff Estimation

It is suggested by Suchet and Probst (1993) that there is a positive relationship between alkalinity flux and runoff from soils developed on granite and basalt, which is well described by the power function of Dunne (1978). The alkalinity flux (meq/m^2 per yr) is given by

$$Alkalinity\ flux = F \times R^{\alpha} \tag{4-4}$$

Therefore, runoff can be expressed as

$$R = \left(\frac{Alkali\ nity\ \ flux}{F}\right)^{\frac{1}{\alpha}} \tag{4-5}$$

where F is an empirically derived rock weathering factor, R is the runoff rate (m/yr), and α is an empirically determined exponent.

The power exponent (α) used here is 0.8, which empirically provides a good fit (Boyle, 2008). The value for factor F varies among different rock types (Table 4-5).

Table 4-5 Rock weathering factors, F, for a selection of rock types. Boyle (2008).

Rock Type	Data from Meybeck (1986)	Data from Bluth and Kump (1994)
Carbonate	1800	1000-2000
Shale		500-1000
Basalt	600	300-500
Acid volcanic	300	
Granite		100-300
Sandstone		50-200
Plutonic and metamorphic	90	

The F values used for the runoff calculation at loess sections are shown below:

Mineral Group	Rock Type	Element used for alkalinity flux	Rock weathering factor F
Calcite	Carbonate	Ca	1800
Chlorite	Basalt	Mg	600
K-spar	Granite	K	100
Plagioclase	Basalt	40% Ca + 60% Na	600

Sensitivity Test

The sensitivity of the runoff model has been tested using climate data collected in Xi'an from 1951-2001 (Climate database for Chinese Loess Plateau, Scientific database website, Chinese Science Academy). It is suggested (Turc, 1954, cited in Boyle, 2008) that runoff, R, can be calculated as:

$$R = P - E_{Act} \tag{4-6}$$

$$E_{Act} = P/[0.9 + (P/L)^2]^{0.5} \tag{4-7}$$

where E_{Act} is the annual actual evaporation rate (mm/yr), P is the annual precipitation rate (mm/yr), and L is a factor given by (op. cit.):

$$L = 300 + 25T + 0.05T^3 \tag{4-8}$$

T is temperature in degrees ℃. Since the recent mean annual precipitation (MAP) and mean annual temperature (MAT) are found from the climate database, the runoff can be estimated using the equations shown above. In comparing the results produced by the model with the data from the climate database, the rock weathering factor F has to be adjusted to fit the runoff calculated based on the climate data (Table 4-6). Further discussion is given in Chapter 5.

Table 4-6 Average runoff calculated using different parameters

Parameters	**Average runoff (mm/yr)**	**F (initial value)**	**F (adjusted value)**
Climate database	88.8		
Calcite	150	1800	2740
Chlorite	13	600	125
K-feldspar	21	100	32
Plagioclase	18	600	170

4.8.3 Mean Annual Precipitation

Mean annual precipitation rate (mm/yr) on a temperature gradient is estimated by comparing the runoff rates obtained by Equations (4-6), (4-7), (4-8) and by Equation (4-5) using the solver function in the Excel program. Temperature range is from 0 to 15 degrees ℃, at an interval of 5 ℃. The results of MAP have been compared with those calculated using the climofunction developed by Maher et al. (1994) and magnetic susceptibility records for samples from Luochuan section.

4.9 ALLOGEN model

ALLOGEN is developed on the basis of the weathering rate sub-model of PROFILE, a chemical weathering model initially proposed by Sverdrup and Warfvinge (1992) for lake sediments. In the natural soil environment, the base cation release rate for a single mineral, r, may be approximated by (op. cit.):

$$r = k_{H^+}\frac{[H^+]^{n_H}}{f_H} + \frac{k_{H_2O}}{f_{H_2O}} + k_{CO_2}P_{CO_2}{}^{nCO_2}$$

where

k_{H^+} = rate coefficient for the reaction with H^+ ($m\ s^{-1}$)

k_{H_2O} = rate coefficient for the reaction with H_2O ($kmol_c\ m^{-2}\ S^{-1}$)

k_{CO_2} = rate coefficient for the reaction with CO_2 ($kmol_c\ atm^{-1}\ m^{-2}S^{-1}$)

n_H etc. = reaction order of individual reactions

f_H, f_{H_2O} = rate reduction factors for product inhibition.

This sub-model has been modified and further developed by Boyle (2007) for a wider range of soil types, named ALLOGEN. However, it is not sensitive to hydrological impacts and to dissolved organic carbon production (Boyle, 2008). Therefore, a new model has been created for the long-term impact of climate on average surface water acidity, partly using the principle of ALLOGEN. Major processes in this model include (op. cit.):

- Runoff control over mineral weathering rate
- Dust deposition
- Temperature influence over soil mineral weathering rate
- Evaporative concentration of dissolved ions
- Within-lake alkalinity generation via sulphate reduction
- Variation in dissolved CO_2
- Variation in dissolved organic carbon

In this study, the first process, i.e. runoff and mineral weathering, will be mainly applied to the study areas. Its principles and procedures have been described in section 4.8.

Chapter 5 Mineral weathering-based estimates of palaeo-precipitation on the Chinese Loess plateau

As mentioned in Chapter 2, although previous studies have applied geochemical and mineralogical methods to palaeoclimate reconstruction from loess records, they are not fully quantitative because no comprehensive mineralogical data have been provided. Therefore, in this chapter, detailed mineralogical data will be presented and discussed, together with some quantitative methods for mineralogical analysis on loess-palaeosol sequences.

Results from geochemical and mineralogical analyses are presented, including bulk geochemical data, Scanning Electron Microscope (SEM) images, X-ray diffraction (XRD) spectra and quantified mineral compositions of the loess-palaeosol sequences. Based on the loess mineralogy obtained from the data mentioned above, runoff and precipitation rates in each lithological unit are estimated using an Excel-based program and numeric formula. According to the findings, changes of weathering process and relevant climate regime on the Chinese Loess Plateau have been discussed.

Sensitivity testing has been undertaken for all the models used in this chapter, including quantitative XRD analysis model (RockJock), mineral quantification model (Normative mineral estimation) and the mineral dissolution model. In addition, method developed here has been compared with the rainfall-susceptibility climofunction developed by Maher et al. (1994), which is based on the magnetic susceptibility records and the modern rainfall rates.

5.1 Dating of the Chinese loess

The age models used for the Duanjiapo and Luochuan loess samples are described in Bloemendal and Liu (2005). Ages of loess samples were obtained by linking the magnetic susceptibility records to the insolation record for 65°N and the marine oxygen isotope record from ODP Site 677 (op. cit.). The derived accumulation rates for the two sites are shown below (Figure 5-1). Because loess-palaeosol sequences during the last 500 ky BP are the focus in this study, accumulation rates 6.12 cm/ky and 5.45 cm/ky are applied to Luochuan and Duanjiapo sections, respectively. This age model is used for the following discussion.

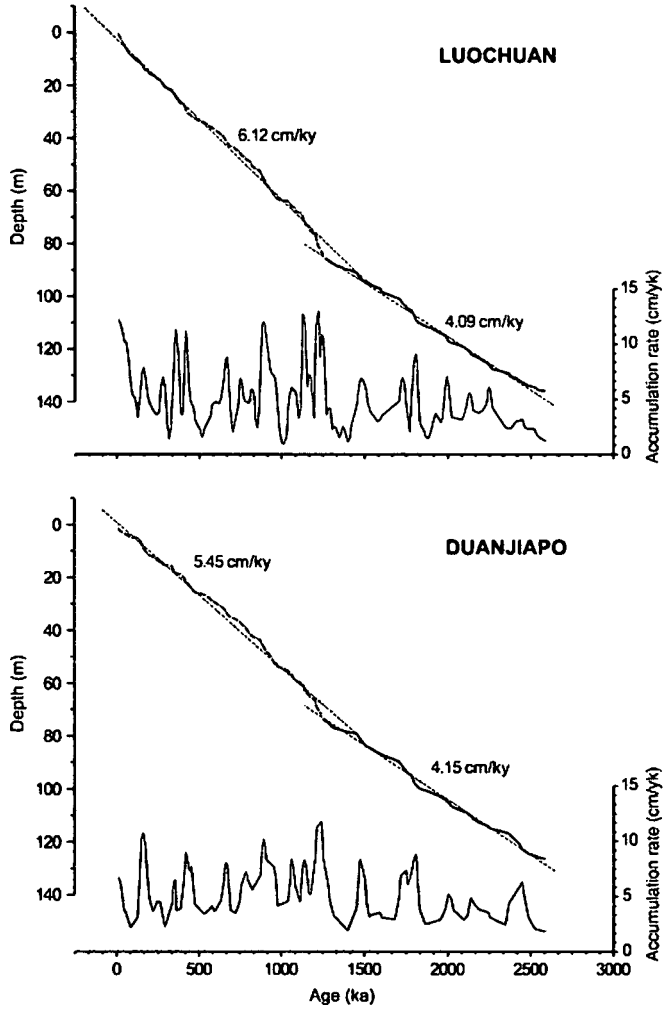

Figure 5-1 Age-depth relationship and accumulation rates for Duanjiapo and Luochuan loess section. From Bloemendal & Liu (2005).

5.2 Bulk geochemical analysis

5.2.1 Geochemical records of the loess-palaeosol sequences

The commonly used geochemical indicators of weathering and pedogenesis in Chinese loess, Rb/Sr ratio and the Ca concentration, for the three sections are shown in Figure 5-2, together with the magnetic susceptibility (MS) stratigraphy. The Rb/Sr ratio shows a high degree of similarity with the MS records at all three sites, although an absence of correlation is evident in some intervals (e.g. 10-11m depth at Luochuan, 39.5-41.5m depth at Caoxian) possibly due to the noise of the Rb/Sr ratios and its smaller amplitude of fluctuation. The overall correlation is in agreement with the results of several workers (e.g. Chen et al., 1999), who showed that the Rb/Sr ratio can be used as an indicator of weathering and pedogenesis, as is the case for MS.

Comparison of the Ca concentrations with the MS records shows that peaks in MS correspond to minima in Ca concentration, although very low values can also be found in both parameters at the same depth, e.g. 16-18 m at Duanjiapo. Calcium has been almost depleted in some intervals at Duanjiapo, i.e. 4.5-7.5m, 12-14m, 16-25m and 26-33m. At the other two sites, Ca variation is clearly inversely-correlated to MS and Rb/Sr ratio, especially the latter. This probably implies that most Ca is in primary calcite, which is indicative of chemical weathering intensity and could also affect Sr mobility to weathering. Assuming that MS reflects variations in weathering intensity, it may not be straightforward for Ca content in loess-palaeosol sequences, especially in loess, to be directly used as a proxy for chemical weathering in some loess sections. For example, since most intervals are Ca-free at Duanjiapo, it is not appropriate to use Ca as an indicator for chemical weathering. In addition, at loess sections with intensely weathered layers, Ca can be depleted and then re-deposited as secondary calcite (Chen et al. 1997). Therefore, a reasonable volume of Ca content may occur in the form of needle-shaped or granular secondary calcite grains, meaning that it would be problematic to use Ca as chemical weathering indicator in

these layers. However, Ca can be used for interpreting mineral chemical weathering at those sites with lower weathering intensity, such as Luochuan and Caoxian, where most of the Ca is in calcite of detrital origin.

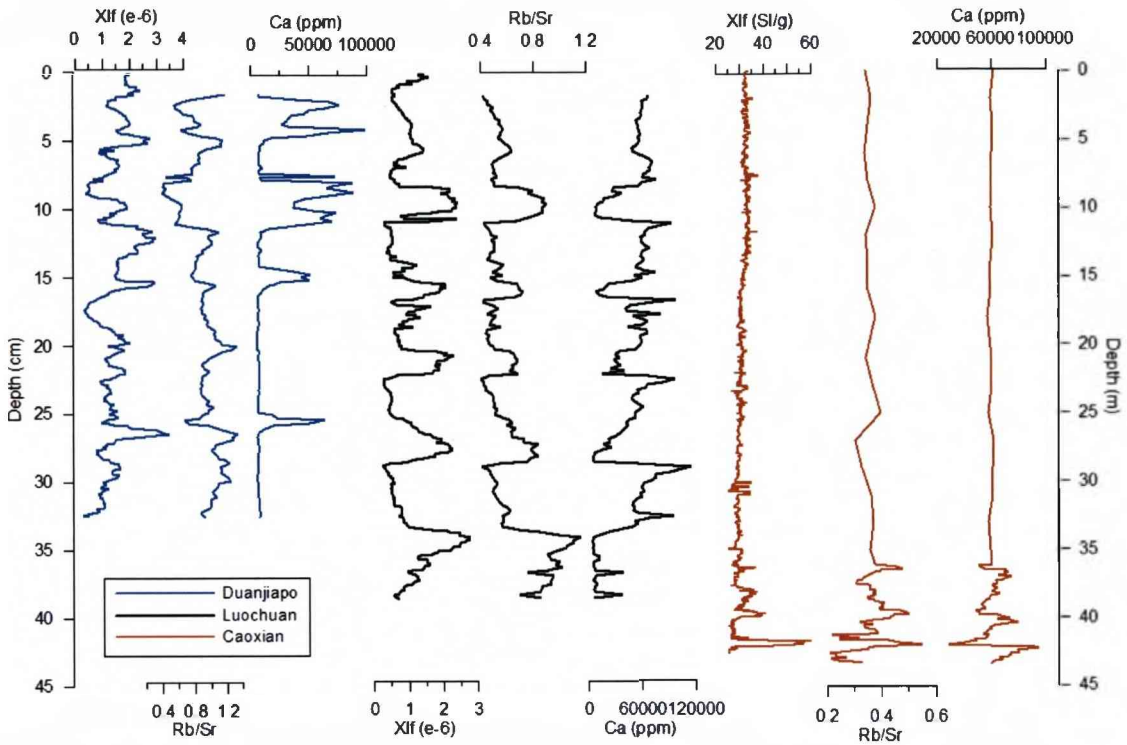

Figure 5-2 Comparison of magnetic susceptibility and independent geochemical indicators for Duanjiapo, Luochuan and Caoxian. Low frequency susceptibility data adapted from Bloemendal et al., (2008) and Parker and Bloemendal (2005). Blue line: Duanjiapo; Black line: Luochuan; Red line: Caoxian.

5.2.2 Detailed element quantification in selected samples

Recent studies (Yang et al., 2006; Jeong et al., 2008) showed that bulk chemical properties of loess could be significantly affected by changes in particle size caused by fluctuations in the strength of the winds transporting the detrital grains. In order to estimate the elemental mobility during the chemical weathering of rocks and sediments, some elements from weathering-resistant minerals, such as Si in quartz and Zr in zircon, are needed as a reference to minimize the effect of variations in detrital grain size. This is based on the assumption that these weathering-resistant weathering minerals can be only affected by physical weathering, e.g. during wind

transportation, and their concentrations are positively correlated to the average grain size of the relevant loess or palaeosols. Although quartz is relatively stable during chemical weathering, aluminosilicates, as another source of Si, are not. Therefore, since Zr in loess/palaeosol sequences is mainly associated with the eolian mineral zircon, which is resistant to chemical weathering, Zr was selected as a reference element instead of Si in Figure 5-3.

Figure 5-3 shows the scatter plots of element/Zr ratios compared with MS values. Most major elements are included. However, some elements such as Na and Ba cannot be measured accurately enough and thus showed very noisy results. Therefore, these elements have not been presented here.

None of the ratios shown in Figure 5-3 are significantly correlated with magnetic susceptibility, except for Ca/Zr and Mg/Zr which show a negative correlation with MS. In addition, at Duanjiapo and Luochuan, Sr/Zr also has a strong negative correlation (Figure 5-3 (1) and (2)), and similarly, both Ca/Zr and Sr/Zr appear to have two different types of correlation with MS. In their scatter plots, some sample clusters have strong negative correlation between Ca/Zr or Sr/Zr and MS, while other sample clusters have no or very weak correlation. Since Sr is mainly present in Ca-rich minerals and is also sensitive to chemical weathering, it is suggested that in unweathered or less weathered layers Ca/Zr and Sr/Zr are negatively related to MS; while in palaeosols and heavily weathered loess units, there is no clear relationship between them.

Aluminium is slightly positively related to MS while S/Zr shows a much weaker relationship with MS (scatter around the regression line) at all the three sites. The other element/Zr ratios can be divided into the following groups according to their type of correlation with magnetic susceptibility (MS):

1) No clear relationship with MS can be found for Fe and Mn from Duanjiapo and Caoxian, but there is a positive relationship at Luochuan. This may imply

that iron minerals, which are normally associated with Mn, are not affected by chemical weathering when the climate is generally very wet-warm (i.e. at Duanjipao) or dry-cold (i.e. at Caoxian), but they can increase during moderate weathering (i.e. at Luochuan). However, this is still unclear. Therefore, it is necessary to convert quantitative chemical data (element concentrations) into quantitative loess mineralogy, since mineralogy is directly related to the weathering, but elements are not;

2) Negative, positive, and positive but non-linear relationships for Si and K with MS are observed at the Duanjiapo, Luochuan and Caoxian sites, respectively. A possible explanation is that different intensities of weathering processes in Si- and K-rich minerals (e.g. K-feldspar) occur at these three sites. At Duanjiapo with intense weathering conditions, these minerals have been weathered. At Luochuan with moderate weathering conditions, these minerals have been weakly weathered while other minerals have been more strongly weathered, resulting in the increasing proportion of Si and K. At Caoxian, where least weathering occurred, these Si- and K- rich minerals together with other highly mobile minerals are largely unaffected by the weathering process, resulting in fairly uniform concentrations. However, another reason for this could be that most of the Si and K are dominated by different mineral groups at different sites.

3) Concentrations of Ti and P are positively and inversely related to MS variations at Duanjiapo and Luochuan, respectively. It is suggested that Ti is weathering-resistant yet P is not. In addition, they have no clear relationship with MS at Caoxian, possibly because the weak weathering process in this area did not have a large influence on the concentrations of most elements, including Ti and P.

4) It is evident that the relationship between Rb and MS is positive non-linear at Duanjiapo and positive at Luochuan and Caoxian. This is possibly due to the high stability of Rb to weathering, although it seems to be slightly weathered at Duanjiapo.

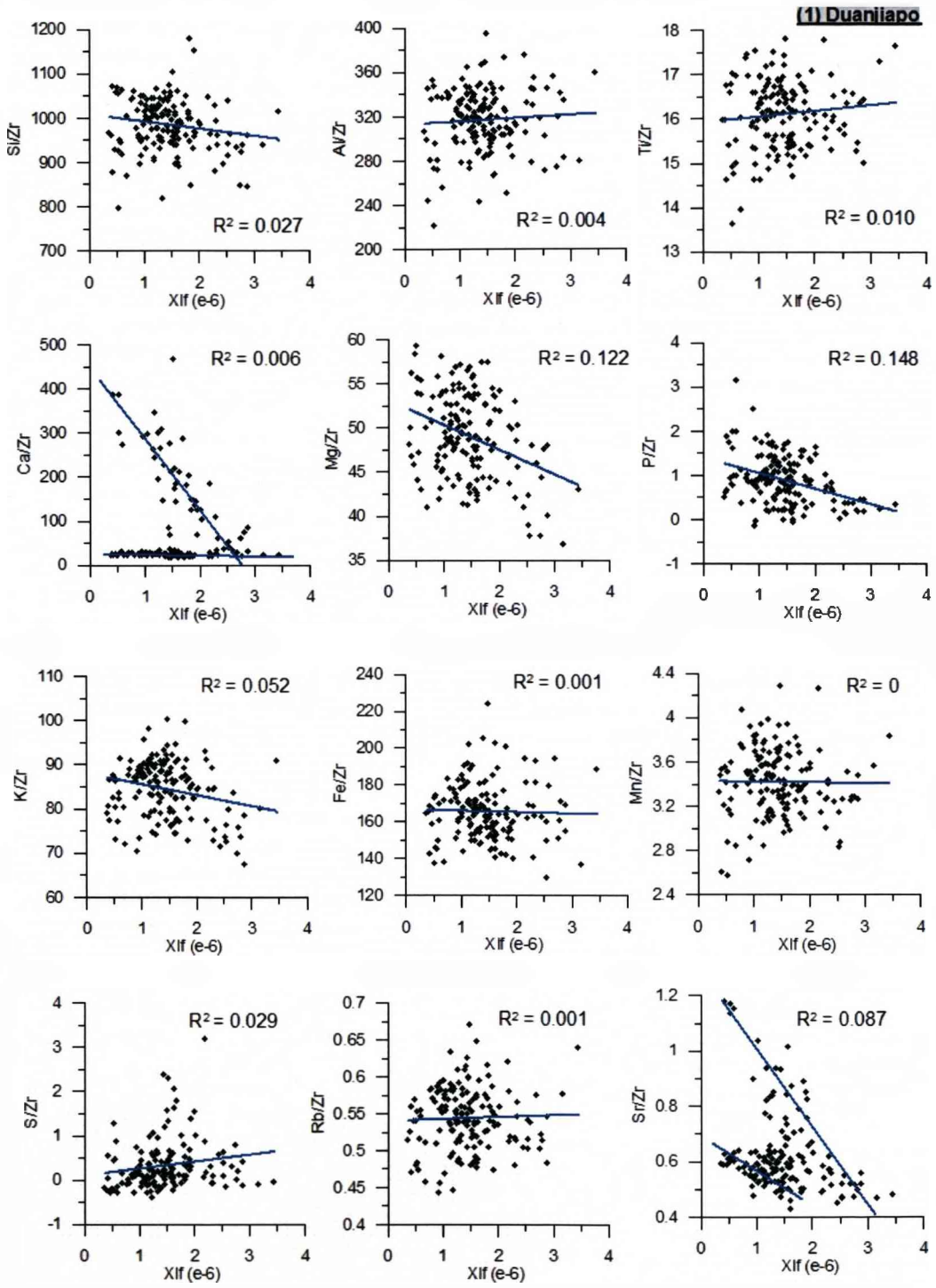

Figure 5-3 Element/Zr ratios compared with low-frequency susceptibility for the Duanjiapo, Luochuan and Caoxian loess sections.

(1) Duanjiapo; (2) Luochuan; (3) Caoxian

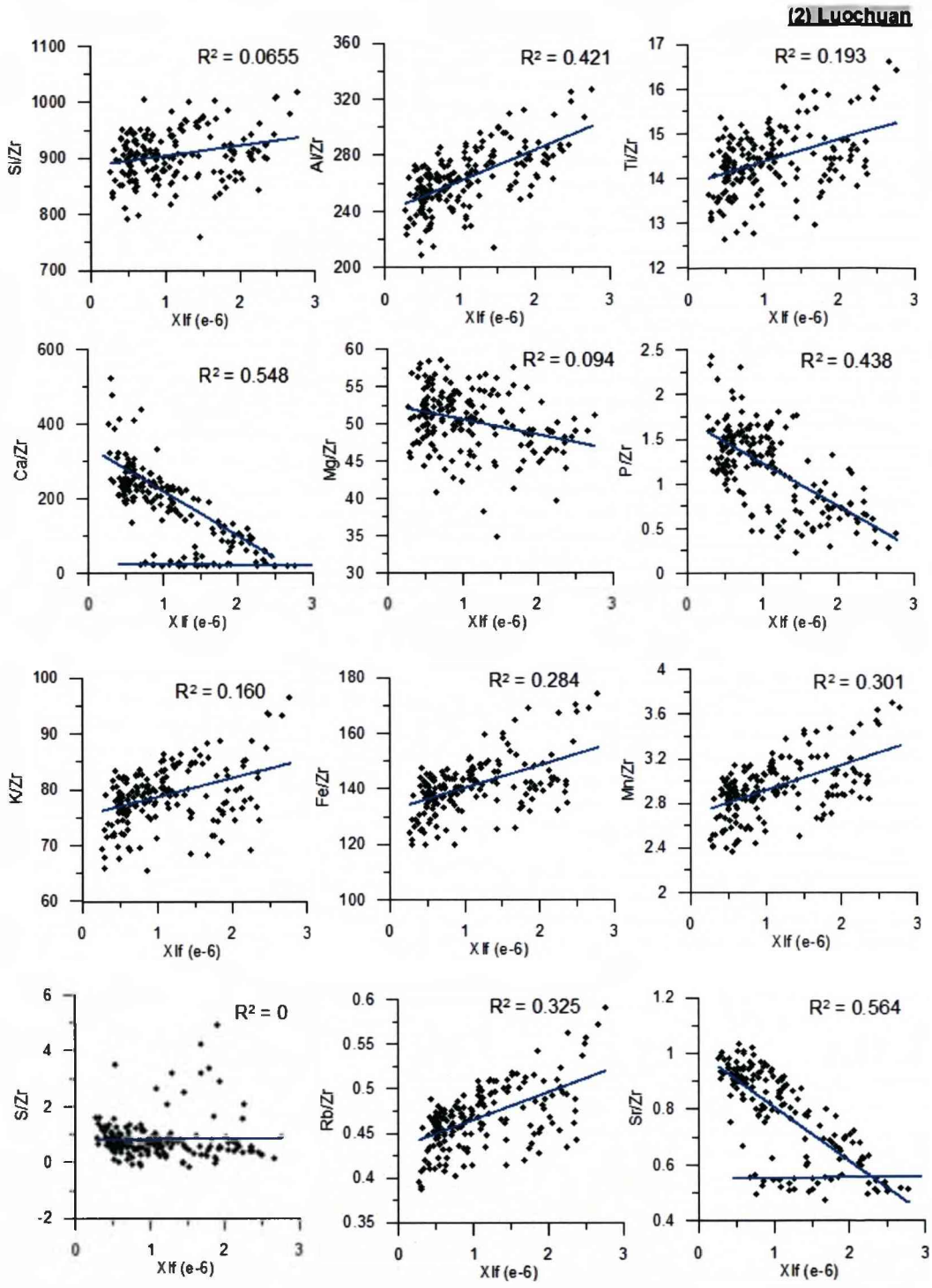

Figure 5-3 Continued. (1) Duanjiapo; (2) Luochuan; (3) Caoxian

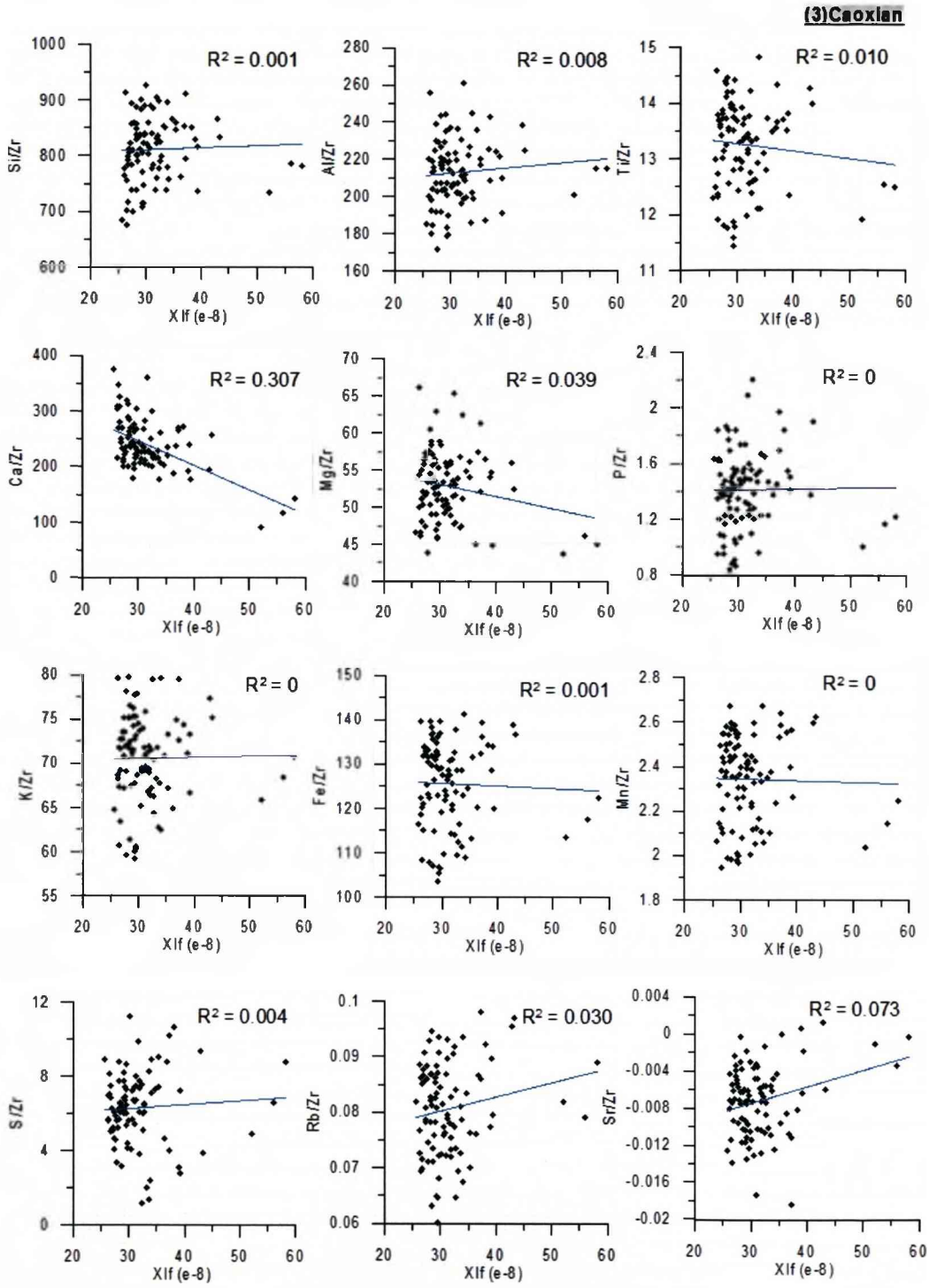

Figure 5-3 Continued. (1) Duanjiapo; (2) Luochuan; (3) Caoxian

5.3 Mineral identification

5.3.1 XRD spectra

Comparing the XRD spectra pattern of unknown samples with pure minerals (standards), the XRD qualitative analysis of the loess-palaeosol sequences at the three sites shows that both loess and palaeosol samples contain albite, calcite, K-feldspar, quartz, calcite, chlorite, illite, kaolinite and amphibole, apart from some non-calcareous or minimally-calcareous layers found e.g. L2, S4, L5 from Duanjiapo (Figure 5-4). However, there are some uncertainties in mineral identification:

- Minerals present in low concentrations (e.g. iron oxides) or which are not sensitive to XRD (e.g. clays) are very likely to be underestimated during bulk XRD analysis.
- Mineral groups such as mica, plagioclase and K-feldspars can complicate the mineral type determination, as they have many subtypes or metamorphs with similar or partially-overlapping XRD spectra (Elton and Smith, 1999).

Therefore, SEM analysis was also used for qualitative mineralogical identification.

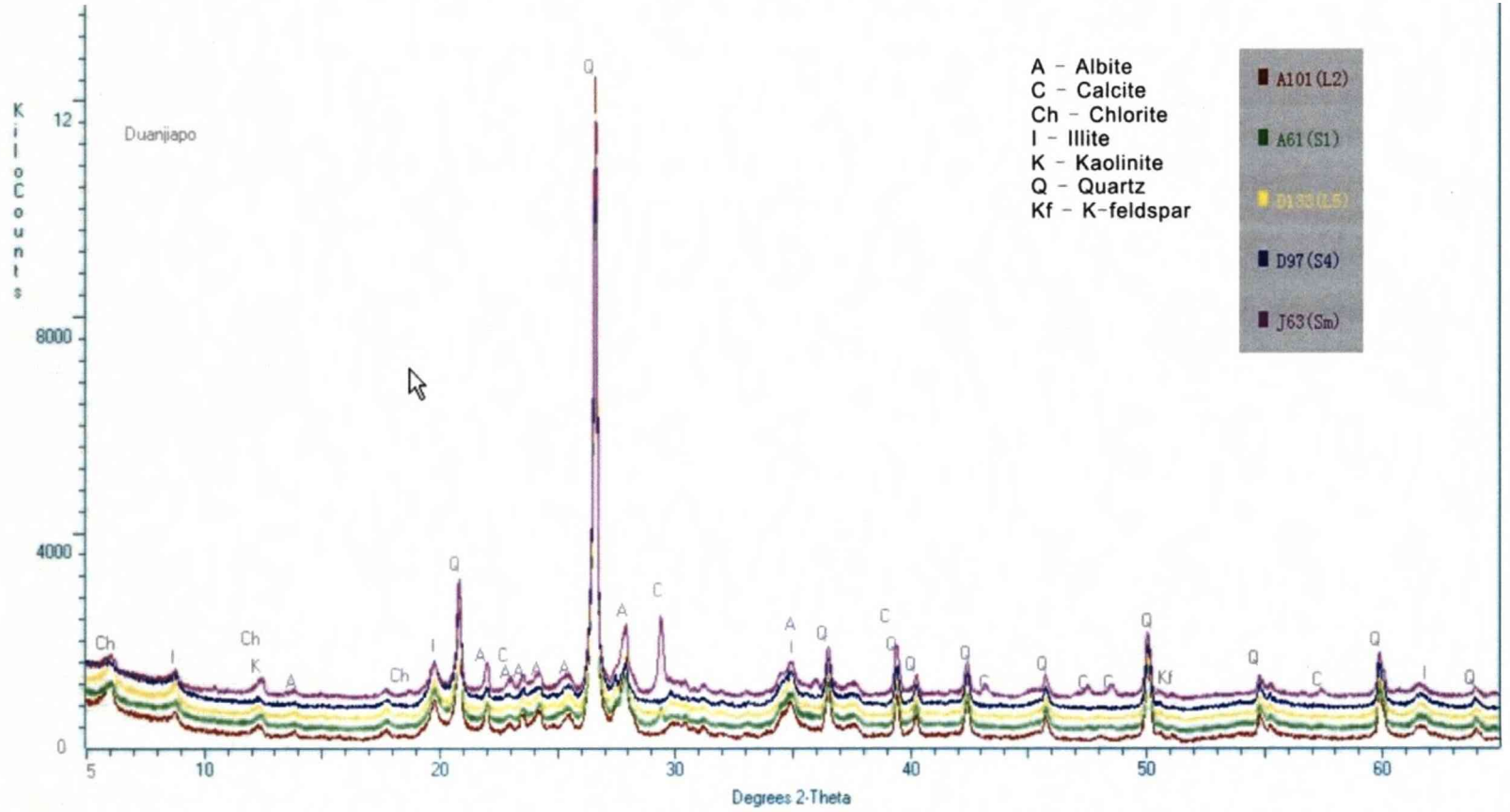

Figure 5-4 XRD spectra of samples from Duanjiapo loess section. Because the spectra of the samples from all the three sections are very similar, only spectra of Duanjiapo samples are shown here.

5.3.2 Microscopic observations - SEM images of loess-palaeosol particles

Four samples, one from L5 layer at Luochuan and three from Sm, S1S2 and S1S3 layers at Caoxian have been observed under the scanning electronic microscope (SEM) after thin sectioning, and chemical analysis data of these samples were collected by energy dispersive X-ray (EDX) detector. Figure 5-5 to Figure 5-8 show the back-scattered electron images of selected mineral particles and rock fragments from different samples. According to the SEM results obtained, the following mineral types were identified: albite, apatite, barite, calcite, chlorite, dolomite, epidote, iron oxides, hornblende (amphibole), illite, ilmenite, K-feldspar, muscovite, Na-Ca plagioclase, quartz, sphene (titanite), and zircon. The size of the grains in the loess samples is generally bigger than in the palaeosol samples (ca. 2-40 μm for loess and ca. 5-60 μm for palaeosols).

Quartz is the most common mineral in both loess and palaeosols. It mainly occurs as discrete particles although some intergrowth with feldspars or clay minerals (e.g. chlorite and illite) can also be observed (Figure 5-5-1 and Figure 5-6-1). Feldspars are divided into three groups based on EDX analysis: K-feldspar, albite and Na-Ca plagioclase (NCP). Feldspars normally occur as single grains, but intergrowth of albite and K-feldspar is still commonly observed in some samples (Figure 5-6-6). In addition, NCP appears to be present in single grains rather than in rock fragments (Figure 5-6-6 and Figure 5-7-1).

Biotite is more commonly found in single particles rather than rock fragments, with a bright needle-like appearance under back-scattered electron images (Figure 5-5-2). In the recent study of Jeong et al. (2008), common inclusions of barite and celestine are found along the basal planes of biotite grains, with lensoid voids and fan-out at the flake edges. In the present study, barite was also found within a palaeosol sample from the Caoxian section (Figure 5-7-1), but it appears to consist of fillings amongst quartz and feldspar grains with a length of nearly 200 μm. Chlorite occurs either in a mixture with quartz (Figure 5-6-2) or as a single grain (Figure 5-6-3).

According to current observation under SEM, the very fine-grained phyllosilicates mainly contain illitic clays and muscovite. No kaolinite or talc has been observed so

far, in contrast to the XRD analysis results. The illitic clays probably contain illite, interstratified illite-smectite and smectite as shown in XRD quantification, but it is unlikely that they can be distinguished one from another under EDX chemical analysis. Both large aggregates of illitic clays (Figure 5-6-5) and mixtures of quartz-illitic clays (Figure 5-8-1) were observed in palaeosol and loess samples, respectively, at different loess sections.

Carbonates exist as fine-grained calcite particles (Figure 5-6-4, Figure 5-8-1), fine-grained dolomite particles (Figure 5-6-2) or coarse grains with a mixture of calcite and dolomite (Figure 5-6-7).

Iron and titanium oxides were also found in most samples observed. They have a wide range of formations: single-grained iron oxides (Figure 5-8-1), single-grained ilmenite (Figure 5-6-4, Figure 5-7-2 and Figure 5-7-3), intergrowth of iron oxides and clays (Figure 5-6-1, Figure 5-6-6, and Figure 5-6-7), intergrowth of rectangular iron oxides-sphene-quartz-K-feldspar within the rock fragment (Figure 5-5-3) and mixture of quartz and very fine single-grained titanium oxides. In addition, the SEM observation also showed the occurrence of single zircon particles (Figure 5-7-2) and large aggregates of apatite and quartz (Figure 5-8-2).

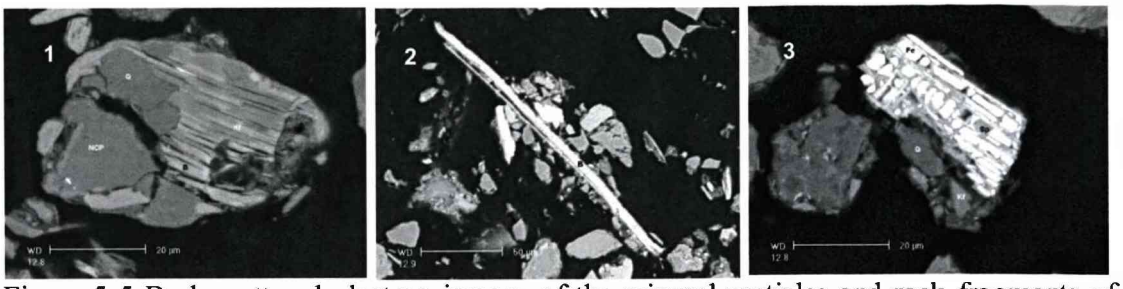

Figure 5-5 Back-scattered electron images of the mineral particles and rock fragments of sample CX2448 within the Sm layer from Caoxian. The length of the largest particle in Figure 5-5-2 is ~150μm. A: Albite; Ap: Apatite; Ba: Barite; Ca: Calcite; Ch: Chlorite; Do: Dolomite; Ep: Epidote; Fe: Fe Oxide; Ho: Hornblende; Il: Illitic clays; Ilm: ilmenite Kf: K-feldspar; M: Muscovite; NCP: Na-Ca Plagioclase; Q: Quartz; Sp: Sphene (Titanite); Zr: Zircon.

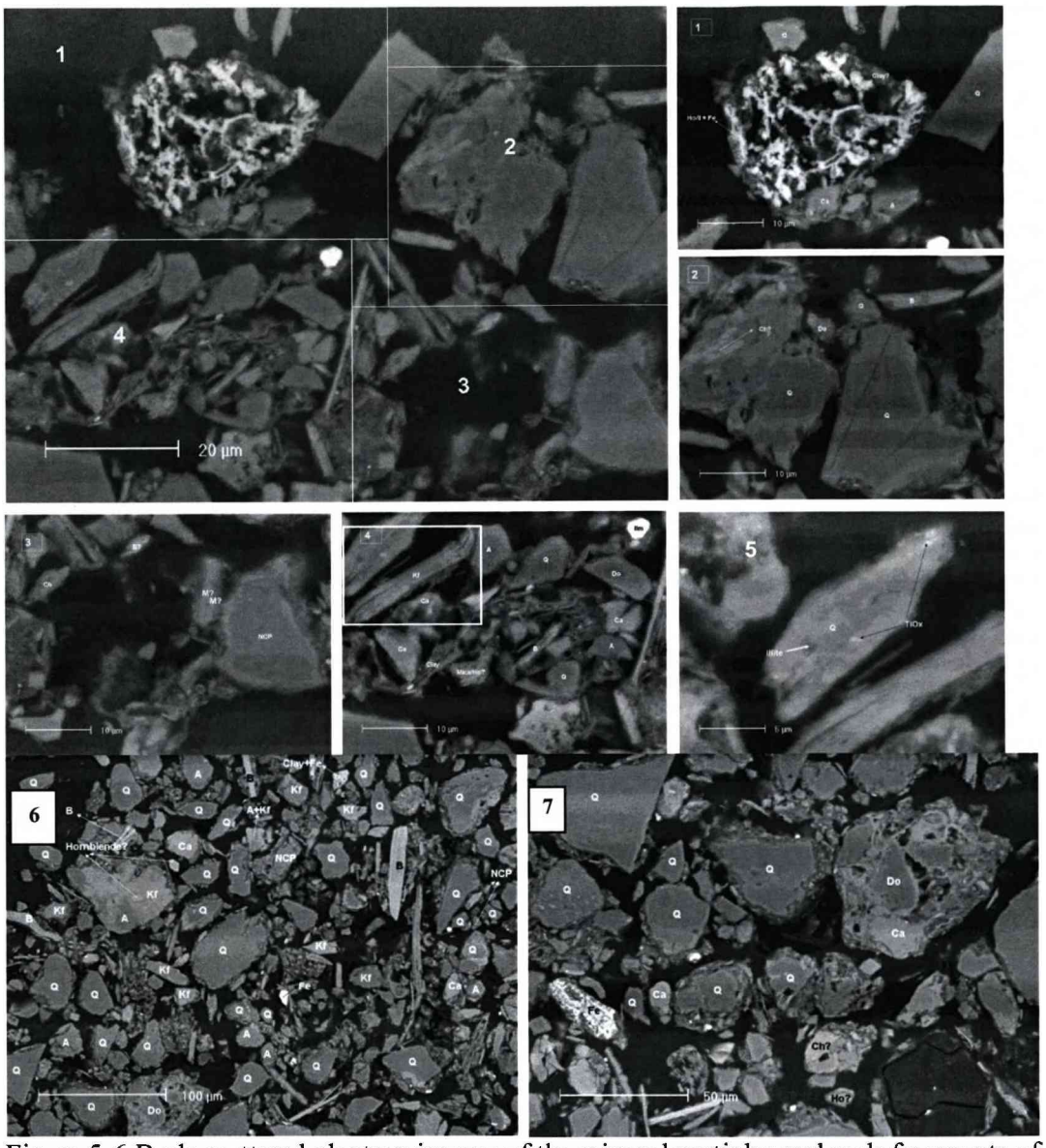

Figure 5-6 Back-scattered electron images of the mineral particles and rock fragments of sample CX3892 within the S1S2 layer from Caoxian. A: Albite; Ap: Apatite; Ba: Barite; Ca: Calcite; Ch: Chlorite; Do: Dolomite; Ep: Epidote; Fe: Fe Oxide; Ho: Hornblende; Il: Illitic clays; Ilm: ilmenite Kf: K-feldspar; M: Muscovite; NCP: Na-Ca Plagioclase; Q: Quartz; Sp: Sphene (Titanite); Zr: Zircon.

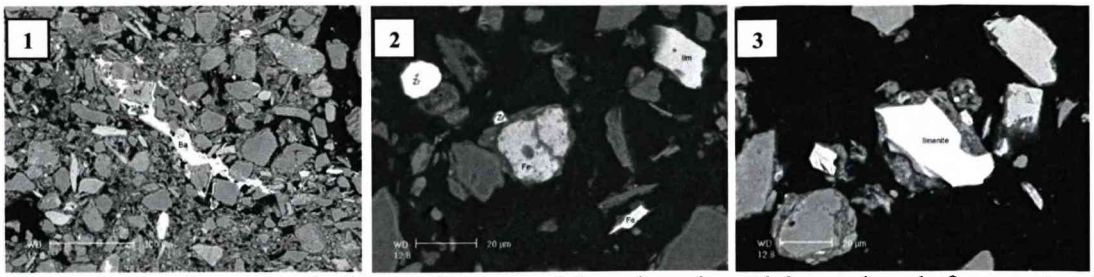

Figure 5-7 Back-scattered electron images of the mineral particles and rock fragments of sample CX4192 within the S1S3 layer from Caoxian. A: Albite; Ap: Apatite; Ba: Barite; Ca: Calcite; Ch: Chlorite; Do: Dolomite; Ep: Epidote; Fe: Fe Oxide; Ho: Hornblende; Il: Illitic clays; Ilm: ilmenite Kf: K-feldspar; M: Muscovite; NCP: Na-Ca Plagioclase; Q: Quartz; Sp: Sphene (Titanite); Zr: Zircon

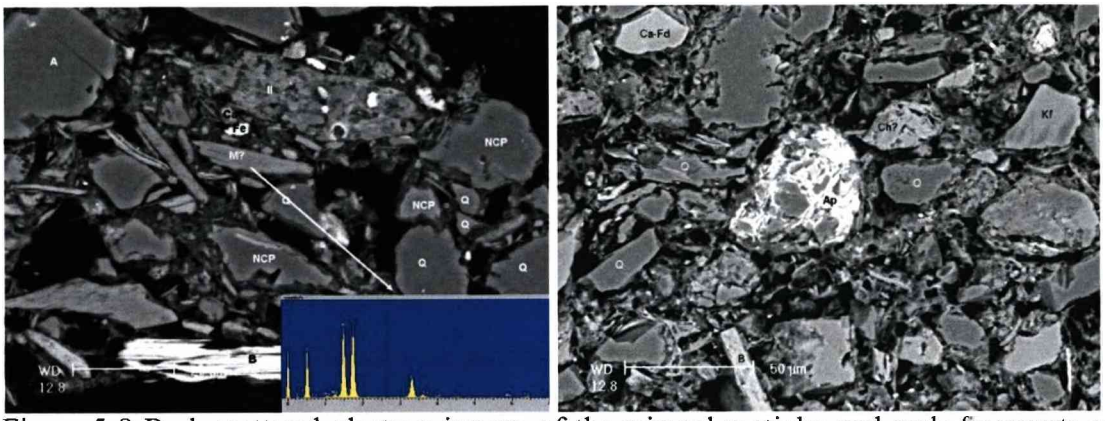

Figure 5-8 Back-scattered electron images of the mineral particles and rock fragments of sample B299 within the L5 layer from Luochuan. A: Albite; Ap: Apatite; Ba: Barite; Ca: Calcite; Ch: Chlorite; Do: Dolomite; Ep: Epidote; Fe: Fe Oxide; Ho: Hornblende; Il: Illitic clays; Ilm: ilmenite Kf: K-feldspar; M: Muscovite; NCP: Na-Ca Plagioclase; Q: Quartz; Sp: Sphene (Titanite); Zr: Zircon

5.4 Mineral quantification

5.4.1 Quantification of XRD results

Mineral compositions of both loess and palaeosol samples were calculated by the RockJock program (Version 5) and the results are shown in Table 5-1. The results of quantitative estimation show that both loess and palaeosols mainly comprise quartz, phyllosilicates, feldspars, carbonates and other minor minerals.

Table 5-1 Mineral compositions of loess and palaeosol samples in weight percentage (%) from the three sections

Sites	Sample No.	Unit	Q	Feldspars			Carbonates				Phyllosilicates						FeOx	Others
				Alkali fd	Pl	Total	Ca	Do	An	Total	Ka	Sm	Talc	Chl	Mica	Total		
Duanjiapo	J63	Sm	29.9	18.9	4.1	22.9	7.3	0.0	0.0	7.3	2.3	3.6	1.8	6.8	22.6	37.0	0.9	1.9
	A61	S1	32.9	14.4	1.9	16.3	1.0	0.0	0.0	1.0	4.2	10.4	1.6	4.5	26.1	46.8	1.4	1.6
	A101	L2	33.0	18.0	4.2	22.2	0.0	0.0	0.1	0.1	3.7	7.4	1.1	3.6	25.6	41.4	1.3	2.1
	D97	S4	31.1	11.3	2.3	13.6	0.0	0.0	0.0	0.0	4.6	13.9	1.5	3.1	29.4	52.5	1.3	1.5
	D133	L5	30.5	13.9	4.9	18.7	0.0	0.0	0.2	0.2	4.3	9.2	1.3	2.8	29.7	47.3	1.3	2.0
		Average	**31.5**	**15.3**	**3.5**	**18.8**	**1.7**	**0.0**	**0.1**	**1.7**	**3.8**	**8.9**	**1.5**	**4.2**	**26.7**	**45.0**	**1.2**	**1.8**
Luochuan	A113	Sm	30.4	17.1	5.4	22.4	10.1	0.1	0.3	10.5	1.6	2.9	1.0	6.5	22.2	34.2	0.9	1.5
	A175	S1	32.9	16.9	4.9	21.7	5.5	0.0	0.2	5.7	2.0	3.5	0.9	6.9	24.1	37.4	1.2	1.0
	A237	L2	30.1	16.0	4.9	21.0	14.9	0.2	0.4	15.4	1.8	3.5	0.9	5.4	19.4	30.9	0.9	1.6
	B249	S4	32.9	15.6	5.4	21.0	4.0	0.0	0.0	4.0	3.1	5.3	1.2	6.5	23.7	39.9	1.0	1.3
	B299	L5	29.4	14.1	5.4	19.6	16.3	0.2	0.2	16.7	1.7	3.3	1.1	6.1	20.5	32.6	0.7	1.0
		Average	**31.2**	**15.9**	**5.2**	**21.1**	**10.2**	**0.1**	**0.2**	**10.5**	**2.1**	**3.7**	**1.0**	**6.3**	**22.0**	**35.0**	**0.9**	**1.3**
Caoxian	2448	Sm	30.8	16.6	6.4	22.9	10.7	0.7	0.8	12.3	1.2	1.6	0.9	6.9	20.6	31.2	0.9	1.8
	3674	S1S1	27.9	17.8	4.9	22.7	16.6	0.9	1.4	18.9	1.3	0.2	1.0	8.2	18.2	28.9	0.5	1.2
	3892	S1S2	30.0	17.6	5.1	22.7	14.1	0.9	1.5	16.5	1.5	0.4	1.0	7.3	18.1	28.4	0.6	1.9
	4288	L2	30.5	18.2	4.6	22.9	13.3	1.2	1.3	15.8	0.9	1.4	1.0	6.6	18.1	28.0	0.7	2.1
		Average	**29.8**	**17.5**	**5.2**	**22.8**	**13.7**	**1.0**	**1.2**	**15.9**	**1.2**	**0.9**	**1.0**	**7.3**	**18.8**	**29.1**	**0.7**	**1.7**

Q, quartz; Alkali fd, alkali feldspar; Pl, plagioclase; Ca, calcite; Do, dolomite; An, ankerite; Ka, kaolinite; Sm, smectite; Chl, chlorite; Mica: illite, biotite and muscovite; FeOx: iron oxides, including hematite, goethite and maghemite; Others: amphibole, apatite, barite, epidote, garnet, gypsum, ilmenite and titanite. Average value for each mineral at each loess section is given in bold numbers.

With respect to the latitudinal/climatic gradient across the Loess Plateau, from Duanjiapo (southeast) through Luochuan (central) to Caoxian (northwest), the concentration of quartz remains similar (~30%) though with a slight decrease towards northwest. The phyllosilicates group decreases significantly along with the climate gradient, from 45% to 29% from southeast to northwest. In contrast to the phyllosilicates, feldspars and carbonates are increasingly abundant, from 18.8% and 1.7% at Duanjiapo to 22.8% and 15.9% at Caoxian, respectively. Phyllosilicates are dominated by mica, which has an average concentration of 18.8-26.7% within loess minerals Table 5-1. Iron oxides show very low abundances in all loess sections, although a slight decrease can be found northwestwards. There is evidence of maghaemite, hematite and goethite in the XRD patterns of the loess and palaeosol samples, but not for magnetite possibly because of its poor sensitivity to X-ray diffraction (Elton and Smith, 1999).

To compare the changes in mineral compositions between different stratigraphical units and different loess sections, quartz was used as a reference material because of its resistance to weathering in temperate environments (Jeong et al., 2008). Major loess mineral groups to quartz ratios were calculated based on the quantification of mineral compositions (Table 5-1) and plotted against loess stratigraphy for all three loess sections (Figure 5-9). The abundance of iron oxides remains at a low level and does not change much between the different units and sections. The results show that within the three sections, feldspars and carbonates are enhanced in loess units and within the sub-loess units within palaeosols; and that carbonate minerals are nearly absent within S1, L2, S4 and L5 from the Duanjiapo section. Phyllosilicates are relatively enhanced in the palaeosols from the three sections. In addition, the magnitudes of the variations in feldspars and phyllosilicates versus depth are relatively similar within the same section, which implies that there could be a quasi-linear relationship between these two mineral species.

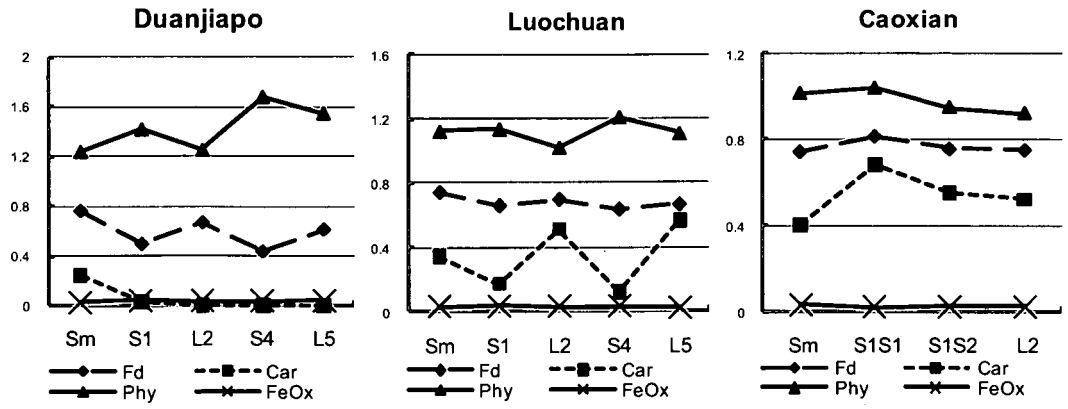

Figure 5-9 Mineral to Quartz Ratios vs. Stratigraphical Units
Fd, Feldspars/Quartz; Car, Carbonates/Quartz; Phy, Phyllosilicates/Quartz; FeOx, Iron Oxides/Quartz.

Sensitivity test for RockJock using XRF results

Although RockJock is an efficient tool for quantitative estimation of mineral concentrations within loess and palaeosols, its reliability still needs to be tested. Under the model, all 14 calculated XRD spectra have broader peaks than the measured ones, probably because the grain size of the sample is finer than expected by the model RockJock (Figure 5-10). In addition, samples are regarded as unknown when their XRD data are quantified, which must be run with unconstrained choice of mineral types. However, this could complicate the selection of some minor minerals when their concentrations are less than 1%. Thus, all these factors could affect the accuracy of estimating mineral species and calculating mineral concentrations. It is necessary to examine the reliability of the model by comparing the XRD quantitative estimation of loess minerals with the XRF data of element concentrations within the same sample.

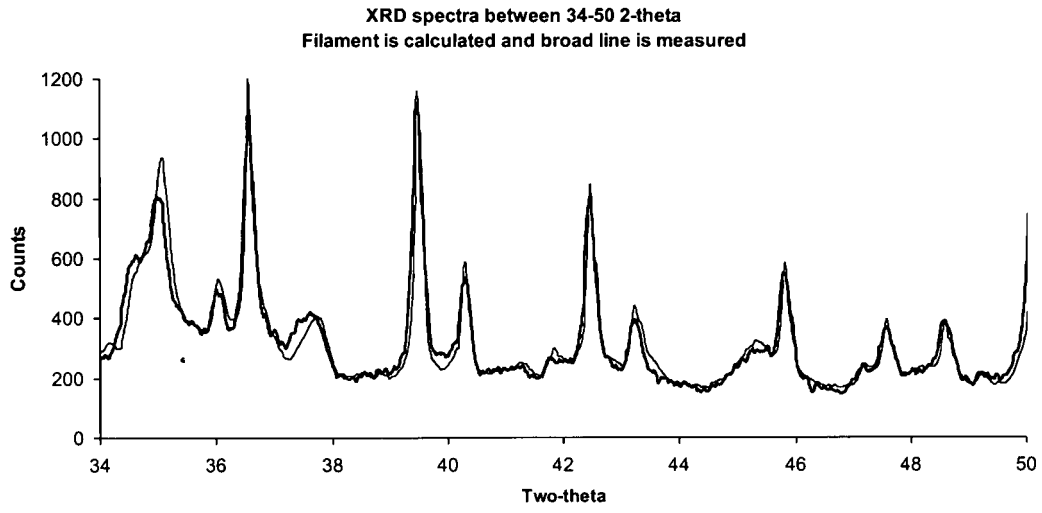

Figure 5-10 Calculated and measured XRD spectra.

The element concentrations of minerals estimated by RockJock are calculated according to the chemical compositions of selected reference minerals. Then the values of element concentrations are divided by those results measured by XRF spectrometer, as shown in Figure 5-11. Among the ten major elements examined in the model sensitivity test, there are six with values close to 1, which means the model and the selection of mineral groups are relatively reliable. Ratios of Na, Ti, Mn and Ba have large deviations, ranging from 0.6 to 0.8. This is possibly because the minor minerals mainly containing these elements have not been selected in the RockJock Model, since the more mineral types selected, the less accurate is the outcome from the model (Eberl, 2003). For Ti, Mn and Ba, this is possibly due to the low concentrations of Ti-, Mn- or Ba- rich minerals with consequent poor measurement by XRD. In addition, another possibility for the high Na content in XRF quantification is that Na could have been over-measured by the XRF spectrometer.

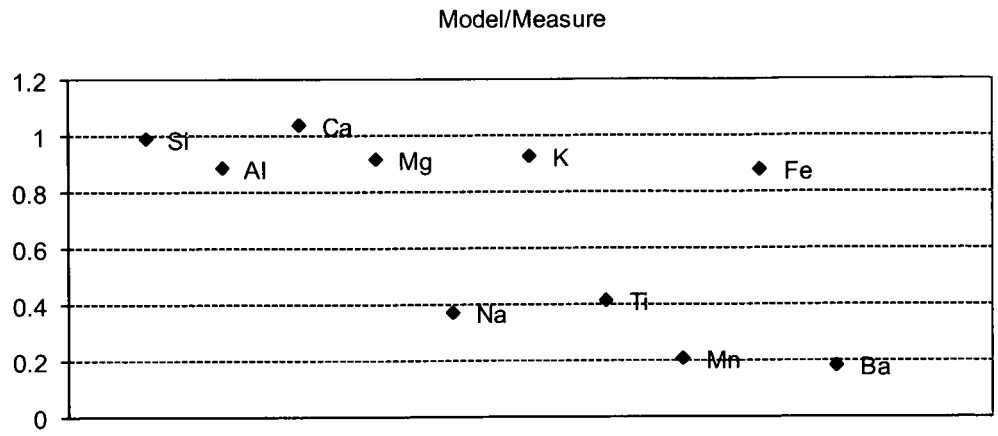

Figure 5-11 Results of sensitivity test for RockJock. Model/Measurement Ratio: element concentrations calculated by XRD quantification are divided by those measured by XRF. Values over and under 1.0 indicate over and under-prediction by RockJock, respectively. The model will be more reliable if the ratio is closer to 1.

5.4.2 Normative mineral estimation

Although quantitative XRD analysis seems applicable to loess and palaeosol samples, it is time-consuming and costly to undertake XRD measurements for all the samples. Therefore, a numerical model is needed for quantifying mineral compositions and ideally on the basis of the available bulk geochemical data. Thus, normative mineral estimation is proposed here as a major method for mineral quantification, but XRD analysis is still needed for mineral identification and sensitivity test of the normative mineral estimation method.

Two different methods have been used in order to get a more accurate and reliable result for the normative mineral estimation. The difference between these two calculation procedures is the order of minerals and the element used for mineral calculation (Table 5-2). Model 1 uses Rb to estimate the concentration of biotite, whereas Model 2 uses Sr for biotite estimation and subsequently the concentration of plagioclase has been calculated prior to that of illite, compared with Model 1.

Table 5-2 Comparison of two models for normative mineral calculation

Model 1			Model 2		
Mineral type	**Oxide used**	**Element concentration (moles/mole)**	**Mineral type**	**Oxide used**	**Element concentration (moles/mole)**
Zircon	ZrO2	1	Zircon	ZrO2	1
Apatite	PO2.5	3	Apatite	PO2.5	3
K-feldspar	BaO	0.0283	K-feldspar	BaO	0.0283
Biotite	RbO0.5	0.0247	Biotite	SrO	0.0213
Illite	KO0.5	0.7	Plagioclase	RbO0.5	0.0014
Chlorite	MgO	3.681	Illite	KO0.5	0.7
Plagioclase	NaO0.5	1	Chlorite	MgO	3.681
FeOOH	FeO1.5T	1	FeOOH	FeO1.5T	1
TiO2	TiO2	1	TiO2	TiO2	1
Calcite	CaO	1	Calcite	CaO	1
Kaolinite	AlO1.5	8	Kaolinite	AlO1.5	8
Quartz	SiO2	1	Quartz	SiO2	1

XRD quantification data have been compared with their equivalent obtained by normative mineral estimation for all of the samples from the three sections (Figure 5-12). Negative correlation in K-feldspar and mica between the model and XRD data can be found in both Model 1 and Model 2 at the Duanjiapo and Caoxian sections. For the Luochuan section, all the mineral concentrations are positively correlated between Model 1 and the XRD quantification model, while quartz and plagioclase in Model 2 are found to be inversely correlated to the results from XRD quantification. In addition, the concentrations of plagioclase based on the Model 2 calculation are all negative for the three loess sections. Therefore, Model 1 appears to be better than Model 2 and thus has been selected for the runoff estimations in the next step (Section 5.5.1).

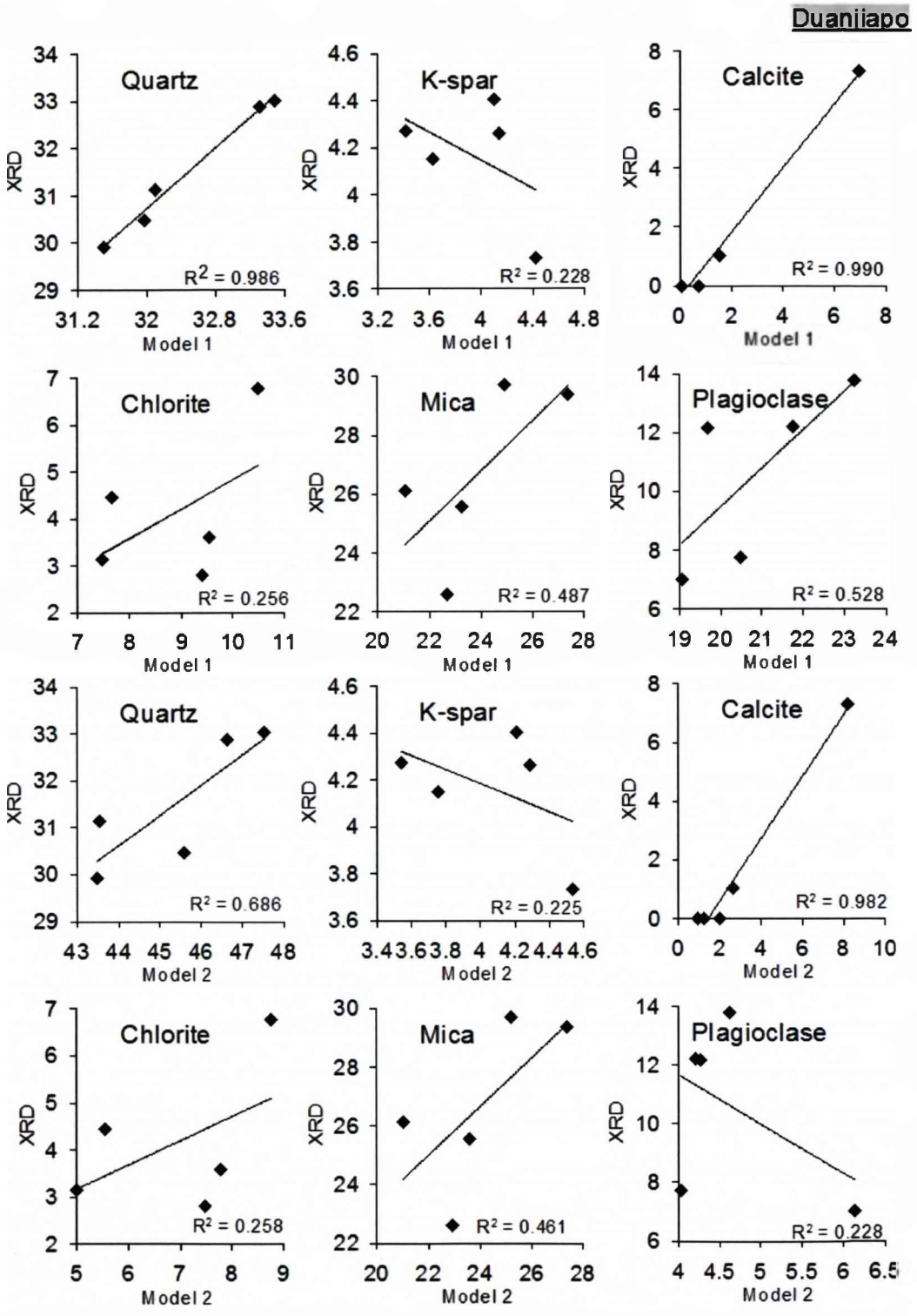

Figure 5-12 Comparison of mineral concentrations calculated by quantitative XRD analysis (RockJock) and the two normative mineral estimation methods, i.e. Model 1 and Model 2, at three loess sections.

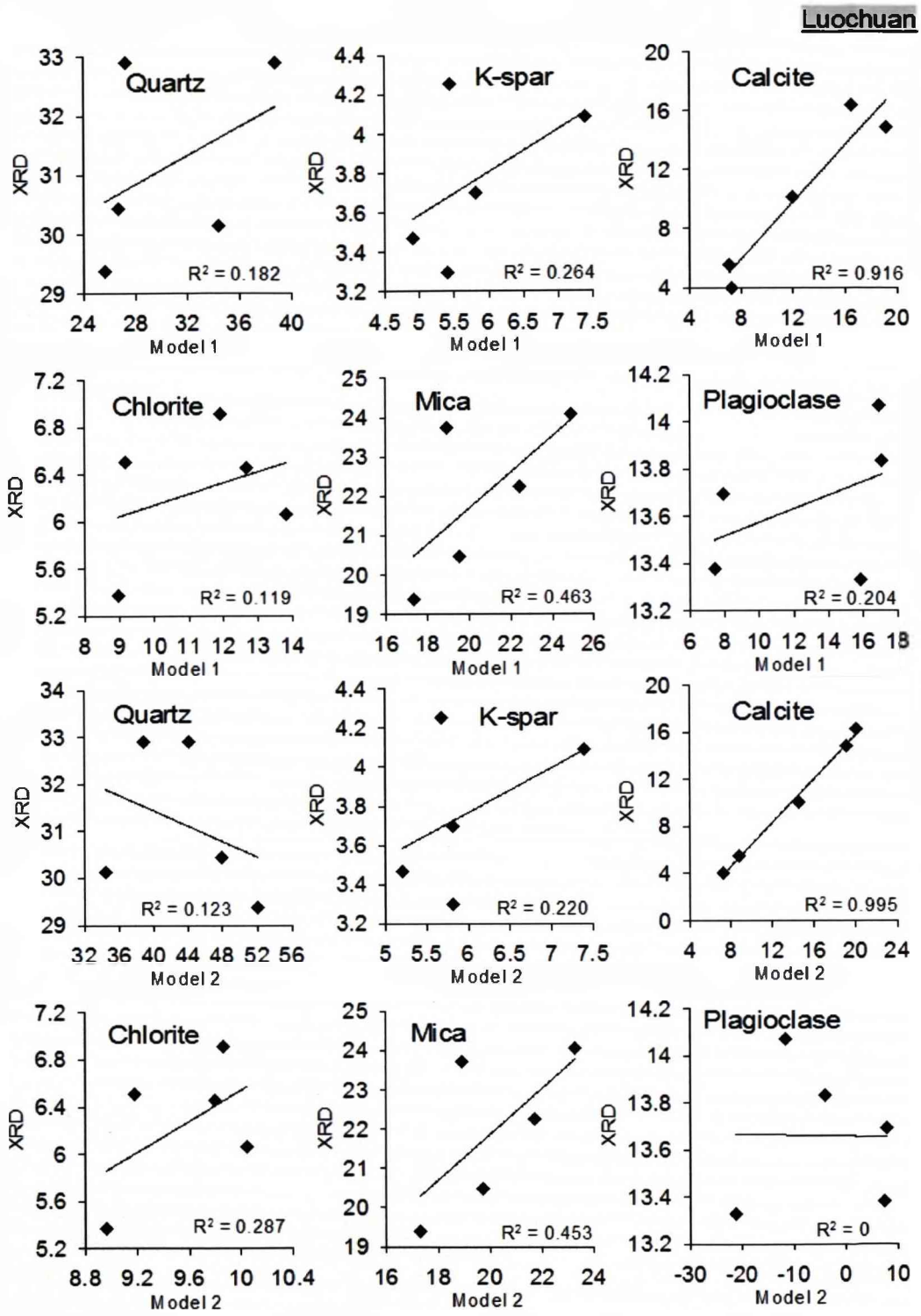

Figure 5-12 Continued.

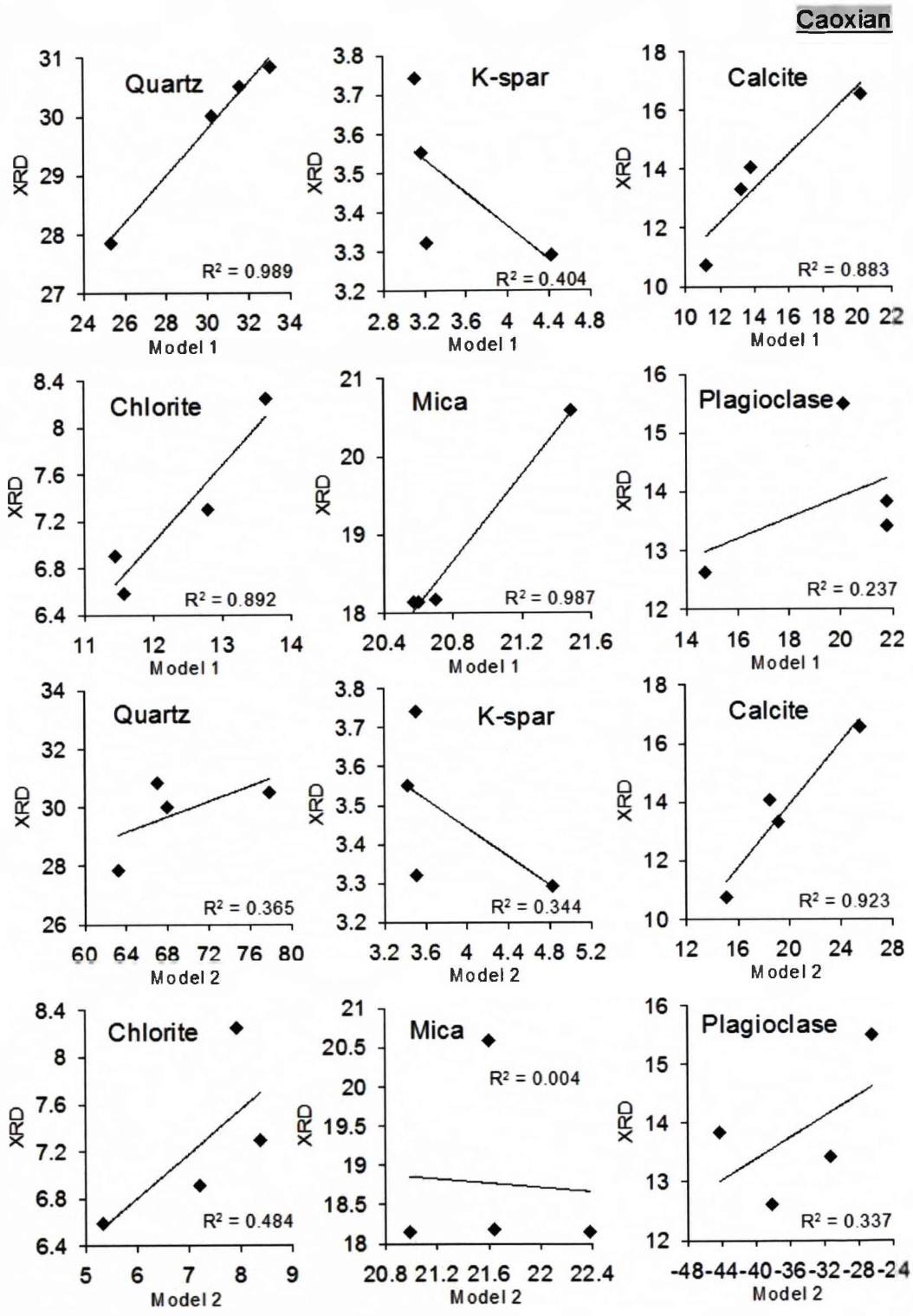

Figure 5-12 Continued.

Sensitivity test for Excel-based mineral estimation

As stated in Chapter 4, Methodologies, in the normative mineral quantification method, the calculation of mineral concentrations depends on the chemical analysis of reference minerals (Appendix I). However, there are many possibilities for the chemical compositions in mineral groups such as feldspar, chlorite, illite, etc. Therefore, the principle for the reference mineral selection is based on the greatest similarity in modern climate conditions of the place where the reference minerals are from to the loess section. Moreover, no example with extreme concentration of certain elements has been selected in order to get a reasonable result. Two different orders in distributing the oxides to the loess minerals have been used, as shown below:

Method 1

1. ZrO_2 = Zircon
2. $PO_{2.5}$ = 3 × Apatite
3. BaO = 0.0283 × K-feldspar
4. SrO = 0.013 × Biotite
5. Remaining $RbO_{0.5}$ = 0.0014 × Na-Ca Plagioclase
6. Remaining $KO_{0.5}$ = 0.7 × Illite
7. Remaining MgO = 3.681 × Chlorite
8. Remaining $FeO_{1.5}$ (total) = Fe oxyhydroxide
9. Remaining TiO_2 = Ti oxides
10. Remaining CaO = Calcite
11. Remaining $AlO_{1.5}$ = 8 × Kaolinite
12. Remaining SiO_2 = Quartz

Method 2

1. ZrO_2 = Zircon
2. $PO_{2.5}$ = 3 × Apatite
3. BaO = 0.0283 × K-feldspar

4. $RbO0.5 = 0.0247 \times$ Biotite
5. Remaining $KO0.5 = 0.7 \times$ Illite
6. Remaining $MgO = 3.681 \times$ Chlorite
7. Remaining NaO0.5 = Na-Ca Plagioclase
8. Remaining FeO1.5 (total) = Fe oxyhydroxide
9. Remaining $TiO2$ = Ti oxides
10. Remaining CaO = Calcite
11. Remaining $AlO1.5 = 8 \times$ Kaolinite
12. Remaining $SiO2$ = Quartz

The sensitivities of these two calculation methods were individually tested by comparing their estimated mineral concentrations with the equivalents using XRD quantification. According to the regression values in the scatter plot of each mineral, Method 1 is more reliable. Because of the high applicability of XRD quantification model in loess-palaeosol sequences according to the sensitivity test of the quantitative XRD analysis method (Section 5.3.2.1), the mineral concentrations estimated by Method 1 have been adjusted using the regression relationship between Method 1 and XRD quantification.

In addition, Model 1 has been applied to a loess-palaeosol sequence at Jiuzhoutai, northwest Loess Plateau (Jeong et al., 2008). Trace elements such as Zr, Ba, Rb and Sr, which are not shown in Jeong et al.'s paper, have been supplemented by the geochemical data from corresponding Caoxian loess samples, because of the high similarity in the magnetic susceptibility records in Jiuzhoutai and Caoxian (Figure 5-13). Model 1 has been used to calculate the mineral concentrations, being compared with the mineralogy obtained by XRD. Figure 5-14 shows that apart from K-feldspar and plagioclase, results derived by normative mineral estimation are well related to the XRD quantified mineralogy, especially calcite. This means that normative mineral estimation can be applied to loess-palaeosol sequences if certain modification is provided by other independent experimental geochemical methods, but it is not sensitive enough for the quantitative prediction of feldspar.

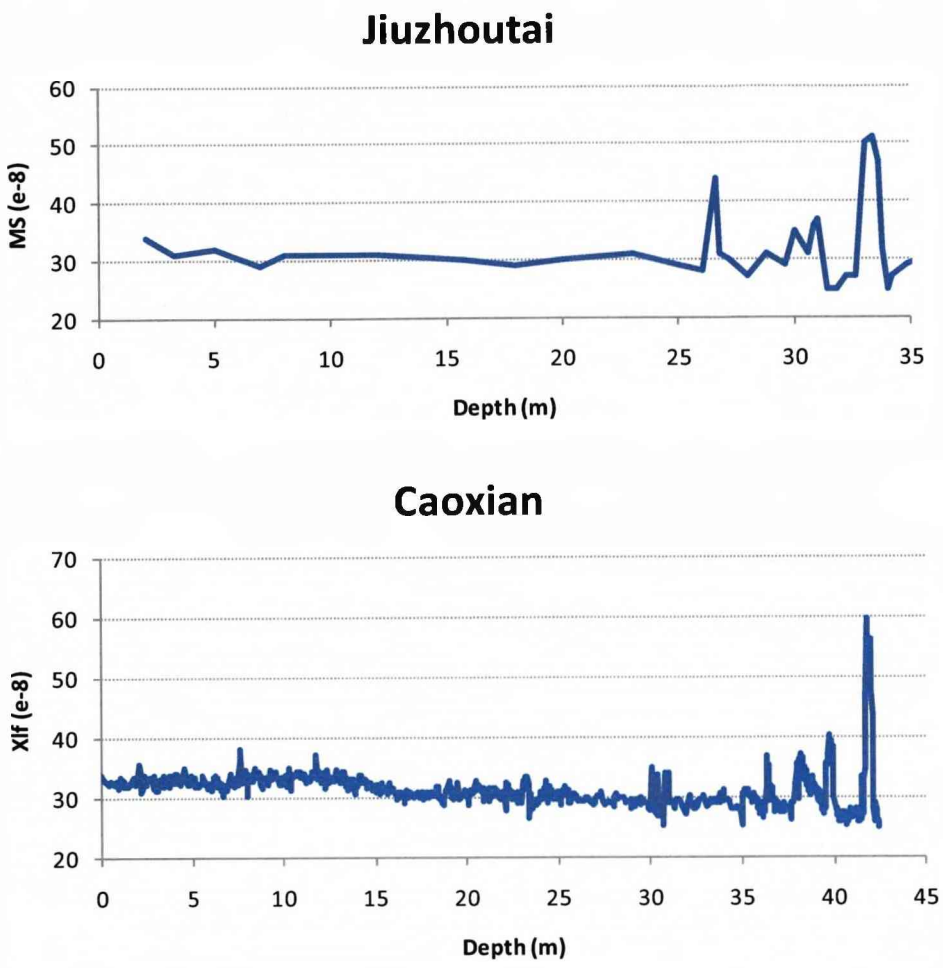

Figure 5-13 Magnetic susceptibility records for loess-palaeosol sequences at Jiuzhoutai and Caoxian, adapted from Jeong et al. (2008) and Parker and Bloemendal (2005), respectively.

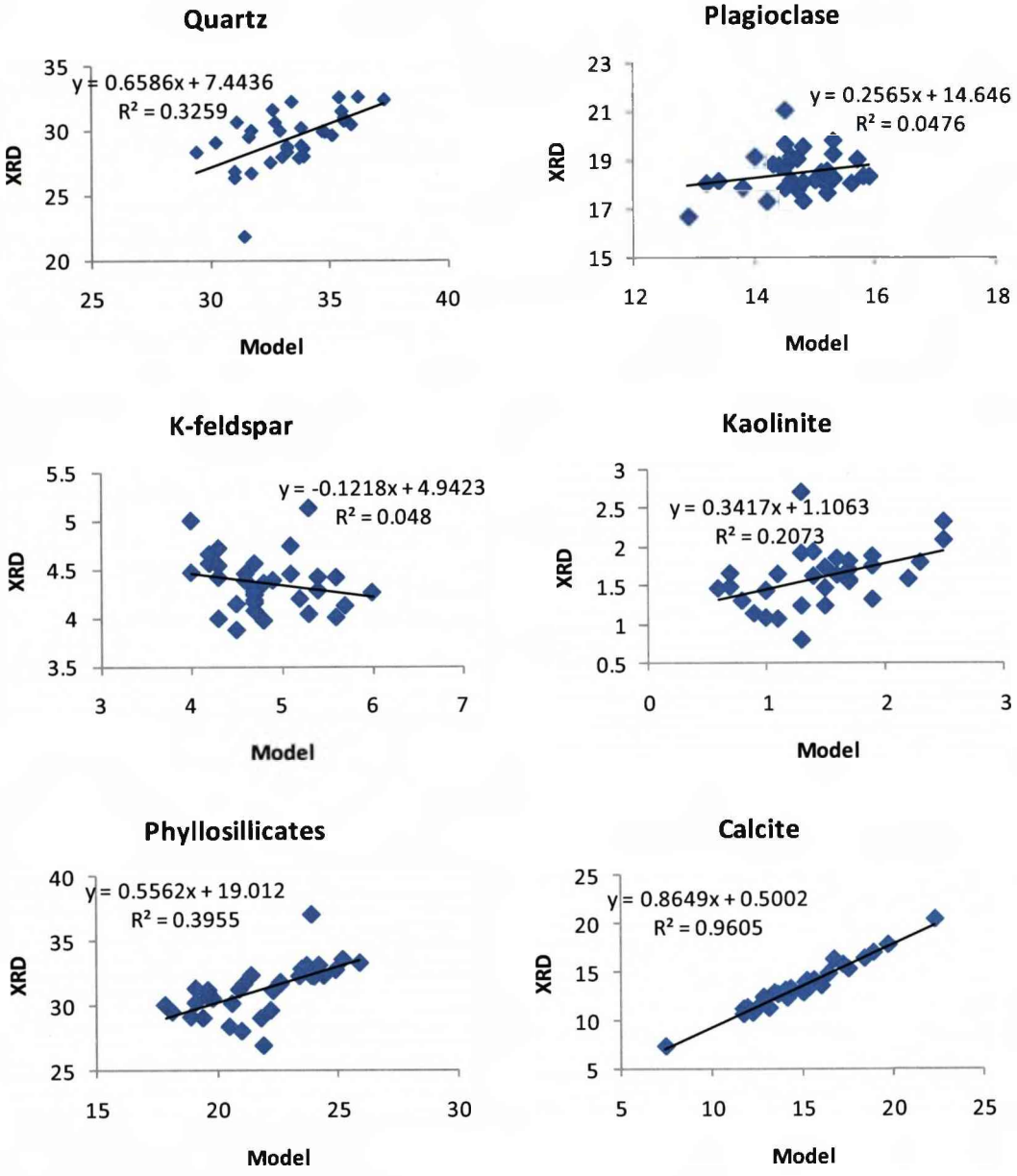

Figure 5-14 Scatter plots for mineralogy obtain by XRD and normative mineral estimation for loess-palaeosol sequence at Jiuzhoutai. Raw element and mineralogical data are from Jeong et al. (2008).

5.5 Variation in mineral concentrations

In this section, changes in mineral concentrations will be demonstrated as mineral to quartz ratios, plotted against depth. In the descriptions below, the named minerals mean the ratios of a given mineral to quartz, e.g. mica means the ratio of mica to quartz.

Duanjiapo

Figure 5-15 shows variations in mineral:quartz ratios for Duanjiapo. K-feldspar, mica and calcite have been heavily depleted within the S1, L2S1, S2, L4, S4, L5 and S5 units, except for two peaks found at ~15m and 25.5m, which occur at the base of the L3 and L5 intervals, respectively. Chlorite concentrations are also relatively low in these units, but are especially depleted at the depths of 5m, 20.1m and 26.3m, corresponding to S1, S4 and S5, respectively. This suggests that palaeosols, as well as loess units L2S1, L4 and L5 at Duanjiapo, have been intensively weathered. In addition, compared with other palaeosol units, higher values can be found in S3 for these four minerals mentioned above, which implies that S3 may have been less intensively weathered.

Comparing the lowest values of the concentrations of the four mineral types in S4 and S5, little difference is observed, in spite of the higher magnetic susceptibility values in S5. This could have two explanations: either that the magnetic susceptibility values cannot be directly used as an indicator of weathering intensity; or that the mineral concentrations have already reached the minima during the weathering in S4, so that no further mineral depletion (K-feldspar, mica, calcite and chlorite) occurred even under even stronger weathering conditions. If the latter is true, caution is needed when using the calculated mineral loss to quantify the runoff rate, especially when using calcite, which has been completely weathered in many palaeosols and weathered loess units. This will be further discussed in the context of the runoff estimations (section 5.9).

Feldspar is slightly positively correlated to phyllosilicates (mainly chlorite and mica, see Figure 5-15), which disagrees with the XRD quantification results (section 5.3.2.1).

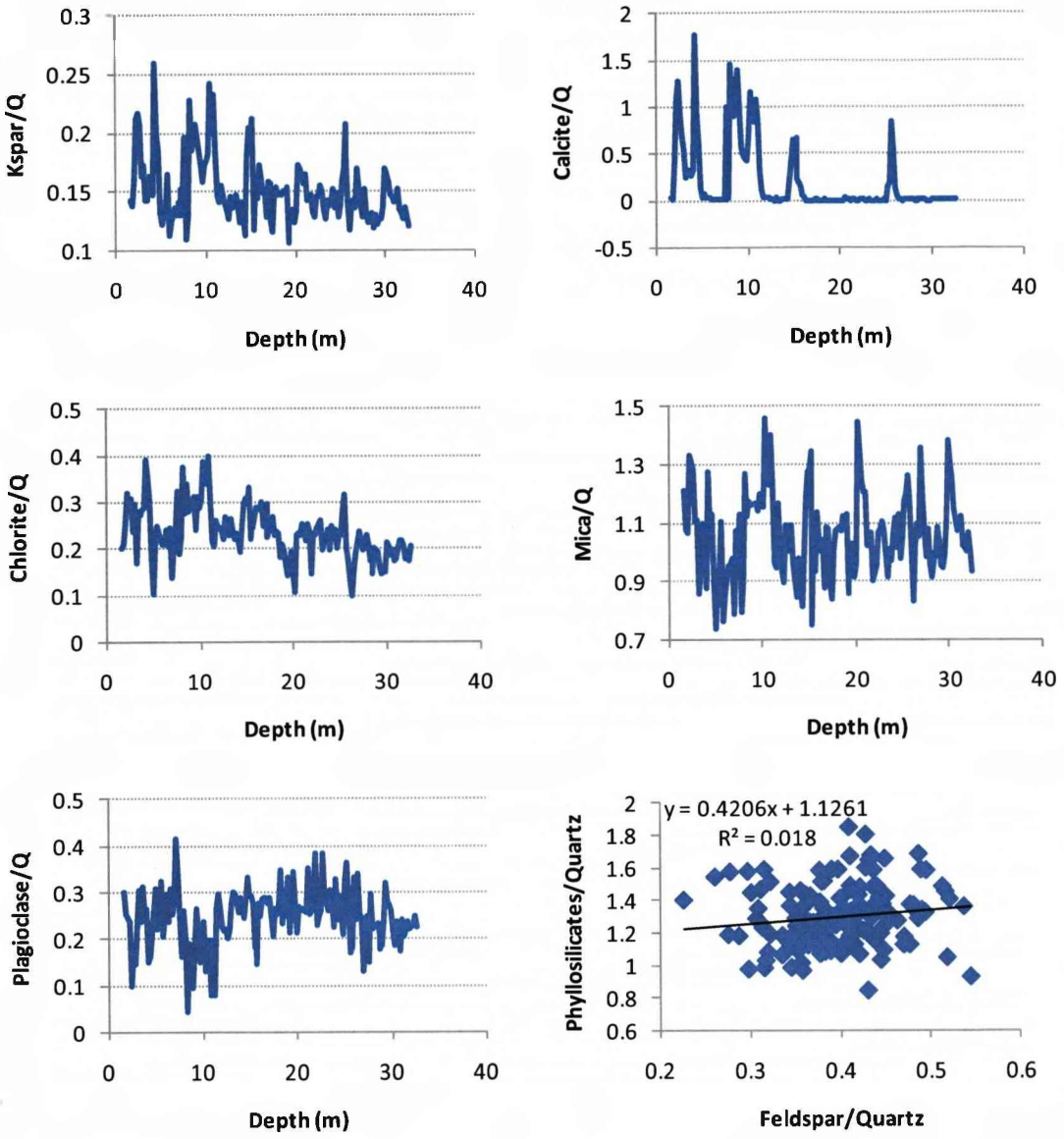

Figure 5-15 Duanjiapo section: Variations in mineral:quartz ratios, and relationship between feldspar and phyllosilicates

Luochuan

Calcite and plagioclase have been heavily depleted in all the palaeosols in question and have relatively high values in interbedded loess (Figure 5-16). In addition, chlorite has been depleted in palaeosols, especially in S1, S4 and S5. There is hardly any calcite in palaeosols S1, S2, S4 and S5, but there is a small amount in S3. Compared with other palaeosol units, higher concentrations of plagioclase and

chlorite also occur in S3, again indicating that weaker weathering processes occurred in S3. In contrast, K-feldspar and mica are relatively abundant in palaeosols and are less abundant in loess, which possibly suggests a different weathering mechanism at Luochuan.

In addition, similar to the Duanjiapo section, due to the higher mobility of calcite in the weathering process, calculating the runoff rate based on calcite loss is problematic, because too much calcite was leached out and so it cannot be used as an indicator for weathering intensity. In addition, there is a slightly positive correlation between feldspars and phyllosilicates, which is still contrary to the findings of XRD quantification.

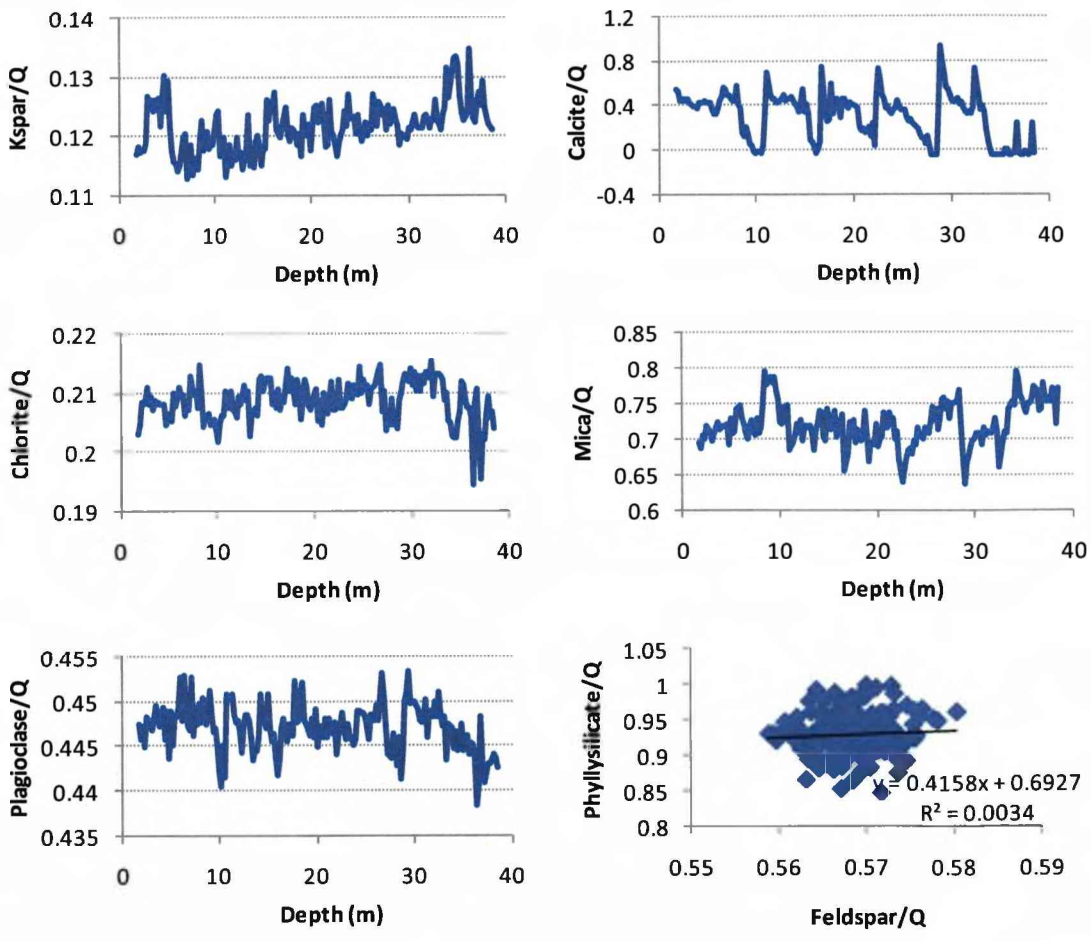

Figure 5-16 Luochuan section: Variations in mineral:quartz ratios, and relationship between feldspar and phyllosilicates

Caoxian

Relatively high concentrations of calcite, K-feldspar, chlorite and plagioclase occur in loess units, L1L1, L1L2, S1L1, S1L2 and L2. However, no significant increase in these minerals occurs in Sm (L1S1), which implies that this interval at Caoxian probably has not been strongly weathered. Mica has a reverse correlation with other minerals, i.e. high in palaeosols/sub-palaeosols and low in loess/sub-loess units. Feldspars are positively related to phyllosilicates (Figure 5-17) and both mineral groups are abundant in loess/sub-loess layers but low in palaeosol/sub-palaeosol layers, which is in agreement with the XRD quantification results.

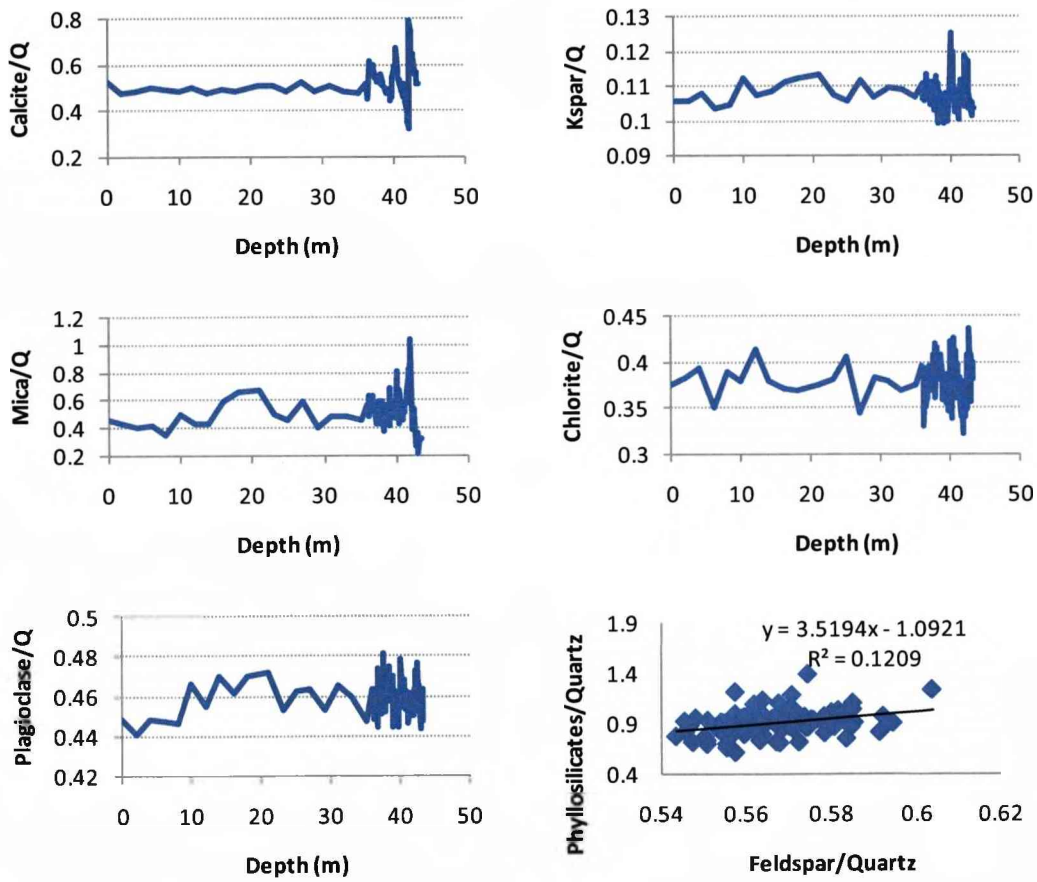

Figure 5-17 Caoxian section: Variations in mineral:quartz ratios, and relationship between feldspar and phyllosilicates

5.6 Origin of the loess minerals

5.6.1 Quartz

Quartz is not mainly of detrital origin, as neither overgrowth between primary and secondary quartz nor quartz cementation has been found under SEM observation.

According to the XRD quantification, there is no significant change in quartz concentration among different lithological units or different loess sections. This proves that quartz is resistant to weathering.

5.6.2 Feldspar

Jeong et al. (2008) suggested that albite has two possible origins: (1) After the erosion from the bedrock but before the material arrives on the CLP, it is precipitated through significant weathering; or (2) bedrock in the source area are rich in albite and are weakly weathered, which forms highly albitic feldspar in loess through transportation. According to the electron microscope observation, the other possible origin is the intergrowth of K-feldspar and albite from cooling granitic magmas, by low-grade regional metamorphism up to greenschist facies, or by contact metamorphism of albite-epidote hornfels facies (Raymond, 1995; Jeong et al., 2008). Na-Ca plagioclase (NCP) and K-feldspar can be easily transformed through chemical weathering, thus their origin is unlikely to be the rock types sensitive to hydrothermal process or other chemical alternations.

5.6.3 Biotite

Biotite can be formed under a wide range of temperature and pressure conditions, and is typically rich in many contact and regionally metamorphosed sediments. In addition, it is also suggested that biotite is found more in intrusive igneous rocks rather than in extrusive igneous rocks (Howie & Zussman, 1966).

5.6.4 Barite

Barite occurs as veins or cavity filling concretions in limestones, sandstones, shales and clays. It can be formed through hydrothermal alternation or limestone weathering which requires relatively warm and wet environment. Since barite has

only been found in one palaeosol sample (Figure 5-7-1), it is difficult to determine its origin.

5.6.5 Chlorite

It is common to find chlorite intergrowing with quartz as a product of hydrothermal alteration in igneous rock. Chlorite is also commonly distributed in sedimentary rocks both as detrital and as authigenic crystals (Howie & Zussman, 1966). However, it has been found that primary chlorite is sensitive to chemical weathering (Dixon and Weed, 1989). Since the mineralogy data obtained during the present study show that chlorite is abundant in the loess at all of the three sections, it can be concluded that chlorite in the loess-palaeosol sequences is mainly a primary mineral.

5.6.6 Illitic clay

Illite can be formed by feldspar weathering, alteration of other clay minerals during diagenesis, by the degradation of muscovite, the recrystallisation of colloidal sediments or by hydrothermal alteration of various rocks (Deer et al., 1996). For both hydrothermal and sedimentary occurrences illite can be more easily formed in alkaline conditions with high concentrations of Al and K. The illite concentrations at the three loess sections show that it is high in palaeosols and low in loess, indicating that the illite in loess-palaeosol sequences could be formed through chemical weathering of other minerals. If so, the enhancement of illite can be a proxy of increasing summer monsoon as suggested by Gylesjo and Arnold (2006).

5.6.7 Calcite and dolomite

The origin of carbonate minerals is debatable, because of their high mobility during diagenetic and weathering processes. Calcite can be derived from calcareous rocks as a detrital origin or from calcic plagioclase weathering as a secondary product.

Dolomite is known as a common sedimentary material formed under normal conditions of temperature or pressure, but its origin remains unclear both in the laboratory and from the observation. Krauskopf and Bird (1995) suggested that most dolomite is not a primary precipitate but forms rather as a product of slow reactions altering originally deposited calcium carbonate. However, recent evidence from the

Chinese Loess Plateau (Liu et al., 2006) showed that the dolomite in loess-palaeosol sequences is detrital in origin, and it only exists in the zones where modern rainfall is less than 540mm/yr. This is in agreement with our SEM observations of dolomite are confined to a loess sample from Caoxian, the only loess section with an annual mean precipitation less than 540mm (~200mm/yr) among those three localities in question.

Therefore single-grained calcite and dolomite in Figure 5-6-2, Figure 5-6-4 and Figure 5-8-1 could be derived from metamorphic rocks rich in carbonates, while intergrowth of calcite and dolomite in Figure 5-6-7 indicates an origin from carbonate and calcareous sedimentary rocks.

5.7 Weathering in source or depositional regions?

Primary chlorite concentration was found to be high in loess and low in palaeosols (Section 5.4) suggesting the enhancement of the winter monsoon during glacial times or the removal of chlorite during warm and wet spells, because chlorite preservation is favoured by a cool, arid environment. Therefore, it is most likely that weathering occurred after deposition. Otherwise chlorite would be depleted during the intense weathering in source region, resulting in low chlorite concentration even in loess units, which is the opposite to what is observed. This conclusion is also supported by the similar variation of plagioclase within alternating loess and palaeosol layers.

However, as mentioned in section 5.4, according to normative mineral estimation results, K-feldspar and phyllosilicates in the three loess-palaeosol sequences have a positive correlation, in contrary to that found in XRD quantification, yet this positive correlation is very weak (R^2<0.13). If both observations could be true, possibly it is the other processes e.g. transportation, tectonic mechanism, etc. that have complicated the mineralogy variation.

From the XRD quantification aspect, the reverse trends of feldspar and phyllosilicates shown in Figure 5-9 indicate a possible alternation between these two mineral groups, in which the variations at Duanjiapo and Luochuan sections show the potential decomposition of feldspar into kaolinite, smectite or illite, composing a large portion of phyllosilicates in palaeosol layers. This assumption is also supported by the fact that illite, the major component in loess phyllosilicates is highly enhanced

in palaeosols rather than in loess. However, it seems to be more complicated for the case at Duanjiapo, because of plagioclase abundant in palaeosols rather than in loess as at the other two sites, since plagioclase preservation is normally favoured dry and arid climate conditions.

On the other hand, if the alternating relationship between feldspar and phyllosilicates can be confirmed, it could suggest that (1) some phyllosilicates mainly kaolinite, smectite and illite, at the Duanjiapo and Luochuan loess sections were formed through chemical weathering at the depositional area; and (2) the amplitude of the fluctuation in feldspar and phyllosilicates can be considered as an indicator of changes in weathering intensity at the depositional area. Since the amplitude in the Duanjiapo samples is higher than that in the Luochuan samples, it is suggested that the intensity of chemical weathering in the former is higher than in the latter. This is also in accordance with the modern climate conditions at these two localities.

From the normative mineral estimation results and the XRD quantification results at Caoxian, in accordance with the possible feldspar weathering at the depositional areas from south and central CLP, feldspar, mica and calcite are found to be abundant in loess/sub-loess rather than in palaeosols.

Taking the uncertainty of the feldspar estimation (Section 5.2.1 and Section 5.3.2) into account, the variation in other loess minerals shows that chemical weathering most likely occurred after deposition, which is also supported by previous isotope (Wang et al., 2007; Yang et al., 2000) and mineralogical studies (Li et al., 2008; Jeong et al., 2008) on Chinese loess.

5.8 Weathered loess

From the mineralogical quantification by normative mineral estimation, it is suggested that the weathering in L1S1 at Duanjiapo and Luochan has reached a reasonable degree, based on the fact that most minerals decrease at L1S1 layer from both sites (Section 5.4). However, the Sm layer at Caoxian has not clearly shown the mineralogical characteristics of weathered loess: weathering-sensitive calcite is unchanged, which is similar to the magnetic susceptibility records in this lithological unit, although a finer grain size was also observed by Parker and Bloemendal (1995).

In contrast, it is also found that chlorite is generally low in Sm at Caoxian, while other minerals including K-feldspar, mica and plagioclase are relatively higher.

From the annual mean precipitation reconstruction, the rainfall in Sm layer is relatively higher than other pristine loess layers from Duanjiapo and Luochuan, suggesting that Sm has been intensely weathered. In Caoxian, however, the rainfall (based on the K-feldspar depletion) within Sm unit has not increased but slightly decreased. This means at least no strong weathering found in L1S1 from Caoxian, in agreement with the interpretation of the mineralogical data. This implies the weathering regime in the northwest Loess Plateau may have been different to that in the central and south CLP. This is possibly because either the summer monsoon during the formation of Sm was significantly weakened and the winter monsoon still dominated at the northwest CLP; or that the pathway of the summer monsoon during this period was different. Nevertheless, the rainfall rate calculated from the chlorite depletion at Caoxian, shows that the summer monsoon was actually enhanced during the Sm stage.

Apart from L1S1, other weathered loess layers, i.e. L2, L4 and L5 at Duanjiapo and L4 at Luochuan, can also be found from the runoff and precipitation data. This is also supported by the mineral estimation data, decrease in K-feldspar, mica and calcite has been identified in these loess units, although it is not clearly shown in the magnetic susceptibility signals. Therefore, the identification of weathered loess only dependent upon magnetic susceptibility enhancement could be problematic.

5.9 Runoff and precipitation estimation

In Section 5.3, mineral compositions within loess and palaeosols are quantified using normative mineral estimation, thus mineral depletion in each lithological unit during weathering can be calculated. Because the relationships of mineral depletion-runoff and runoff-precipitation can be quantified using the numerical model, runoff and precipitation rates were calculated accordingly.

5.9.1 Runoff and precipitation rates calculation

Figure 5-18 shows the estimated runoff rates in m/yr for the three loess sections based on the chemical denudation of calcite or K-feldspar. Generally, high runoff rates can be found in palaeosols from all the sites. However, relatively intense runoff can also be found in some loess units, i.e. Sm (L1S1), L2, L4 at Duanjiapo; Sm and L4 at Luochuan; L1L1 and L1L2 at Caoxian. This suggests that these loess units could possibly have been weathered, especially the Sm sub-loess units at Duanjiapo and Luochuan which have been shown to be a weathered loess layer by magnetic susceptibility records, in agreement with the runoff estimation results (Figure 5-18).

Similar to the mineral concentration records as mentioned in the previous section (Section 5.4), the results indicate that the runoff rate in S4 was higher than that in S5 at both Duanjiapo and Luochuan, which is also supported by the annual mean precipitation calculation (Figure 5-19). This means that the average weathering intensity in S4 may have been stronger than that in S5 under the same temperature, although the maximum annual precipitation rate could occur during a short term (a period of time shorter that S4 and S5 stages) within S5 stage. This could perhaps explain why the higher peak in magnetic susceptibility is found in S5 at Duanjiapo and Luochuan, and yet a higher estimated average rainfall rate occurred in S4 at both sites. If the mean temperatures are similar between these two interglacials during which S4 and S5 were developed, it can be concluded that according to the magnetic records from different loess sites in the central CLP (Kukla and An, 1989; An et al., 1990; Xiao and An, 1999; Hao and Guo, 2005; Sun et al., 2006), although the summer monsoon intensity could have increased sharply from S5, which is believed to have higher weathering intensity than S4, the summer monsoon could still have influenced the palaeosol S4 for a longer time than was the case for S5.

Similar to Sm, the calculated average rainfall rate in L4 was also relatively high at Duanjiapo and Luochuan, but no evidence can be found in the magnetic susceptibility records – values are consistently very low within L4. This is possibly due to 1) the inappropriate definition of parent material, which can make the mineral loss larger than the amount in reality and thus overestimate the average rainfall rate. This is more likely to have occurred in those loess units where the loess accumulated faster during a long period (this will be further discussed in the sensitivity test, Section 5.9.2); 2) more goethite has formed under its favorable climate conditions, i.e. higher soil moisture and cooler temperatures (Balsam et al., 2004). This could reduce the magnetic susceptibility signal despite relatively high precipitation; and 3) during intensely weathered units at Duanjiapo especially, loess could have been significantly depleted during subsequent interglacials.

Generally, a decrease in runoff and precipitation rates is observed to have occurred with time at Duanjiapo and Luochuan, indicating a possible weakening of the summer monsoon or an enhancement of the East Asian winter monsoon from S5 to present, in agreement with the work done by Wang et al. (2007) and partly in agreement with Gylesjц and Arnold (2006). However, a reverse change in runoff and rainfall occurred in L1 at the Caoxian section (Figure 5-18), which could suggest a different weathering mechanism or climate regime has affected the Northwest CLP. Nevertheless, this is still not clear because data can be only collected down to S1 unit at Caoxian and no further data are available at the moment.

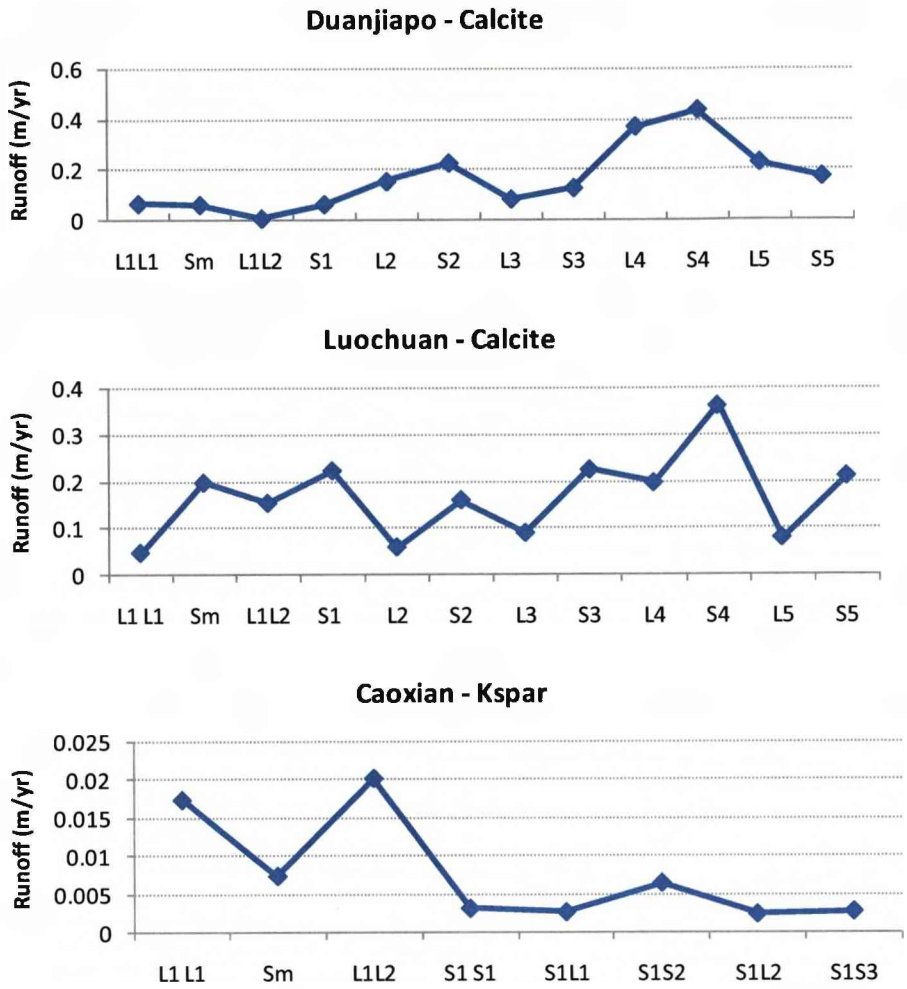

Figure 5-18 Runoff rate (m/yr) calculated from mineral loss at three loess sections

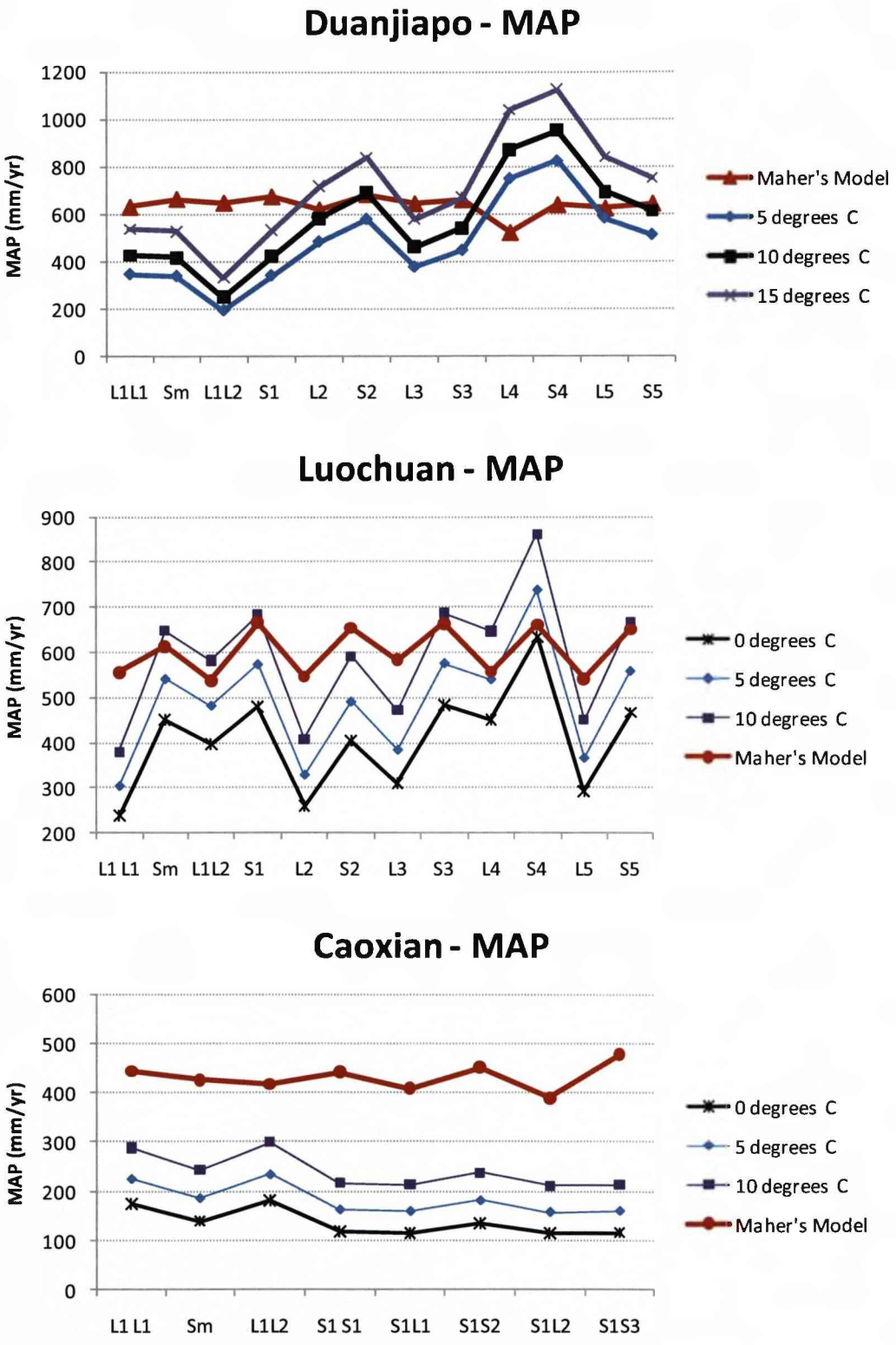

Figure 5-19 Estimated annual mean precipitation rates (mm/yr) at three loess section

5.9.2 Sensitivity test in runoff estimation

As mentioned in the last section, the runoff rate is calculated based on the power function equation adapted from Dunne (1978). The alkalinity flux (meq/m^2 per yr) is given by (Boyle, 2008):

$$\text{Alkalinity flux} = F \cdot R^{\alpha} \quad \textbf{(5-1)}$$

Therefore, in order to test the sensitivity of this quantitative method, two variables in this equation (F and α) need to be discussed.

The value of α

It is suggested that the lower the soil solubility, the higher the α value is. However, it is empirically indicated that this relationship is weak (Boyle, 2008). Therefore, a single value for α of 0.8 has been used for this calculation, since it has been proved that the value of 0.8 provides a good fit for silicate rock weathering (Boyle, 2008), which is similar with the geological conditions for the formation of the loess-palaeosol sequences.

The rock weathering factor F

The F value cannot be considered as constant according to different soil types and weathering conditions (Boyle, 2008). Previous studies (Meybeck, 1986; Bluth and Kump, 1994) show that the F value varies for different rock types. In the calculation of the runoff on the CLP, the F values of different rock types have been used as reference for different mineral weathering processes. The runoff calculations for Duanjiapo and Luochuan are based on the alkalinity flux of calcite, while for Caoxian K-feldspar depletion (F value for granite: 100 – 300, Table 4-5) has been used because the negative values in the alkalinity flux of calcite cannot be used in the equation.

In addition, based on the rock/soil weathering intensity quantification, Boyle (2008) suggested that 1) the rock weathering factor can drop significantly over a millennial or greater timescale; 2) the F value can be adjusted in proportion to the fractional soil coverage. This means that the rock weathering factor can be affected by the grain size distribution, which is affected by loess density. Therefore, F values for runoff reconstruction on different lithological units have been adjusted according to its relationship with the densities of corresponding loess or palaeosol, and the subsequently calculated runoff rates have been tested using modern runoff data for the same site. If the rock weathering factor F can be regarded as an indicator of the minerals in the soil, i.e. they are positively correlated, a lower runoff rate could lead to higher mineral content, and thus a higher F value.

For example, in the case of using calcite depletion to calculate the runoff rate at a certain temperature, when the runoff rate has reached a certain value (threshold value *T*), the calcite in soils should have reached a certain level, where no more calcite can be dissolved – the carbonate in runoff has be saturated. Theoretically, at this time, the reference F value in **Error! Reference source not found.** should have been used for the runoff calculation, which is supposed to be most accurate under this circumstance. In other words, in order to obtain the runoff rate closest to the real runoff rate, if the runoff in reality is higher than the threshold *T*, the F value should be tuned lower than the recommended value in **Error! Reference source not found.**, and vice versa. For reference, this threshold *T* is about 300mm/yr as a world average suggested by Holland (1978, cited in Bluth and Kump, 1994). According to the climate data over the past 50 years collected by the Chinese Loess Plateau Soil and Water Conservation Database (CLPSWCD), the average runoff rates in the three loess sections are all much lower than 300 mm/yr, so the F value for loess-palaeosol weathering is expected to be higher than the reference value, especially in loess units.

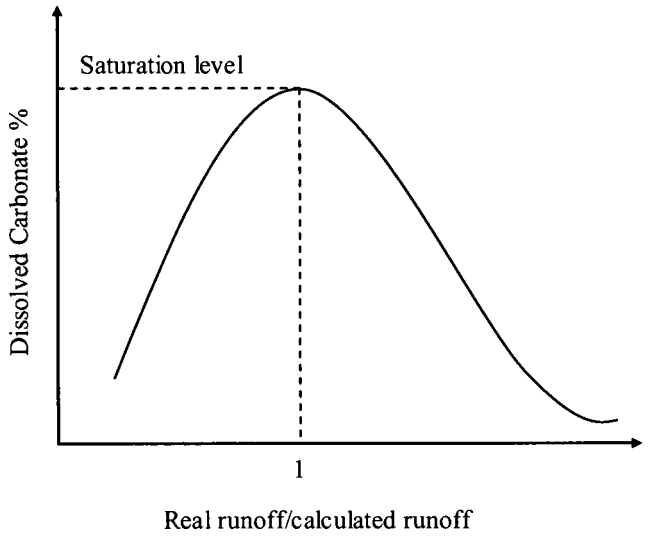

Figure 5-20 Concept of the relationship between dissolved carbonate concentration and the ratio of real runoff to calculated runoff. When the ratio is 1, dissolved carbonate reaches its saturation level, and thus at this time calculated runoff is equal to the threshold runoff rate *T*.

Take calcite depletion at Duanjiapo for example, the F value was modified as follows:

1. Comparing with the reference value (1000 – 2000), set a higher F value for loess and a relatively lower value for palaeosol, e.g. 3000 for all loess units and 2000 for all the palaeosols, when the runoff rate reaches the threshold *T*.
2. Use the loess density data and the set values of F to draw a scatter plot and find the regression between the two parameters. Afterwards, use the regression equation and the loess density data to refine the F value (Figure 5-21).
3. Apply the refined F values on each lithological unit and calculate the runoff rates, and then average them. The averaged value (158 mm/yr) is considered as the threshold value *T*, which is compared with the modern runoff data at Duanjiapo (CLPSWCD).
4. According to the statement above, the modern runoff (174 mm/yr, the real runoff) seems higher than the calculated value *T* (158 mm/yr), so the set F values should be adjusted lower than the initial values i.e., 3000 and 2000 for loess and palaeosols, respectively.

5. Use the re-adjusted set F value to repeat Steps 1 to 4 until the calculated average runoff (T) is close to the value in reality (174 mm/yr).

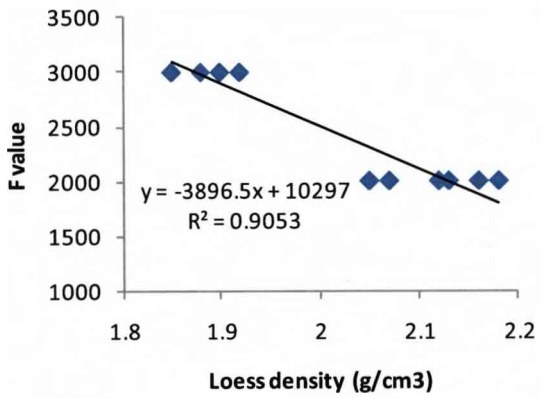

Figure 5-21 Correlation between set F values and the densities of loess and palaeosols at Duanjiapo.

Table 5-3 Adjusted F values for calcite weathering in loess-palaeosol sequences from Duanjiapo and Luochuan.

Adjusted F value (calcite)	Lithological unit	Density (g/cm^3)
2965.5	L1	1.88
2077.1	S1	2.07
3105.8	L2	1.85
1796.5	S2	2.13
2965.45	L3	1.88
1656.3	S3	2.16
2778.5	L4	1.92
1562.8	S4	2.18
2872.0	L5	1.9
1843.3	S5	2.12

Table 5-4 Adjusted F values for K-feldspar weathering in loess-palaeosol sequences from Caoxian.

Adjusted F value (K-feldspar)	Lithological unit	Density (g/cm^3)
261.9	Sm*	2.05
394.3	L1	1.88
246.3	S1	2.07

*the density of Sm (L1S1) refers to the density of S0 as a reference value.

Table 5-3 shows the calcite weathering factors modified based on the loess density. F values of calcite weathering in palaeosols are mostly within the range 1000 – 2000 suggested by Bluth and Kump (1994) and close to the maximum of the range, but those in loess are much higher than the reference value. Similarly, in the runoff calculation for the Caoxian section, the K-feldspar weathering factor in S1 and Sm (the sub-palaeosol layer within L1) is within the reference range 100 – 300, but the one for L1 is higher (Table 5-4).

Runoff rates estimated based on the chlorite depletion (Figure 5-22) have shown similar variation to those calculated by calcite or K-feldspar weathering, except for the Caoxian section. Differing from the runoff rate derived from K-feldspar weathering, it is higher in Sm and the palaeosols from Caoxian and lower in loess. The F values used for chlorite are shown in Table 5-5. It is experimentally proved that the variation in runoff rate does not change significantly if the F value for chlorite weathering is set to be constant for each loess section, respectively. Due to the positive correlation between the rock weathering factor F and the grain size distribution, this means chlorite weathering is not affected by grain size variation very much, which is also suggested by Li et al. (2008). This is possibly because chlorite is preferentially abundant in the fine grain-size fraction in both loess and palaeosols, and thus its weathering will not largely depend on the wind transportation process, which generates different grain size variations in different depositional areas (Yang et al., 2006). This is also suggested by the SEM observations that chlorite in loess and palaeosols mainly intergrows with fine-grained quartz. Another possible explanation is that chlorite weathering could be largely affected by the internal void within the structure of chlorite, rather than by the grain size variation.

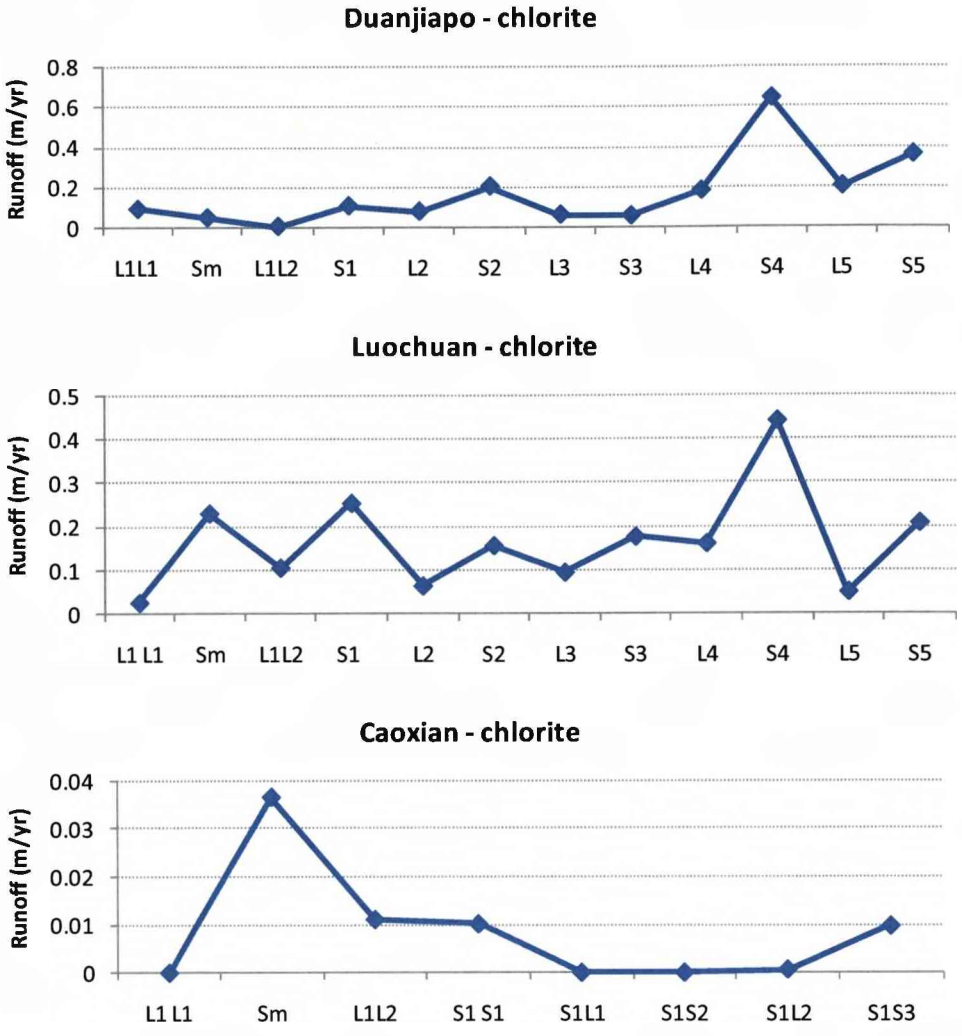

Figure 5-22 Runoff rate in m/yr for three loess sections based on chlorite weathering

Table 5-5 Rock weathering factor (F) for chlorite at three different sites

Strat. Layer	F – Duanjiapo	F - Luochuan	F - Caoxian
L1L1	74.212	98.8632	582.4968
Sm	55.665	72.367	448.513
L1L2	74.212	98.8632	582.4968
S1	53.483	69.2498	432.7502
L2	77.485	103.539	
S2	46.937	59.8982	
L3	74.212	98.8632	
S3	43.664	55.2224	
L4	69.848	92.6288	
S4	41.482	52.1052	
L5	72.03	95.746	
S5	48.028	61.4568	

However, weathering of silicate minerals like chlorite is largely affected by the accumulation rate of loess-palaeosol sequences, which could lead to changes in weathering time. The higher the accumulation rate, the shorter the weathering time, and vice versa (Li et al., 2008). This is the most likely reason for the very low F value for chlorite weathering at Duanjiapo and Luochuan but similar F values within the reference range (300-600) at Caoxian. The average accumulation rate within L1 and S1 at Caoxian is 32.6 cm/kyr, much higher than those within equivalent intervals at Duanjiapo (4.1 cm/kyr) and Luochuan (8.3 cm/kyr), and thus the weathering time of chlorite at Caoxian was significantly limited. Since the weathering intensity depends on both weathering time and chemical weathering rate (Vidic et al., 2004; Li et al, 2008), the weathering intensity of chlorite at Caoxian has been weakened by the relatively short duration of the reaction. Therefore, the weathering rock factor F for chlorite in the Caoxian loess-palaeosol sequence is much higher than for the two other sites. In other words, when there is a very weak grain-size effect or when it is constant, the F value will largely depend on the accumulation rate, i.e. they are positively correlated. Therefore, the F values for chlorite at Duanjiapo is slightly lower than that at Luochuan, as the corresponding accumulation rate of the former is slightly lower than the latter.

Thus chlorite, as one of the silicate minerals, seems to be the proxy of weathering intensity which is not affected by grain-size effects. However, its relationship with temperature remains unclear; on the other hand, compared with the XRD mineral quantification, the quantitative analysis of K-feldspar by normative mineral estimation is not accurate enough (R^2 = 0.0035), leading to some uncertainties in the

calculation of K-feldspar loss and runoff rate based on it. This has also been proved by the unclear relationship between Ba concentration and the magnetic susceptibility, as mentioned in Section 5.1.3, as the K-feldspar concentration is determined by its BaO component according to the normative mineral estimation method. Thus caution must be used when interpreting the difference in runoff variation between methods based on K-feldspar and chlorite weathering.

Baseline problem – parent material prior to weathering

For the runoff reconstruction, mineral loss is needed for the alkalinity flux calculation. Thus, mineral amounts both before and after weathering are required. The mineral amount after weathering can be calculated based on the mineral concentration data (section 5.4), but the determination of the mineral amount before weathering is not so straightforward. Samples with highest CaO and lowest ZrO_2 or TiO_2 content have been considered as parental material within the loess-palaeosol sequence before weathering because of the high weathering mobility of CaO and low weathering susceptibility of ZrO_2 and TiO_2. However, this definition of parent material could constitute a 'baseline problem'. For example, in the case of calcite, although the mineral loss at a certain depth within palaeosols could be higher than that in loess, the calculated total mineral loss in loess can be much higher than that in palaeosols if a particular baseline has been selected (Figure 5-23). In addition, due to the relatively high accumulation rate in loess, the same depth interval in loess covers a shorter period of time than that in palaeosol. As a result, mineral loss per year in loess could be even higher than that in palaeosols, and thus the runoff in loess appears to be higher, because the alkalinity flux calculated from mineral loss per year is positively related to runoff rate according to Equation 5-1:

$$\text{Alkalinity flux} = F \cdot R^{\alpha} \qquad (5\text{-}1)$$

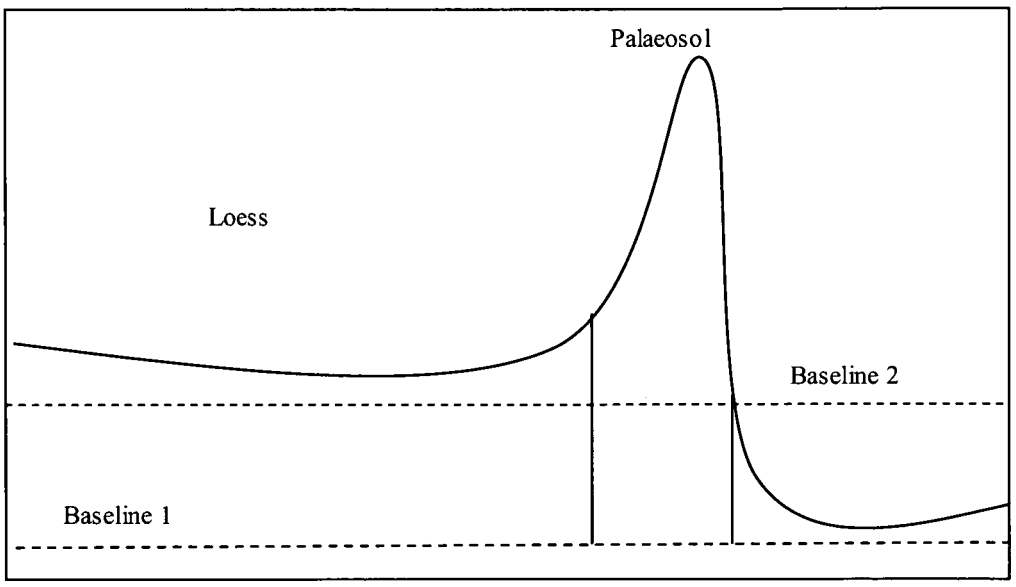

Figure 5-23 Baseline problem in the mineral loss calculation. Mineral loss in loess is higher than that in palaeosol if Baseline 1 is selected; but if mineral amount is subtracted by Baseline 2, mineral loss in loess will be lower than that in palaeosol.

5.9.3 Mineral dissolution model vs. rainfall-susceptibility climofunction

As mentioned in Chapter 4, this rainfall quantification model will be compared with the rainfall-magnetic susceptibility climofunction proposed by Maher et al. (1994). Based on the low-frequency susceptibility records of the loess samples in question, the average annual precipitation rate is given by (Maher et al., 1994):

$$P_A \text{ mm/yr} = 222 + 199 \log 10 (\chi_{B-C} 10^{-8} m^3 kg^{-1}) \qquad 5\text{-}1$$

where P_A is annual precipitation in mm/yr, χ_{B-C} is the difference in susceptibility of the B (subsoil) and C (parent material) horizons, as give in $_{\chi B-C}$ = **χB - χC** **5-2**:

$$\chi_{B-C} = \chi_B - \chi_C \qquad 5\text{-}2$$

χ_B is the average susceptibility value in each lithological unit. χ_C is equal to the susceptibility of the local loess unit L9.

The rainfall rates calculated by these two independent quantitative models have been plotted as a scatter graph in Figure 5-24. A relatively high similarity is observed between the two different approaches. In Figure 5-19, it can be seen that the rainfall is relatively high in palaeosols/weathered loess and low in loess/least weathered palaeosols, yet higher variations occur in results obtained by the mineral dissolution model. In addition, in the Caoxian section, the average rainfall (431.6 mm/yr) calculated by Maher's climofunction is much higher than that estimated by the mineral dissolution model and is also much higher than the modern annual rainfall rate in this area (228 mm/yr, according to the Chinese Loess Plateau Soil and Water Conservation Database, CLPSWC database). Therefore, it is suggested that in areas with very low precipitation and extremely low runoff rate (8 mm/yr, CLPSWC database), Maher and others' (1994) rainfall-susceptibility climofunction model gives less reliable results than the mineral dissolution model.

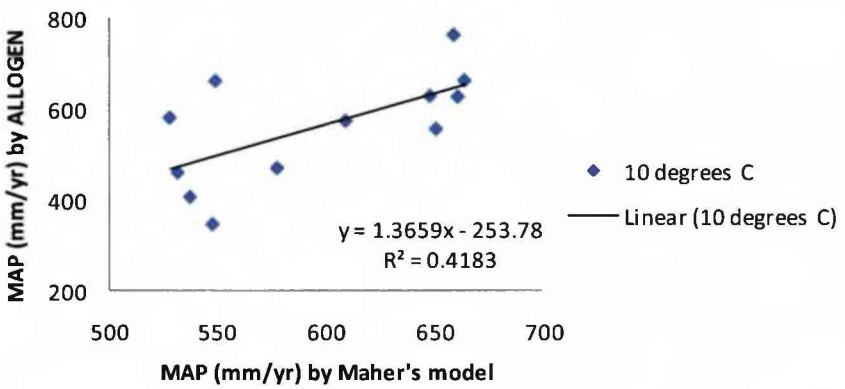

Figure 5-24 Annual rainfall calculated by Maher's climofunction compared with the mean annual rainfall calculated by the mineral dissolution model using calcite weathering at a MAT of 10 ℃degrees.

However, both models have the 'baseline problem'. In the magnetic susceptibility climofunction model, the definition of the parent material before weathering is the average susceptibility value in loess L9. As is the case with the mineral dissolution model, this can give more uncertainty in the rainfall reconstruction. Additionally, this definition method is not applicable to samples younger than L9, such as the Caoxian loess samples in this study. Thus, in contrast to Duanjiapo and Luochuan, the parent material at Caoxian is empirically defined, which has limited the comparability among the rainfall rates at the three loess sections.

Temperature variation is another factor affecting the calculation procedure of both models. The equation in the susceptibility climofunction is based on the recent annual rainfall data and pedogenic susceptibility records of modern soils on the Chinese Loess Plateau, meaning that mean annual temperature over a short period does not change significantly, and thus the effect of temperature variation on the rainfall reconstruction has not been well demonstrated in this model – smaller amplitude of variation in rainfall rates along with lithological units. Nevertheless, the temperature effect on weathering intensity and precipitation is actually highly significant, as suggested by Boyle (2008). In contrast, the mineral dissolution model has provided possible rainfall rates according to different mean annual temperature values (Figure 5-19), but the determination of the temperature for a specific lithological unit remains uncertain.

5.10 Conclusions

Detailed and quantitative geochemical and mineralogical analysis as well as scanning electron microscopy of loess-palaeosol sequences on the CLP has enabled the identification of various mineral species and estimations of their concentrations within different lithological units. Based on the qualitative XRD analysis and SEM observation, loess mineralogy including mineral types and their origin can be generally obtained. The RockJock program is a sensitive tool for estimating the mineral concentrations with reasonable accuracy, although it is not reliable for minor mineral quantification and needs the definition of mineral types for higher accuracy. However, due to the high cost and long processing time of the XRD analysis, it is not suitable for bulk analysis on a large volume of samples. Therefore, a mathematical approach, termed normative mineral estimation, can be used on the basis of known element concentrations, which can be easily measured by XRF spectrometer. It is experimentally proved that normative mineral estimation is useful for the determination of mineral compositions if the reference mineral selected is similar to the mineralogy of the sediment. The fewer the number of mineral types and the simpler the mineral chemical composition, the more accurate is this approach.

Mineral depletion can be estimated based on the quantitative mineralogical data obtained when parent material before weathering is defined as loess unit with highest calcite and lowest ZrO_2 or TiO_2 concentrations. Subsequently, mineral weathering

rate can be calculated if the duration of each weathered layer is provided. Using the numerical approach from the mineral dissolution model, the mineral weathering rate has been converted into runoff rates in loess and palaeosol units. However, by comparing the estimated runoff rate with the modern runoff rate at the same site, the rock weathering factor F in the model needs to be adjusted according to different lithological units and mineral types, so that the relatively accurate results can be obtained. Finally, the precipitation rates at a certain temperature can be estimated by its quantitative correlation with runoff rates.

Based on the mineral concentrations and the runoff and rainfall rates derived from the mineral dissolution model, the intensity of weathering, i.e. precipitation rate, is suggested to decrease from SE to NW loess plateau along with the climate gradient. In terms of timescale, the rainfall estimates show that the average rainfall rate has been decreasing at southeast and central Loess Plateau from 500 ky until present; while it has been increasing in the northwest Loess Plateau area during the last 130 ky. Therefore, it is suggested that there could have been a shift in the intensity of the summer and winter monsoon on the CLP from southeast to northwest at least during last 130 ky. In addition, the intensity of the summer monsoon in the southeast and central Loess Plateau area reached its maximum at about 420 ky BP rather than 600 ky BP as suggested by previous studies (Kukla and An, 1989; An et al., 1990; Xiao and An, 1999; Hao and Guo, 2005; Sun et al., 2006), and subsequently it started to decrease and the intensity of the winter monsoon increased.

On the CLP, the influence of weathering in the depositional areas on loess mineralogy is much stronger than that in the source region. However, electron microscopic and mineralogical analyses of more loess sites are needed to determine the origin of loess minerals. In addition, the L1S1 layer in loess-palaeosol sequences is known as a weathered loess layer according to its enhancement in magnetic susceptibility. This is confirmed by the mineralogical and precipitation data. However, loess units such as L2, L4 and L5 at Duanjiapo and L4 at Luochuan, have also been shown to be significantly weathered in this study, although there is no strong magnetic susceptibility signal in these units. This suggests that 1) the weathering intensity may increase from northwest to southeast Loess Plateau; and 2)

magnetic susceptibility of loess-palaeosol sequences is possibly not able to be directly used as a proxy of weathering intensity.

Mineralogical data-based the mineral dissolution model is useful and reliable for palaeoprecipitation reconstruction. However, it is still an empirical process to define the rock weathering factor F in the equation, which is largely dependent on the grain-size effect for non-clay minerals and on the accumulation rate of the loess-palaeosol sequence for silicate minerals such as chlorite. In order to further test the model and find well-defined F value for Chinese loess, more loess sections are needed for future work.

Compared with the rainfall-magnetic susceptibility climofunction, the mineral dissolution model appears to be more applicable although both of them have suffered from the 'baseline' problem. Rainfall results derived from both models have similar variation associated with the lithological units, but a larger amplitude of variation in rainfall is exhibited by the results from the mineral dissolution model. In addition, the mineral dissolution model has also well demonstrated the rainfall variation corresponding to different temperature levels, while the rainfall-susceptibility climofunction based on the modern climate data cannot well represent the temperature effect on the precipitation.

Chapter 6 Environmental change and human impact during the late Holocene: a geochemical study of sediments from Chaohu Lake, Anhui Province, East China

In order to deconvolve environmental change and human activity during the late Holocene around the Chaohu lake area, various analyses were undertaken on the sediment samples, including radiocarbon dating, magnetic susceptibility, bulk geochemical analysis, palynology and quantitative mineralogy. According to the variation of these parameters, the sediment records have been divided into four zones (A-D), and results are described and discussed within each zone. Possible human activities are also revealed mainly based on the pollen and charcoal data. Finally, quantitative mineralogical analysis (QMA) is compared with other proxies for historical environmental study.

6.1 The age model

6.1.1 Radiocarbon dates

Six calibrated AMS radiocarbon dates were obtained (See Table 6-1). Four bulk samples were used as no suitable macrofossils were found, and the other sample was dated by two different methods, using organic sediment and a macrofossil (a shell-half), respectively.

Considering all of the radiocarbon dates together, it is clear that their interpretation is not straightforward. The ages do not increase clearly with depth. There is an overlap between the dates for samples Cl-112 and Cl-130 (see Table 6-1), but this overlap is acceptable since it lies within the error range because those two samples are very close. However, the date for Cl-85 is much older than expected. It is possible that Cl-85 (square-shaped point on Figure 6-1) has been contaminated with 'old' carbon (i.e. which is significantly older than the date of its incorporation in the sediment). One possibility is the presence of carbonate from the catchment. Also noteworthy is the contradictory results for the two discrete sub-samples from Cl-41, which comprised dates for both bulk organic sediment (Cl-41a) and a half-shell (Cl-41b) found in the

sample. Sample CI-41 was closest to the sediment surface (20.25cm depth), and so should have a significantly younger radiocarbon age than the other samples. However, sample CI-41a has an age of ~1910BP; while CI-41b has a post 0BP age. Therefore, it is possible that sediments at the depths of 20.25 and 42.25cm include a significant amount of 'old' carbon materials. One possibility is that the significant amount of human activity within Yangtze Delta (including Chaohu Lake and its catchment) since ca. 2000 yr BP (Jia et al., 2008), resulted in increased input of catchment-derived material into the lake basin, perhaps including carbonate material. Taking these factors into account the decision was made to exclude dates CI-85 and CI-41b from the age model, which is based on the best fit linear regression line between the remaining dates. This age model will be used in the subsequent discussion (Chapter 6, Section 6.1).

Table 6-1 ^{14}C AMS ages and calibrated years in the Lake Chaohu sediments

Sample Name	Depth (cm)	Measured 14C Age (yr BP)	Calendar Age (cal. yr BP)	Average (cal. yr BP)
CI-41[a]	20.25	1920 +/- 40	1990 – 1830	1910
CI-41[b]	20.25	112.3 +/- 0.5 pMC*		
CI-85[a]	42.25	2360 +/- 50	2710 – 2630 2620 – 2340	2575
CI-112[a]	55.75	1420 +/- 50	1500 – 1500 1490 – 1470 1420 – 1290	1445
CI-130[a]	64.75	1400 +/- 40	1400 – 1290	1345
CI-220[a]	109.75	2000 +/- 40	2120 – 1920	2020

NB: a – the material used for dating is organic sediment; b – the material used for dating is a half-shell found in CI-41. * - pMC stands for "percent modern carbon". The result here means that Sample CI-41 could be younger than the modern reference standard (AD 1950).

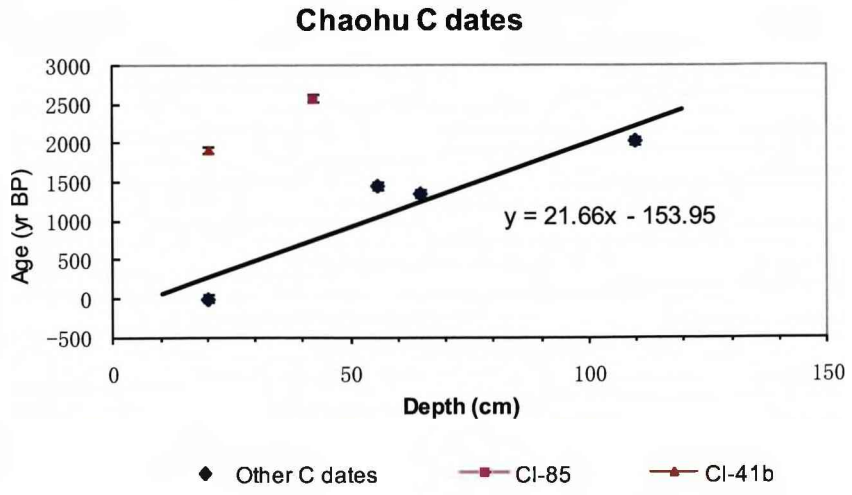

Figure 6-1 Age versus depth relationship based on the AMS radiocarbon dates for the Chaohu lake sediments.

6.1.2 Determination of the age model

As mentioned in Chapter 4 (Section 4.2.2), there are some problems with the dating results for the lake sediments. Therefore, attempts were made to refine the age model and which are described below. Based on the comparison of radiocarbon dates, low-frequency susceptibility records and pollen data from the lake core and the alluvial core, four alternative age models have been developed. In addition, another age model published in the study of Wang et al. (2008) has also been used as assistance for determining the most reliable age model.

By comparing the lake sediment core with the alluvial (ACN) core in terms of magnetic susceptibility and palynology, using correlation points chosen based on similar prominent peaks and troughs using an empirical approach (Figure 6-2), the consistency of their age records can be assessed. The ages in the ACN record are not considered more reliable, but this procedure simply increases the age information available for the site as a whole. Points from the lake sediment records were linked with their equivalent ones from the ACN records by plotting the corresponding depths from one record against the other (Figure 6-4). Correlation points from the pollen records were also selected in this way, but according to the similar shifts between different pollen taxa.

The dated depths in the ACN record could then be converted into equivalent depths in the lake sediment core, using the regressions from the correlation points shown in Figure 6-2. Using this approach, four initial age models were produced: AM1, AM2, AM3 and AM4. The first two models were developed using magnetic susceptibility correlations, because two possible correspondences were found. AM3 was created on the basis of changes in pollen stratigraphy. AM4 was developed by using both magnetic susceptibility and pollen records.

Because of the high similarity in the susceptibility variation records of the lake core and the ACN core, peak and trough points have been selected on both records. However, there are two possibilities by which the two records can be correlated – in the lake core, the prominent peaks at the depths of 107cm, 61cm, 52cm and 36cm (point 3, 5, 6 and 8 on AM1, Figure 6-2) and troughs at 120cm, 88cm and 43cm (point 1, 4 and 7 on AM1, Figure 6-2) can have two sets of correlation points on the ACN records, which formed two initial age models AM1 and AM2. AM1 places correlation points 5 and 6 at 210cm and 160cm, respectively; and AM2 places them at 380cm and 360cm, respectively (Figure 6-2). The correlation points in AM3 are determined by the variation of three major pollen and spore taxa, i.e. tree, herb and fern, where significant changes can be found in all of these taxa, e.g. correlation points 1, 2 and 3 (Figure 6-3). Comparison of the pollen and magnetic susceptibility records for both cores suggests that peaks in *Pinus* pollen correspond to minima in magnetic susceptibility irrespective of fluctuations in any of the other pollen taxa. This is because while different factors in the environment can affect the *Pinus* population, significant changes in *Pinus* population can only be affected by large-scale environmental change, which can also affect the magnetic susceptibility signals considerably. Therefore, the correlation points in age model AM4 were created using this principle (Figure 6-3).

Based on the correlation points selected on the four models, scatter plots can be developed for correlation points against depths of both the lake core and the ACN core (Figure 6-4) and four regressions can be calculated. Using these regressions, four sets of ages from the ACN core can be converted into ages for the lake core (Figure 6-5).

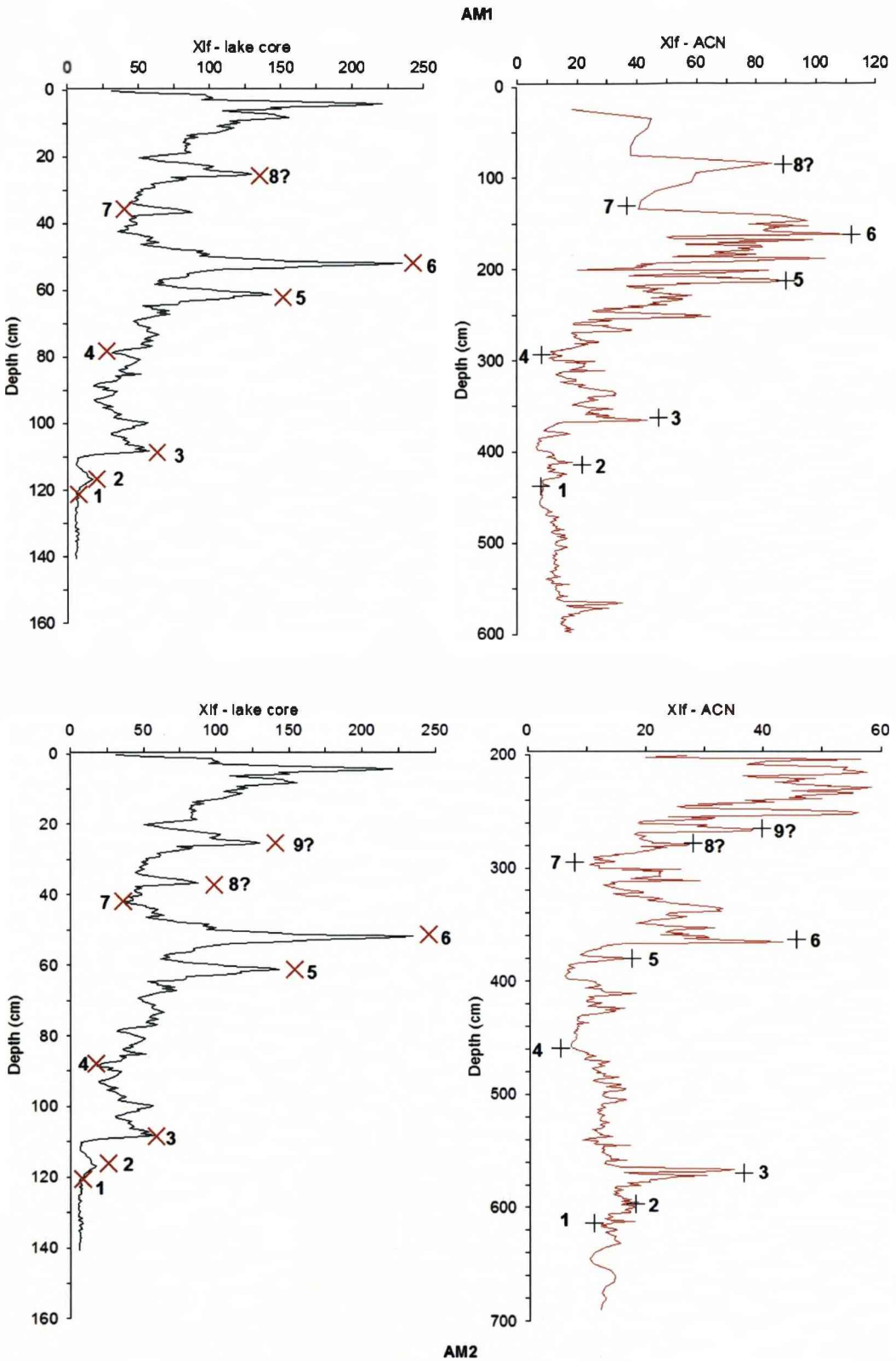

Figure 6-2 Correlation points of the initial age models AM1 and AM2. The same number on both records from the lake core and the ACN core refers to a selected correlation point. Numbers followed by a question mark refers to those points which are plausibly correlated to each other.

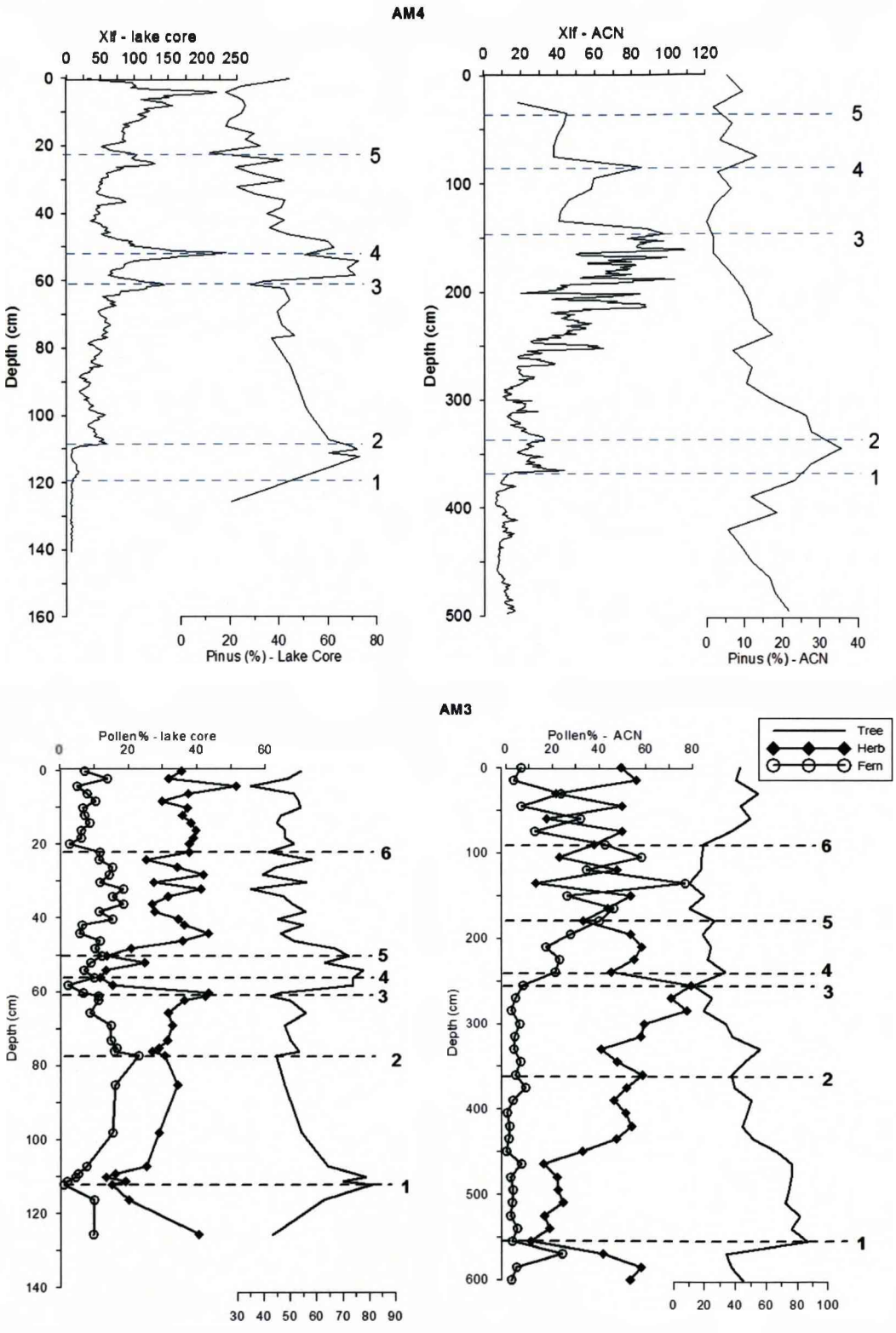

Figure 6-3 Correlation points of the initial age models AM3 and AM4. The same number on both records from the lake core and the ACN core refers to a selected correlation point.

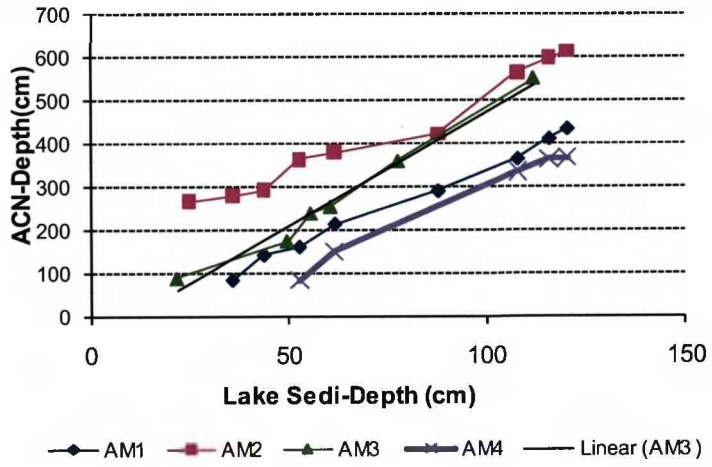

Figure 6-4 Correlation points on the depths from the lake core and ACN core.

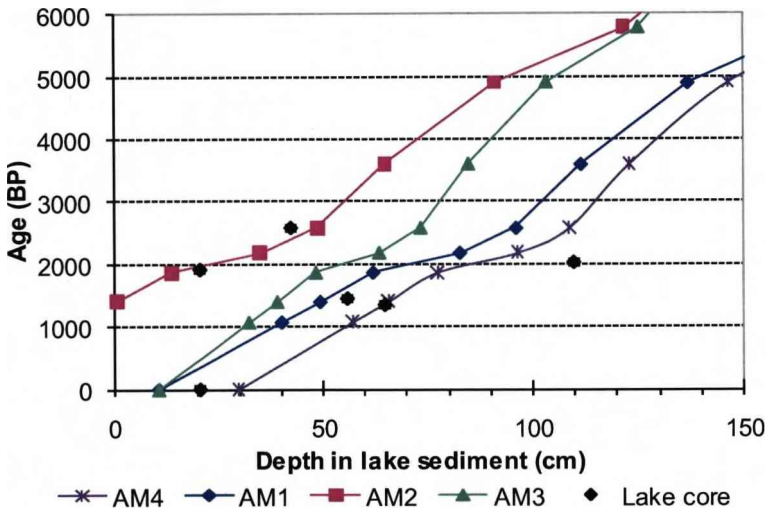

Figure 6-5 Radiocarbon dates from the lake core, and four initial age models created using correlation points. Points labelled as Lake Core refer to the radiocarbon dates from the lake sediments.

Figure 6-5 shows in the four initial age models that two radiocarbon dates from the lake core are older than any dates at the same depths shown by any of the four age models. The reason for this is unclear, but one possibility is that the top of the sediment core has been contaminated by old carbon as mentioned in Chapter 4. The other four ages seem younger than any equivalent data calculated by the age models. In addition, all the four models are scattered or non-linear with a low degree of

similarity. Therefore, it is difficult or impossible to choose an unambiguous age model based on the results available so far. However, AM1 is more plausible than the other two, since AM2 and AM3 cause a significant divergence of the Lake Core ages (Figure 6-4).

Compared with AM1 which is based on the correlation of magnetic susceptibility records from both cores, the overlap between AM4 and the measured ^{14}C AMS dates makes AM4 seem more reliable. Therefore, AM4 is the preferred age model and is used subsequently. In addition, because of the similar regression values between four of the radiocarbon ages for the lake core obtained by this study and by Wang et al. (2008), ages proposed in Figure 6-6 are also possible. Comparing AM4 and the age model in the study of Wang et al. (2008), their regressions are close to each other (Figure 6-6), especially from 0 to 150 cm. Thus, an age model (Figure 6-7) is defined as ages in the envelope margin, from which one extreme is the AM4 ages, and the other extreme is the radiocarbon dates for the lake sediment or those in the study of Wang et al. (2008). For example, the depth of 130 cm corresponds to the age of 2800 ± 500 BP. This dating system will be used for data interpretation below.

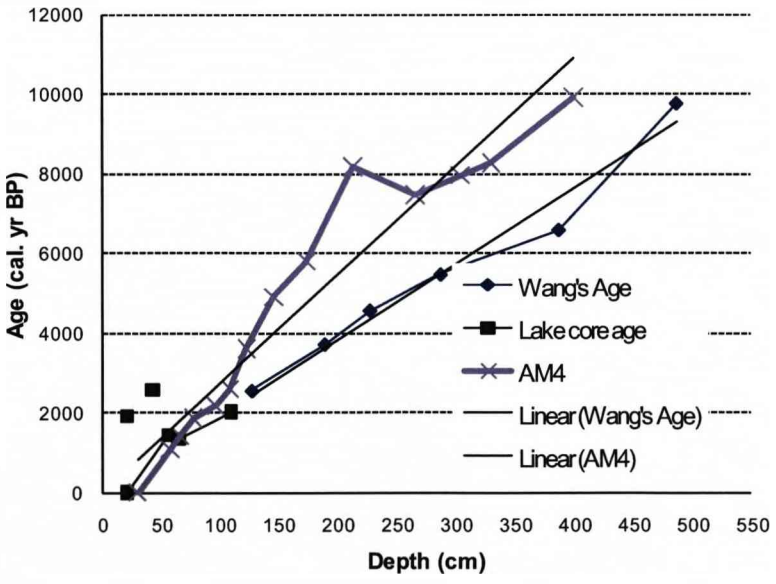

Figure 6-6 Comparison between AM4, the AMS ^{14}C dates for the Chaohu lake sediments and those dates published by Wang et al. (2008).

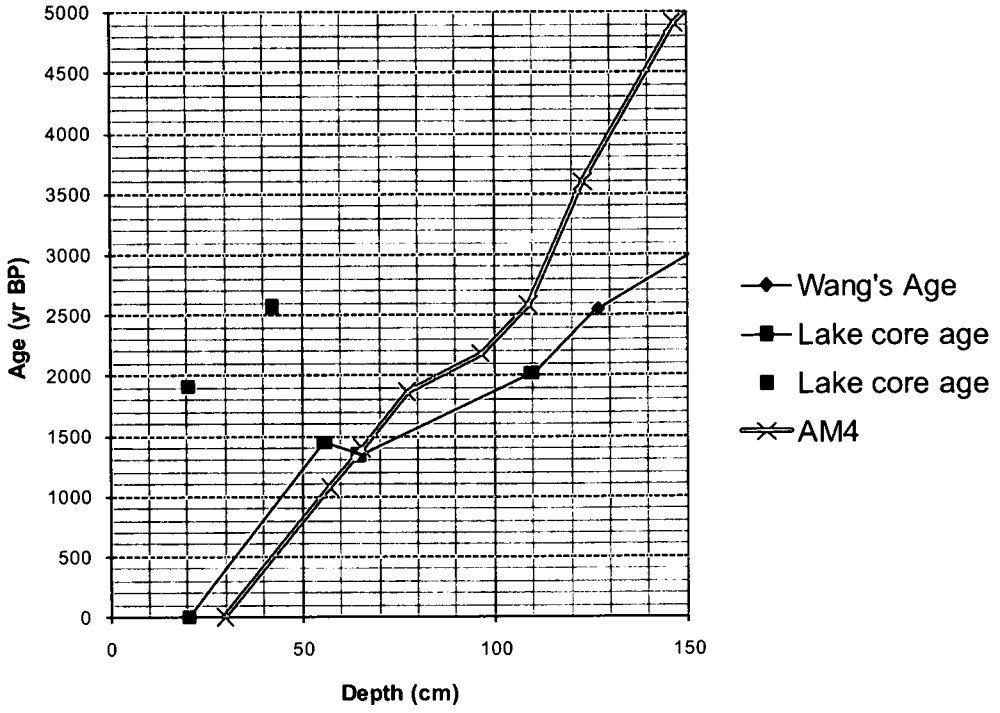

Figure 6-7 AM4 vs. the ^{14}C AMS ages of the lake sediment and those published by Wang et al. (2008). Depth in AM4 refers to the depth in ACN core converted to the depth in the lake sediment core using the regression equation of AM4. AM4 is based on the pollen and MS records.

6.2 Climate and environmental proxies

Apart from geochemistry and mineralogy, it is also important to have a good understanding of the changes in other climate and environmental proxies from the Chaohu lake sediments, so that further comprehensive interpretation can be provided on the late-Holocene environment in this area. Therefore, data from different analyses on the lake core, including magnetic measurements, bulk geochemical analysis, pollen and charcoal analysis and quantitative mineralogy, are presented in this section. A general description of the overall data is given for each climate and environmental proxy, and four zones have been defined according to the similar variations against depth in all the proxies. Detailed data description will be provided in the next section using this zonation system (Section 6.3).

6.2.1 Magnetic properties

Unpublished data for magnetic properties of the lake sediment core provided by J. Dearing (personal communication) are shown below (Figure 6-8). Because focus is

put on the mineralogy and geochemistry of the lake sediment, only two major magnetic parameters i.e. low-frequency susceptibility and frequency dependent susceptibility, have been presented here.

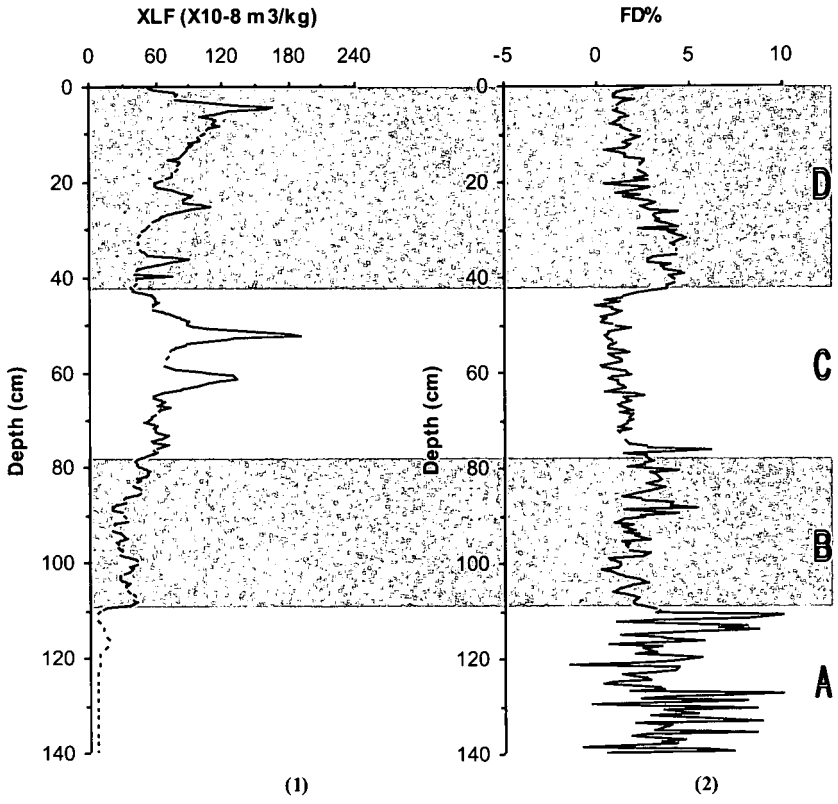

Figure 6-8 (1): Mass-specific low-field susceptibility vs. depth; (2): Percentage frequency-dependent susceptibility vs. depth

Figure 6-8-(1) shows the mass-specific low-frequency susceptibility (XLF) along with depth in the lake sediment core. It is clear that there is an overall trend of rising susceptibility upwards, except for two decreases at the depth of ~40 cm and above ~5 cm, respectively. The percentage frequency-dependent susceptibility (FD %) is calculated as:

$$FD\% = \frac{\chi_{lf} - \chi_{hf}}{\chi_{lf}} \times 100\%,$$

where χ_{lf} and χ_{hf} are the low and high frequency mass specific magnetic susceptibility, respectively.

The FD% of the sediment (Figure 6-8-(2)) shows more frequent fluctuations compared with the χ_{lf}, which is mainly measurement noise. According to the variation in χ_{lf} and FD% against depth, four zones are established to present and interpret the results: Zone A (140 – 110 cm), Zone B (110 – ca. 78 cm), Zone C (ca. 78 – ca. 42 cm), and Zone D (ca. 42 – 0 cm). Detailed interpretation for the results will be undertaken in Section 6.3.

6.2.2 Results of bulk geochemical analysis

Element concentrations and their ratios could be related to the sedimentary environment of the lake. In addition, chemical composition of the lake sediment is also considered as the primary data needed in the procedure of quantitative mineralogical analysis. Therefore, bulk geochemical analysis has been undertaken using X-ray Fluorescence spectrometry and the results are shown in Figure 6-9.

Variations of elements and low-frequency susceptibility with depth in the lake core are illustrated in Figure 6-9. The results from bulk geochemical analysis include most elements, i.e. Si, Al, Ti, Ca, Mg, K, Fe, Mn, S, P, Cl, As, Ba, Br, Cr, Cu, Ga, Ni, Nb, Pb, Rb, Sr, V, Y, Zn, Zr, and some ratios, i.e. Fe/Mn, Sr/Ca, Rb/K, Ca/K, Fe/Al, Cu/Zn and Rb/Sr. Similar to the magnetic properties, most elements have significant changes at the following depths: 110cm, 78cm, 42cm and 5cm. Therefore, the same zonation system as applied to the magnetic data is used for interpreting the bulk geochemical data. Emphasis is placed on the variation of the major elements present in the lake sediment samples. For example, elements traditionally regarded as high mobile, such as Ca, Sr, Zn and K, and those with high stability, including Fe, Mn, Al and Ti (Deer et al., 1996), will be used as indicators of chemical weathering intensity.

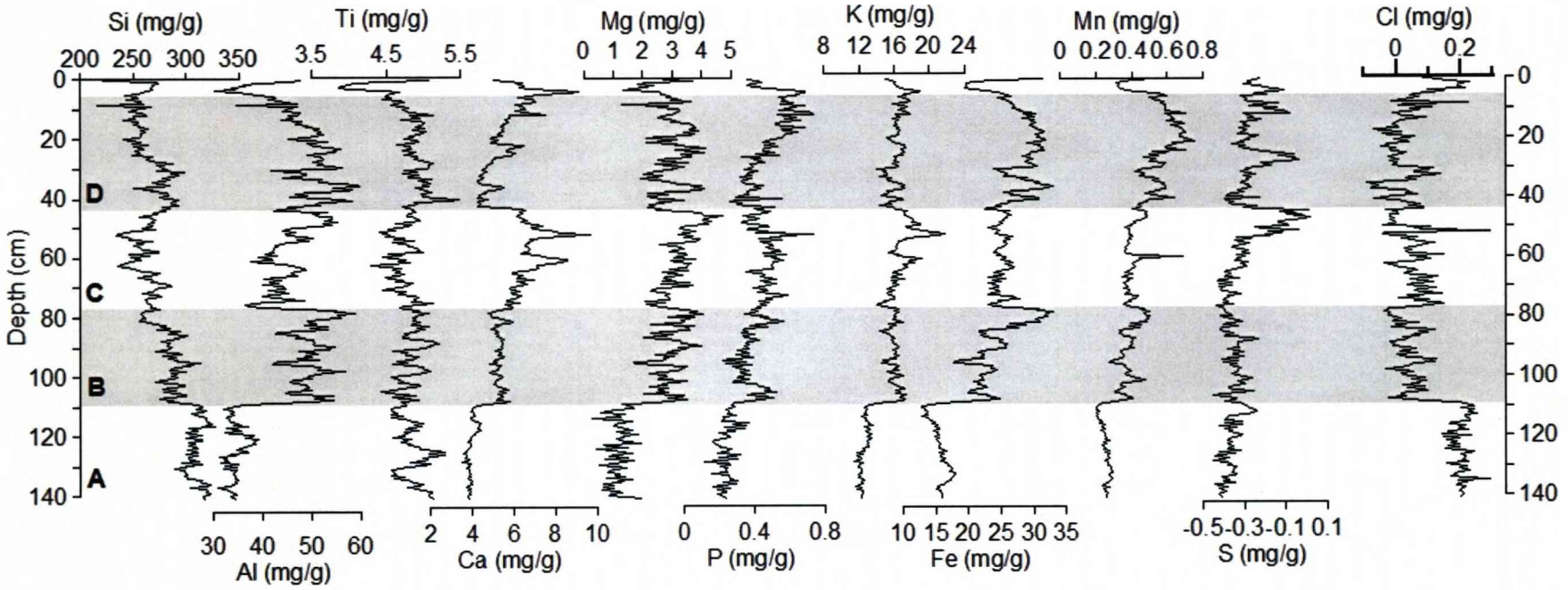

Figure 6-9 Depth variation of element concentrations, selected element ratios and low-frequency magnetic susceptibility of the lake sediment records. D-A are zones of relatively uniform element concentration. The magnetic and geochemical records of the ACN core are from X. Dai and J. Dearing (personal communication).

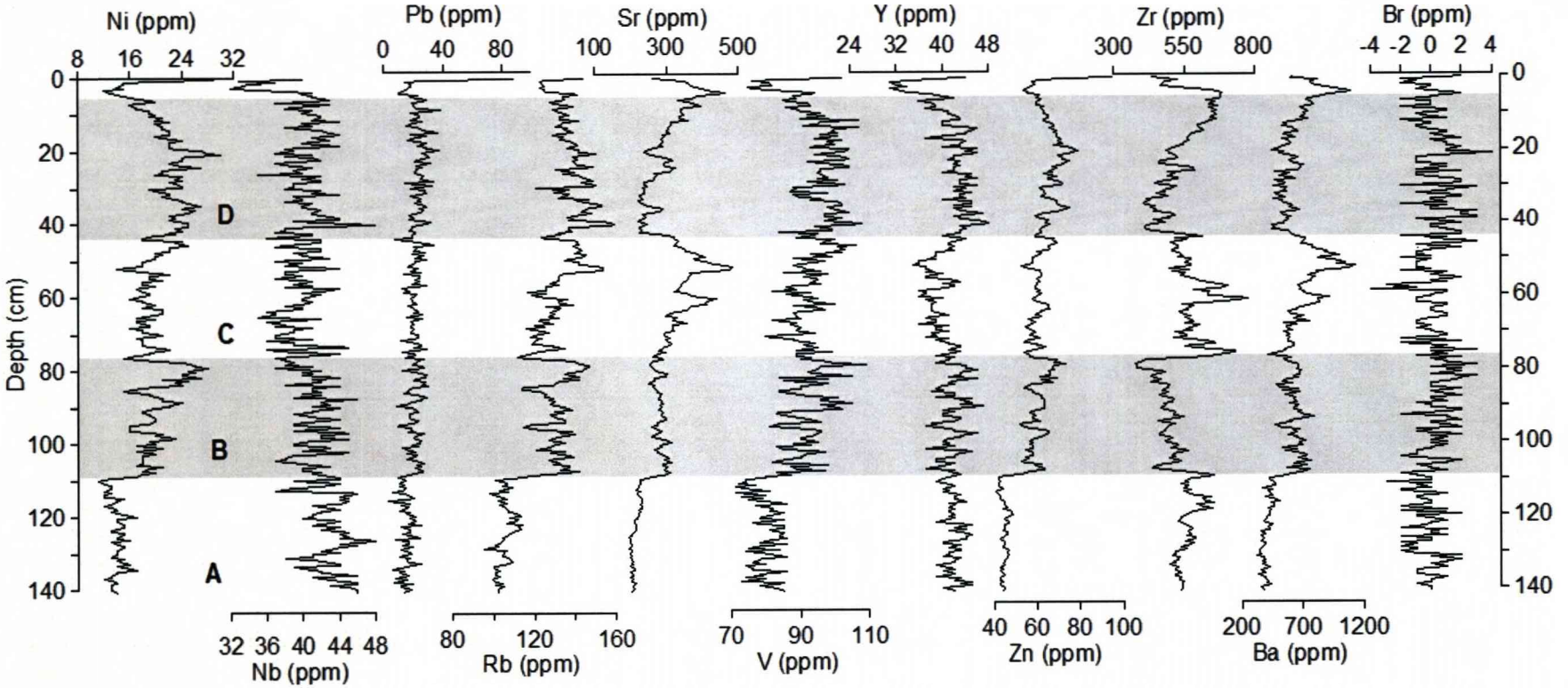

Figure 6-9 (continued)

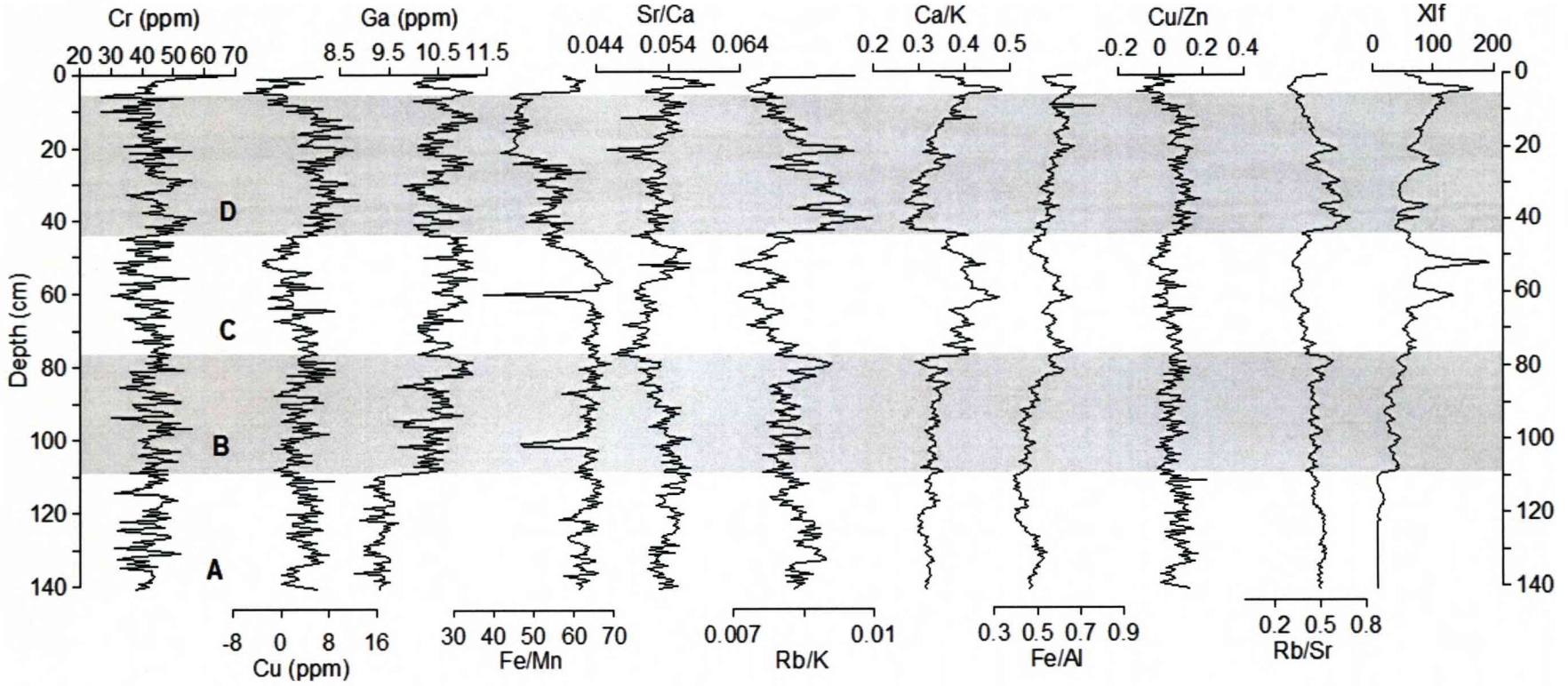

Figure 6-9 (continued)

6.2.3 Pollen and charcoal analysis

Since magnetic susceptibility, geochemistry and mineralogy of the lake sediment could be affected by variations in grain size, it is useful to use an independent proxy which is little affected by grain size and which can also provide palaeoenvironmental information. Therefore, the results of pollen and charcoal analyses of the Chaohu lake sediments were used.

Unpublished pollen data from R. Jones (personal communication) are shown in Figure 6-10. The pollen assemblages are rich in arboreal types (54.5% on average), together with the significant representation of herbaceous taxa and ferns with average values of 30.8% and 40.3%, respectively. The arboreal pollen taxa are dominated by *Pinus*, together with *Carpinus, Ulmus, Fagus, Quercus, Q.gilliana, Castanea/Castanopsis/Lithocarpus, Juglans, Pterocarya* and *Liqidambar*. The proportion of shrubs is very low, mainly composed of *Spiraea, Forsythia, Syringa, Porana, Moraceae, Capparis* and *Osmunthus*, whose percentages are all less than 0.4%. Terrestrial herbs are mainly comprised of Gramineae, with other taxa such as *Artemisia, Aster, Taraxacum,* Chenopodiaceae, Ranunculaceae, *Polygonum, Verbena, Premna* and Liliaceae. Gramineae species were divided into four groups according to size: <30μm, 30-46μm, 46-60μm and >60μm. A small amount of herb pollen types indicating wetland in this study are found including *Caryophyllaceae* and *Cyperaceae*. Monolete spores are the major fern types found in the lake sediment. Finally, there is the minor presence of various algal taxa, including *Pediastrum, Zygnema* and *Concentricystis*.

The pollen taxa presented in Figure 6-10 are those with values greater than 1% and their ecological significance in the interpretation of the palaeo-vegetation change and thus the palaeoenvironmental study (Figure 6-10). Charcoal fragments are also presented in Figure 6-10 in two groups: those with maximum diameter less than 50 μm, and those with maximum diameter greater than 50 μm. Both detailed pollen diagram and a pollen and charcoal summary graph are presented here. These data are described and discussed in Section 6.4.

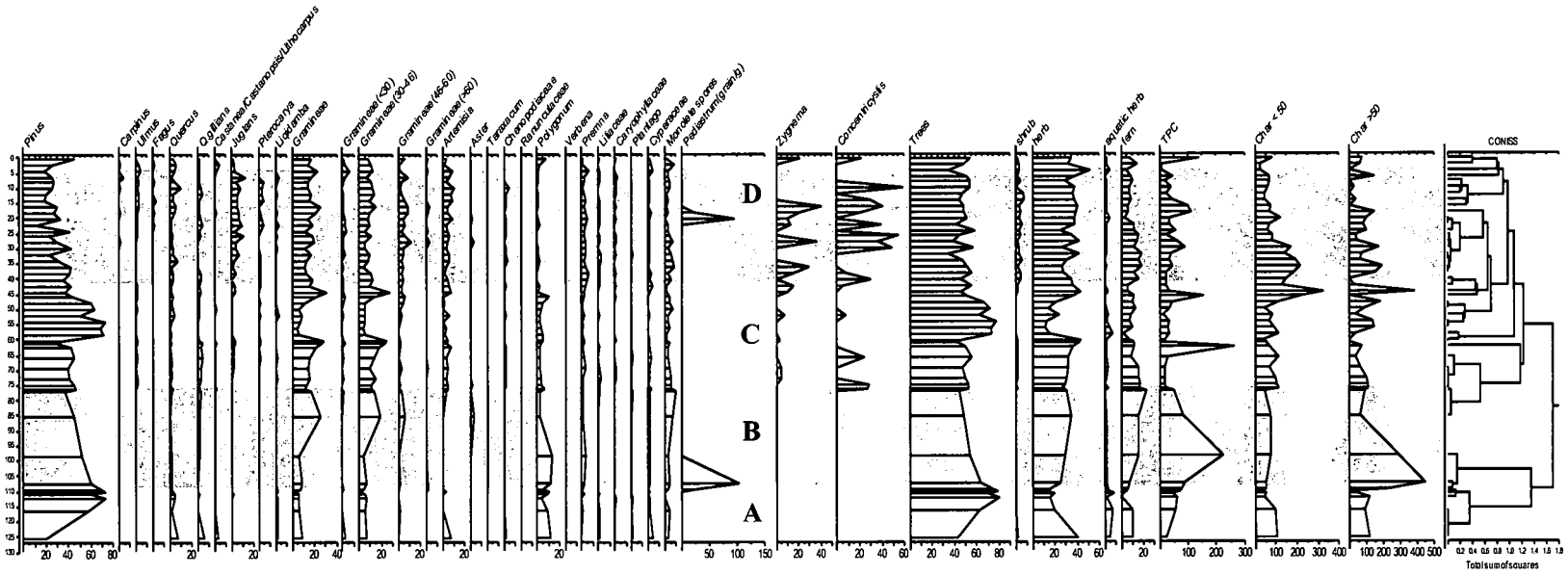

Figure 6-10 Pollen percentage diagram for the Chaohu Lake sediment core

6.2.4 Quantitative mineral estimation

The mineralogy of the lake sediments has been quantitatively analysed using the normative mineral estimation method described in Chapter 4. However, the procedure used is slightly different to that which was applied to the Chinese loess. For the Chaohu Lake sediments, the following steps were followed:

1. It can be assumed that most of the minerals within the lake sediments are from those materials carried by the Hangbu River, and which are likely to be the weathering products of granite and basalt. Therefore, it is likely that the sediment mainly contains quartz, feldspars, zircon, clay minerals, iron oxides and some mafic minerals.
2. All of the major elements were included in the calculation. The element concentrations were recalculated as wt% oxides, and the sum of the oxides was normalized to 100%.
3. Triangle plots were used to obtain oxide ratios and to examine the correlation between different oxides, and then to refine the assumptions regarding the mineral composition. Figure 6-11 shows that quartz, zircon, K-feldspar, plagioclase, biotite, illite/smectite, kaolinite, Ti oxides and Fe oxides are the minerals most likely to be present in the lake sediment. Illite/smectite and biotite are relatively Mg rich and their MgO/Al_2O_3 ratios are 0.112 and 0.413, respectively. Because the average MgO/Al_2O_3 ratio in sediment samples is about 0.05, there are two possibilities amongst the Mg-rich minerals: 1) illite/smectite dominates with some kaolinite; or 2) biotite dominates with some kaolinite. According to the clay mineralogy already obtained for the ACN core, which shows that illite comprises

most of the clay minerals in the samples (average 55.1% of the total clay; unpublished data from Chengjun Gu, personal communication), it is most likely that illite is the major clay component of the lake sediment. Therefore, the mineralogy of the lake sediments can be assumed to comprise the following minerals: quartz, zircon, K-feldspar, plagioclase, illite, kaolinite, Ti oxides (TiO_2) and Fe oxyhydroxides (FeOOH).

4. The value for each oxide was divided by its molecular weight to obtain the molar concentration in moles/100g.
5. Reference minerals for these mineral types were chosen and chemical analysis data for these reference minerals was obtained (Deer et al., 1966). The oxides in the reference minerals were are also converted into moles/100g.

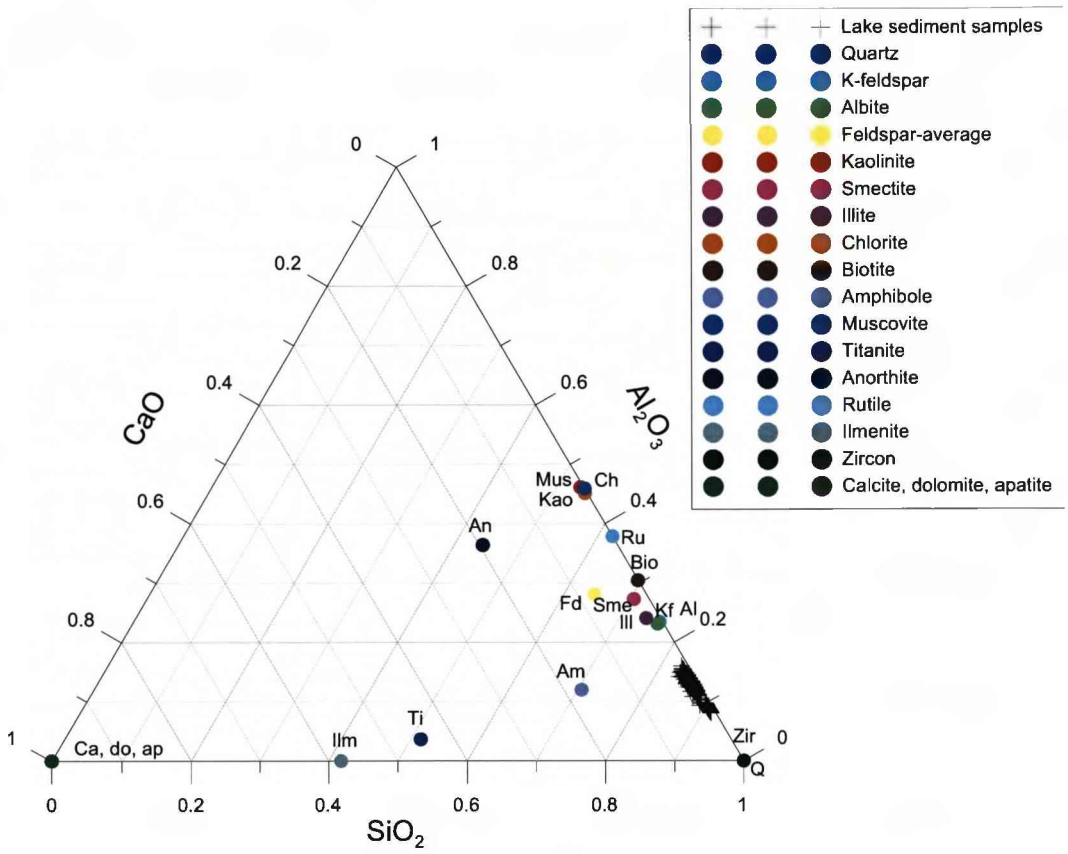

Figure 6-11 SiO_2-Al_2O_3-CaO triangle plot for lake sediment samples and reference minerals

Consequently, molar concentrations of the mineral were calculated using the reference minerals. Idealized minerals were used unless some trace elements were needed for the calculation. Zircon ($ZrSiO_4$); illite (Deer et al., 1966, p251 no. 3); K-feldspar (ibid: p300 no.10); plagioclase (ibid: p325 no. 8, $CaAl_2Si_2O_8$); kaolinite ($Al_4[Si_4O_{10}](OH)_8$); quartz (SiO_2); Ti oxides (TiO_2); Fe oxyhydroxide (in the form of FeOOH).

The distribution of the oxides to the minerals was determined as follows: after each step the total concentration of each oxide was subtracted by its concentration within the mineral of that step.

1. ZrO_2 = Zircon
2. MgO = 0.8 × Illite
3. BaO = 0.03 × K-feldspar
4. K-feldspar (K excess) = remaining $KO_{0.5}$
5. CaO = 0.961 × Plagioclase
6. Kaolinite = remaining $AlO_{1.5}$
7. Quartz = remaining SiO_2
8. Ti Oxides = remaining TiO_2
9. Fe oxyhydroxide = remaining $FeO_{1.5}$

Finally the sum for each mineral was multiplied by its molecular weight to estimate the wt% concentration (zircon: 179.22, illite: 764.796, K-feldspar: 277.6519; plagioclase: 277.4546; kaolinite: 520, quartz: 60.09; Ti oxide: 80; Fe oxyhydroxide: 89).

Comparing the K-feldspar concentrations (moles/mole) calculated from the BaO concentration and the excess of $KO_{0.5}$, the BaO based K-feldspar is higher than the other, so it is more sensible to use the K-excess based K-feldspar to calculate its weight concentration.

The results of detailed mineralogical analyses together with low-frequency susceptibility records for the lake sediments are shown in Figure 6-12. Generally, the lake sediment consists of quartz, feldspar (including K-feldspar and Ca-rich plagioclase), illite, kaolinite, and FeOOH with average weight percentages of 55%, 12%, 22%, 7%, and 3.5%, respectively. In addition minor minerals, e.g. Ti oxides and zircon, are presented because of their mineralogical significance. A more detailed discussion will be given in section 6.3 (below).

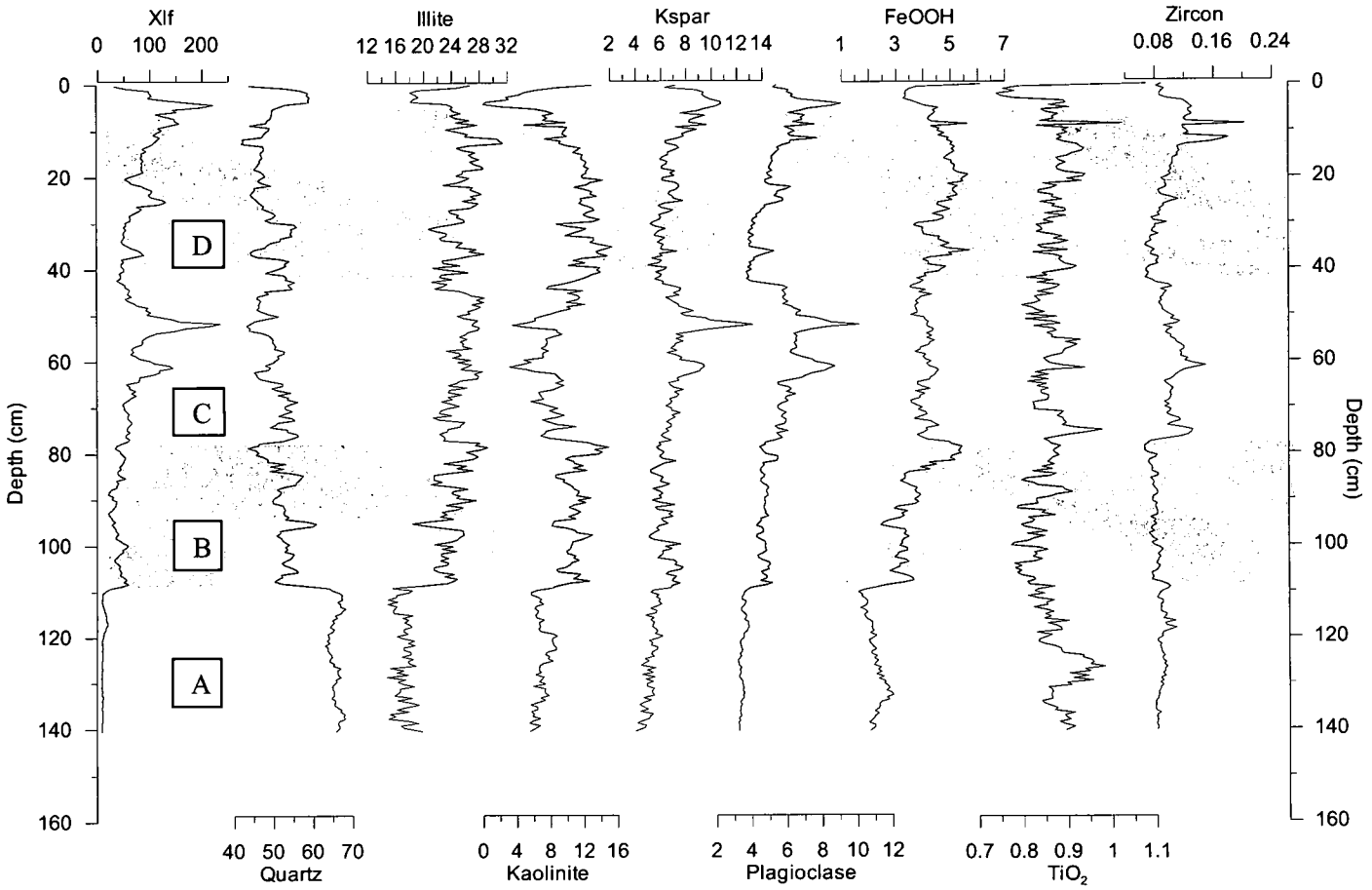

Figure 6-12 Results of quantitative mineralogy calculations together with magnetic susceptibility for the Chaohu Lake sediments. Concentrations of minerals are shown in percentage (%).

6.3 Environmental change and the evolution of Chaohu Lake during the late Holocene

According to the variations in the climate and environmental proxies, i.e. magnetic parameters (mainly low-frequency susceptibility and frequency-dependent susceptibility), bulk element analysis, pollen/charcoal analysis and mineral quantification, as discussed in Section 6.2, four zones are defined: Zone A (140 – 110 cm), Zone B (110 – ca. 78 cm), Zone C (ca. 78 – ca. 42 cm), and Zone D (ca. 42 – 5 cm). Changes in all of the various proxies are described and discussed below in the context of this zonation system. The sediment above 5 cm depth is significantly disturbed by recent local human activity (Wang et al., 2008) and is excluded from the following discussion.

6.3.1 Zone A (140 – 110 cm, 3650 ± 850 – 2300 ± 300 BP)

Elements including Ca, Sr, Zn, K, Fe, Mn and Ti in this zone are at the lowest concentrations for the entire record. Zr fluctuates around the average value of its concentration, and Si reaches its highest concentration during this interval. This implies that quartz-rich sand or silt may dominate the lithology within this zone. Ratios of Fe/Al and Rb/Sr are low and show an overall trend of decreasing values upwards, which may indicate a weakening weathering intensity resulting from cold and dry climatic conditions.

Most minerals in this interval are very low except for quartz and titanium oxides, especially quartz comprising 67% of the total material. This indicates that the lake sediment in Zone A could mainly consist of sand and/or sand silt. This possibly implies that the lake sediment mineralogy could be mainly affected by the sorting process of the lake water itself.

The values of χ_{LF} in this zone are very low and stable, around 6 – 7 $\times 10^{-8}$ m^3/kg, except for a small peak at ~115cm, and returning to a low level again at ~110cm. The variability of χ_{FD}% in Zone A is mainly noise possibly because of low concentration of magnetic minerals, as FD% can be difficult to determine when concentration of ferrimagnetic material is very low (Thompson & Oldfield, 1986). Therefore, the magnetic properties of this zone may be dominated by paramagnetic and/or diamagnetic material.

During this interval, *Pinus* pollen increases from 20% to nearly 75% and herbs and ferns decline by 20% and 10%, respectively. The total pollen concentration was relatively low. This is supported by the decreasing ratios of Fe/Al and Rb/Sr as mentioned above, consistent with a cooling and drying period between 3650 – 2300 cal. yr BP. Previous pollen analysis of the Chaohu Lake sediments (Wang et al., 2008) showed that it was cold and dry between 3760 – 2170 cal. yr BP, which supports this finding.

6.3.2 Zone B (110 – 78 cm, 2300 ± 300 – 1750 ± 150 BP)

Zr and Si concentrations decrease in this zone. Elements such as Ca, Sr, K and Zn decrease but then slightly increase at the very top of this zone. Al, K and Fe are present in much higher concentrations than in Zone A, indicating a possible increase in K-rich clays such as kaolinite and illite. This is supported by the mineralogical reconstruction: there is an abrupt increase in illite and kaolinite at a depth of 110 cm. This suggests that the lake sediments were dominated by fine silt and clay during this period.

Most minerals in Zone B, including illite, kaolinite, Fe oxyhydroxide and Ti oxide, show significant increases, at the expense of a decrease in quartz; however, the Ti oxides and zircon content show little variation.

There is an abrupt rise in both χ_{LF} and χ_{FD}% between Zone A and B, at ~110 cm. The concentration of magnetic material is clearly higher in this zone than in the preceding one. It appears to be that the 'baseline' of FD% values in Zone B has not been changed, but the amplitude is much smaller than in Zone A. This is in agreement with the decreasing Zr and Si, indicating a possible introduction of finer materials.

Within Zone B, the arboreal pollen decreased by nearly 20%, while herb pollen and ferns increased by 10% and 20%, respectively; in addition, algal taxa such as *Pediastrum* begin to occur. The vegetation within the pollen source area changed with a decline in pine forest and the increased occurrence of herbs such as Gramineae. These characteristics together with the increased abundance of illite and kaolinite in the sediment are indicative of a more stable catchment, possibly indicating a warm and wet climate during 2300 – 1750 cal. yr BP. This is also supported by increasing Fe/Al and Rb/Sr ratios.

In addition, between Zones A and B, at a depth of 110cm, there is a sudden shift in all the four proxies. This could indicate a sudden change from cold to warm phases at the age of 2300 cal. yr BP.

6.3.3 Zone C (78 – 42 cm, 1750 ± 150 – 800 ± 200 BP)

Compared with Zone B, elements like Fe, Mn, Al and Ti shows slight increases while elements like Ca, Sr, Zn and K decrease. There are decreases in Fe/Mn and Rb/Sr ratios and increases in Sr/Ca ratios. The concentrations of zircon and titanium oxides are higher in this interval, indicating an increased silt or sand/silt content. This evidence is compatible with the interpretation of a shallowing lake and drier climate (cf. Wang et al., 2005; Sly, 1978; Luo & Chen, 1997; Chen et al., 2003).

Since the formation of kaolinite is favoured by a temperate and humid environment, the decrease in kaolinite content possibly suggests a cooler and drier climate, but may also indicate a change in sediment source within the catchment. The increases in zircon and feldspar indicate a greater proportion of silt.

There are two significant peaks in χ_{LF} within this interval, at depths of ~60cm and ~52cm. However, χ_{FD}% shows a gradual decrease through the zone from ~2.5% to ~0%.

The total pollen concentration is much lower than in Zone B in spite of a slight increase at the top of Zone C. *Pinus* has slightly increased while herbs and ferns have declined slightly. In addition, it is apparent that within this zone there was more *Pinus* pollen yet less herbs and ferns after ca. 1325 a. BP (at the depth of 62 cm) than before. Pollen of the broad-leaved trees such as *Quercus* also started to increase at the depth of 62 cm. Therefore, it is suggested that a shift in environmental conditions occurred during this period, i.e. a cold and dry stage occurred before ca. 1325 a. BP and a slightly warmer and wetter phase afterwards. According to historical documents (Chu, 1973; cited in Yi et al., 2003), it was very cold in the lower Yangtzi River region during the Northern and Southern Dynasties (about AD 350–580, 1600-1370 BP), which is in agreement with the assumption made for the interval between 1750 – 1325 a. BP in Zone C.

The interval from 62cm (ca. 1325 ± 75 a. BP) to 46cm (ca. 850 ± 200 a. BP)

There are abrupt peaks in Sr, Ca, Zr, K, Mn, Ba and in the ratios of Ca/K and Fe/Al at 62cm and 53 cm depth. Feldspars significantly increased at both depths, but only at the depth of 62 cm are there peaks in Ti oxides and zircon. Thus silt/fine silt bands could be

expected at these two layers. This is also supported by the decline in quartz and kaolinite at the same time. These characteristics suggest an increased fluvial influence at these depths, which supplied more coarse material to the lake.

The pollen records show that peaks in herb pollen (predominantly Gramineae) occur at 62 cm (ca. 1325 ± 75 a. BP) and 46 cm (ca. 850 ± 200 a. BP), as well as two remarkable decreases in *Pinus* concentration. This suggests the occurrence of two relatively warm events at ca. 1325 BP and 850 BP. According to the historical literature (Chu 1973, cited Yi et al., 2003), warm periods are recorded during the Tang Dynasty (AD 618–AD 907, ca. 1332-1043 BP) and the North Song Dynasty (AD 907–AD 1127, ca. 1043-823 BP), in agreement with the findings of the present work. However, another explanation could be the expansion of agriculture in this area, because it is recorded that the area around Chaohu lake catchment had already been established as a town in the Qin Dynasty (221 and 206 BC, ca. 2170 – 2155 a. BP) (op. cit.).

There was a reverse trend between 1325 and 850 BP, as *Pinus* dominated again and herbs especially Gramineae, *Artemisia,* and *Premna* decreased. This is consistent with a cold stage. However, it is difficult to detect the factors triggering these changes, because of the combination of anthropogenic influences and changes in sedimentary environment caused by hydrodynamics.

Nevertheless, combining the observations from mineralogy and pollen data, it can be suggested that:

1) At 61 – 63 cm depth, the major influence on the lake sediment composition was the river, which supplied more terrigenous minerals to the lake - evidenced by peaks in K-feldspar, Ca-rich plagioclase, Ti oxides and zircon at 62 cm depth (ca. 1325 ± 75 a. BP). Moreover, increased fluvial activity may have affected the pollen assemblages by supplying more pollen from the catchment (e.g. grasses) into the lake, which may be the reason for the peaks in herbs dominated by Gramineae and in the total pollen concentration. This is supported by the grain size analysis on the ACN core undertaken by Jia et al. (2006), which showed a peak in mean grain size at the depth of 150 cm, corresponding to the depth of 62cm in the lake core according to the AM4 age model (Figure 6-7). Jia et al. (2006) suggested that a sand silt layer occurred during this period in the ACN core from the catchment, due to enhanced river dynamics. Wang et al. (2008) also provide evidence from their study of the lake core from Chaohu Lake, which shows a sand/silt layer at the age of~1280 a. BP.

2) The other peak in feldspars at the depth of 53cm (ca. 1100 ± 200 a. BP) is not associated with maxima in Ti oxides or zircon. In addition high concentration of tree pollen and low concentration of herb pollens, mainly Gramineae, occur at this depth, suggesting an arid period. Therefore, since abundant Ti oxides and zircon in the lake sediment are indicators of a significant amount of coarse-grained probably fluvially-derived material, the predominant factor affecting these changes in the lake was most likely a drier climate rather than hydrodynamic processes within the lake.

3) At 46 cm depth (ca. 850 ± 200 cal. yr BP), the increase in herb and sharp decrease in tree pollen may reflect a shift to a warmer and wetter climate. However, because of a sudden increase in charcoal at the same depth and the fact observed by Jia et al. (2006) that the catchment began to be filled by artificial earth-fill at ca. 850 a. BP, it can be assumed that local population started to fill in the lake marginal areas with artificial fills in order to increase the area available for cultivation (e.g. Gramineae); and for the same reason, they may also have burned the surrounding forests Additionally, since no significant changes in the mineral concentrations occur at the same time, the artificial earth-fill material can be assumed to have a similar mineral composition to the lake sediment.

6.3.4 Zone D (42 – 5 cm, 800 ± 200 BP - present).

There are decreases in Si, Ti, Rb/Sr, Rb/K and increases in Zr, Sr, Ca, K, Ba. Other elements like Mn, Cu, Al, Zn, Fe, Ni and Ti, are found increasingly concentrated from 44cm to 20 cm, while from the depth of 20 cm, these elements start to decrease until 5 cm, and then increase again towards the top of the core.

Compared with Zone C, the average values of illite and feldspars in Zone D are lower, while kaolinite is higher. However, within Zone D, illite and feldspar contents increase and kaolinite decreases. This may reflect changes in grain size of the sediment or source areas of the minerals. Iron oxyhydroxide concentrations are generally increasing, while quartz is slightly decreasing. Zircon and feldspars increase, indicating an increasing proportion of silt. The causes of these mineralogical changes in the lake sediment are not clear. The following factors are possible: 1) the increasing effects of the Hangbu River as

a major water source of the lake; 2) shrinkage of the lake, either by human activity or climate change, enabled the increased supply of coarse material to the core site; 3) from ca. 850 cal. yr BP (at the depth of ~80cm from the alluvial core) local residents started to fill the lake bank with artificial soils for agriculture (Jia et al., 2006).

A shift to higher χ_{FD}% values occurs at the Zone C/Zone D boundary (~44 cm depth) and the average χ_{FD}% value is about 1.5 – 2.0% higher in Zone D than in Zone C. After that, χ_{FD}% values decrease, while χLF values generally increase up to ca. 5cm depth with small peaks at ~35cm, 25cm and 5cm. At the top, from 5cm onwards, χLF values suddenly decline and χ_{FD}% remains the similar average value of about 2%. The sudden change in χ_{FD}% at ~44cm may suggest a shift to a finer-grained sediment during this period; however, this could be also due to the input of the artificial fill with more fine-grained material.

During this interval, although total tree pollen concentration did not change significantly, pollen of the evergreen species (e.g. *Pinus*) gradually decreased while that of the deciduous trees increased (e.g. *Quercus*, *Juglans Carpinus, Ulmus, Fagus, Q. gilliana,* and *Pterocarya)*. Total shrubs, herbs, ferns and algal taxa started to strongly increase during this period. Shrubs like *Artemisia* and *Premna* and algae like *Zygnema* and *Conentricystis* increased much more than during previous stages. This may suggest a warmer and wetter period compared to Zone C, which probably is the reason for the higher water level.

6.4 The charcoal record - Evidence for human activity

During the mid to late Holocene, the lower Yangtze River watershed was significantly affected by human activities such as deforestation and agriculture (Yi et al., 2006). Jia et al. (2006) also suggested that from 1827 ± 308 a. BP, Chaohu Lake started to be significantly affected by human activity. According to the results presented here, pollen taxa like Gramineae and *Artemisia*, regarded as indicators of human activity (Yu et al., 2000), started to increase significantly at 85 cm depth (1800 ± 150 a. BP), in agreement with Jia et al. (2006). According to the historical literature, cultivation was extensively developed in the counties of Lujiang (southwest to the lake) and Wuwei (southeast to the lake) from the Three Kingdoms Dynasty (220 – 265 AD, 1730 – 1685 a. BP) (Sima, 1084).

In general, small-sized charcoal (<50 μm) varies between 25 and 325 grains/g, and large-sized charcoal (> 50μm) varies between 0 and 450 grains/g, indicating that both regional- and local- scale fire events occurred during the late Holocene (Huang et al., 2006). In Zone A (3650 – 2300 a. BP), concentrations of small- and large- sized charcoal were at a relatively low level (~100 grains/g on average), indicating limited human activity in the catchment.

In Zone B (2300 – 1750 a. BP), small-sized charcoal was still very low (80 grains/g on average) but the large-sized charcoal increased significantly with a peak of 450 grains/g at the depth of 107 cm (2200 ± 225 a. BP), the maximum value recorded for the entire large-sized charcoal record. Although there is evidence for human settlement in the surrounding area during this period possibly, it had not reached a significant size, because

the most populous areas at that time were in North China (Zhong et al., 2006). Therefore, it is possible that the charcoal record for this interval reflects the wildfire that dominated in the local area.

At ~ 1750 a. BP, small-sized charcoal shows a sudden increase, indicating a regional fire event. This is within the Three Kingdoms Dynasty (220 – 265 AD, 1730 – 1685 a. BP), when Anhui Province became the second place for high fire occurrences (Zhong et al., 2006). However, both large- and small- sized charcoal did not changed dramatically since then until the depth of ~53cm (ca. 1100 ± 200 a. BP), where both sizes of charcoal began to increase and reached a maximum at ~43cm (ca. 700 ± 200 a. BP). This suggests that both regional- and local-scale fire events remained at a relatively low level at the beginning of Zone C until 1100 ± 200 a. BP, but then started to increase significantly between 1100 and 700 a. BP. According to the historical literature, the national economic centre began to move southwards at 755 AD (1195 a. BP), and had completely moved to the south by the late Southern Song Dynasty (1127 AD–1279 AD, 823 – 671 a. BP) (Zhong et al., 2006). The increase in charcoal occurs within this period. Additionally, during ca. 1100 – 700 a. BP, a significant drop in tree pollen and a sudden decrease in herb pollen especially Gramineae and *Artemisia* are associated with the charcoal peak, suggesting that deforestation was carried out to increase the area available for agriculture.

After 700 a. BP, both sized charcoal groups were relatively abundant in the lake sediment until ~32cm (300 ±200 a. BP), suggesting that human-set fire events were frequent due to the intense human activity. This is also supported by the fact that the high fire occurrences moved to the middle and lower reaches of the Yangtze River including

Anhui Province during the Yuan and Ming Dynasties (671 – 306 a. BP) (Zhong et al., 2006). Because no significant decrease in trees is evident during this period, it could be concluded that no large-scale deforestation has occurred in the area in spite of the frequent fire events at that time. From 300 a. BP to the present, charcoal concentration was decreasing and the historical observation shows that the population was moving back to northeastern China during this interval (Zhong et al., 2006). Assuming that the increase of charcoal during this time is mainly due to the contemporary man-made firing activities, it probably can suggest that the decreasing charcoal contents may be a result of the migration from this region to northeast China after 300 a. BP.

From 1800 a. BP, large-sized charcoal shows a similar pattern of variation with the small-sized charcoal, indicating that local fire history is closely correlated with regional-scale human activity. Since then the lake and its catchment were significantly affected by human disturbance, especially in Zone D (800 a. BP – present), where agriculture has been well developed and the catchment has been filled with artificial soils (Jia et al., 2006).

6.5 Results of quantitative mineralogical analysis (QMA) compared with other environmental and climate proxies

6.5.1 QMA vs. magnetic susceptibility

Magnetic susceptibility and related rock magnetic parameters have already been used to estimate the concentration, grain size and mineralogy of magnetic mineral assemblages in lake sediments (e.g. Dearing, 1999; Shen et al., 2005; Thompson and Oldfield, 1986). The magnetic parameters used at the Chaohu Lake (mainly χ_{LF} and χ_{FD}%) can reflect the

changes in grain size and concentration of the magnetic minerals within the lake sediment, and which may in turn reflect changes in the grain-size and composition of the detrital materials coexisting with them. However the magnetic mineral content of rocks, soils and sediments is typically only a minor proportion of the total mineral assemblage, and thus magnetic measurements alone cannot be used to characterize bulk mineralogy. In contrast, QMA provides a more reliable measure of changes in bulk mineral concentration and composition.

The iron minerals in the lake sediment are quantified in the form of iron oxyhydroxide (FeOOH), which cannot provide further details of its composition as magnetic susceptibility does. It is difficult to distinguish different magnetic minerals by using QMA only. Therefore, QMA is not suitable for detailed magnetic mineralogical analysis, unless it is known that a single type of magnetic mineral or distinguishable species of these minerals are present in the samples.

6.5.2 QMA vs. bulk geochemical analysis

Bulk geochemical analysis can provide estimates of element concentrations in the lake sediment. It is crucial for QMA, as mineral estimation is based on the element concentrations; but these two approaches are still different. In this case, although element concentrations and their ratios are useful for characterising changes in mineralogy and grain size within lake sediments which can then be used to reconstruct environmental and climate change, there are still many uncertainties in the use of this approach. QMA can show the variation of minerals. For example, due to the high mobility of Ca in calcite and relative stability of Ca in Ca-feldspars, it is difficult to define the correlation between Ca

content and environmental change because there are various processes that can affect it. If QMA is used, however, particular types of Ca-rich minerals can be calculated; therefore more detailed interpretation is possible with regard to the environmental effect on these minerals.

In comparison with bulk geochemical analysis, the drawback of QMA based on normative methods is that it can only estimate the concentrations of those major and minor minerals with simple chemical compositions, and therefore changes in those trace elements that have not been used in the QMA calculation cannot be assessed. Some of them may have geochemical and mineralogical significance. For example, the high variability of Sr in feldspars and biotite results in the various Sr concentrations in different species of feldspars and biotite. This makes the selection of reference minerals more difficult and complicates the mineral calculation procedure. Therefore, in the present study Sr is not included in the QMA calculation, but its chemical mobility may be important for understanding the mechanism affecting the lake water.

Therefore, it is better to combine both methods when interpreting mineralogical and chemical data for palaeoenvironment study. In addition, bulk geochemical analysis can also be considered as a preparatory stage for QMA as described in Chapter 4.

6.5.3 QMA vs. grain size analysis

The grain-size distribution of lake and stream sediments is an important source of information on the hydrodynamics of Lake Catchment systems. As mentioned above, QMA can provide qualitative information on sediment grain-size changes, because of the

tendency for particular minerals to occur within specific grain size fractions. In the case of Chaohu Lake, for example, variations in K-feldspar, zircon, and titanium oxides content have been used to infer variations in grain size. Clearly, the use of sieving, gravitational settling, and laser and X-ray analysis provides more precise grain-size data. However, QMA can provide useful complementary information by indicating the nature of possible changes in sediment source that are accompanied by changes in sediment grain size. In addition, a potential weakness of conventional grain size analysis is that it cannot accurately reflect any mineralogical variations. In other words, even if the grain size does not change significantly, the lake sediment could still show a large alternation between different mineral groups. For example, the sharp increase in feldspars and decrease in kaolinite and quartz at the depth of 53 cm (ca. 1100 ± 200 a. BP) are not clearly demonstrated in the grain size records of Wang et al. (2008).

6.6 Summary and Conclusions

According to the mineralogical, magnetic and geochemical analyses of the Chaohu lake sediments, combined with reference to published pollen, charcoal and grain size data from both the lake core and the alluvial core (ACN core) (Jia et al., 2006; Wang et al., 2008), environmental changes and the evolution of the Chaohu Lake can summarized in the following four stages:

1) 3650 – 2300 a. BP: The lake sediment during this interval mainly consists of sand or sand/silt. The sedimentary environment is mainly lacustrine. It was cold and dry in the region around the lake. There is no evidence of human activity at this stage.

2) 2300 – 1750 a. BP: More terrigenous materials were transported into the lake because the fluvial system was enhancing its influence on the lake. The sediment in the interval is mainly composed of clays and fine silts. More herbs and ferns were growing at the catchment and its surrounding area, while the amount of trees was decreasing. The lake was expanding during this period and the water depth was increasing. At ca. 2300 a. BP, the climate has changed significantly – from cold and dry to warm and wet conditions. Human activity began to occur, associated with the development of agriculture in this region at ca. 1800 a. BP. This is reflected by the significant representation of taxa associated with human activity, e.g. Gramineae and *Artemisia*.

3) 1750 – 800 a. BP: During this period, the lake was possibly shrinking under the arid climate conditions resulting in increased fluvial influence at the core site which caused more coarse-grained material to be deposited. According to the variation in the lake sediment mineralogy during this period, it is concluded that sedimentation was affected by alternating fluvial and lacustrine influences. Changes in vegetation and mineralogy during this stage were determined by hydrological, climate and anthropogenic factors. At ca. 1325 a. BP, much more terrigenous minerals (possibly sand/silt) were brought into the lake, indicating the river flux may have dominated the hydrodynamics at that time. At ca. 1100 a. BP, significantly more feldspars occurred, and the most likely cause for this is drier climate conditions based on the pollen observations. At ca. 850 a. BP, the shift between trees and herbs is possibly due to the artificial soil filling for cultivation and slash-and-burn agriculture. After a sudden cooling phase at ca. 1750 a. BP, the

climate conditions in this region started to fluctuate. It was generally less temperate and humid than during the previous stage, although it could still have been warmer than during the first stage (3650 – 2300 a. BP). During this period, however, at least two warm phases occurred: at ca. 1325 a. BP and later at ca. 850 a. BP.

4) ca. 800 a. BP – present: Feldspar-rich silt was increasing in the lake sediment although clay minerals i.e. kaolinite and illite were still abundant. The enhancements of the fluvial effects on the lake and the intense human disturbance are suggested for this period. The climate seems to have been increasingly warm and wet again from ca. 800 a. BP.

Human settlement at the catchment of the Chaohu Lake began at ca. 1800 a. BP, but its influence on the environment was weak until 1100 a. BP. During 1100 – 700 a. BP, there was a boost in human activities, leading to relatively large-scale deforestation because of agricultural burning. This is possibly because of the population migration from North to East China. After this period, human activity was kept in a relatively high level till 300 a. BP, when the population started to migrate back to Northeast China again. Although human disturbance at the catchment was very frequent since 700 a. BP, no large loss of forest has been found, meaning that the deforestation level could be relatively low here during this period.

Compared with other climate and environmental proxies, mineral quantitative estimation appears to be more applicable to the lake sediment. It can be used for qualitative grain size determination like mineral magnetism and grain size analysis do, for climate and

environmental reconstruction like palynology does, and for the lake evolution study like bulk geochemical analysis does. None of these approaches is perfect. It is better to be mixed with other methods to get a more comprehensive understanding on the limnological sedimentology.

Chapter 7 Overall Conclusions

According to the studies undertaken on the two typical landforms in China, quantitative mineralogical analysis is proved to be applicable for reconstructing historical climate and environmental changes in different timescales and localities. Mineral compositions of samples are calculated by normative mineral analysis approach for both sites. The values obtained by this method coincide with those by XRD quantification model except for the feldspar groups. Comparing with other climate and environmental proxies, quantitative mineralogy appears to be more easily applied to interpretation from data into environmental changes. However, it does not mean quantitative mineralogy is an all-around method. Other methods are still needed for supplementary information, some of which could even be essential for the preparation of quantitative mineralogical analysis, such as bulk geochemical analysis. Therefore, the new quantitative mineralogical approach is actually an integrated system with different geochemical and mineralogical methods/parts, including mineral identification, bulk geochemical analysis and the calculation of mineral compositions.

It is also suggested in this study that rainfall rates calculated by the mineral dissolution model have similar variation with those values obtained from susceptibility-rainfall climofunction model in spite of higher amplitude in variation found in the former. However, the former model seems work better in more arid areas. Nevertheless, both models have similar problems: 1) the 'baseline problem'. The 'parent soil' before weathering is defined empirically, which could result in problematic baseline and thus faulty precipitation estimation; and 2) the 'temperature effect'. White and Blum (1995) have suggested the coupling of precipitation and temperature and indicated that the positive relationship between rainfall and weathering rates can increase exponentially with increasing temperature. In the susceptibility-rainfall climofuntion model, this has not been demonstrated properly, while the mineral dissolution model has provided different possibilities in rainfall

rates according to different levels of temperature, although it is still difficult to find out the average temperature for individual weathered soil units.

This study shows that the new quantitative mineralogical method and the numerical model can be applied to different landforms for reconstructing palaeoclimate and historical environmental change. It fills the gap that no detailed and comprehensive mineralogical analysis has been conducted on geochemical sediment records for environmental change study. It can also help improve the understanding of the effect of changes in weathering intensity and duration on mineral composition within sediment, and the relationship between mineral chemical weathering and East Asian Monsoon regime. From this respect, this study has its significance in palaeoclimate study, although improvement and refinement of constants and reference minerals are needed and a selection of various sites is necessary for further study on the approach in order to avoid site-specific problems.

References

An Z.S., Wang J.D, Li H.M., 1977. Paleomagnetic research on the Luochuan loess section. *Geochemica,* 6(4): 239-249 (in Chinese).

An Z., 2000. The history and variability of the East Asian palaeomonsoon climate. *Quaternary Science Reviews,* 19: 171-187.

An, Z. S., T. S. Liu, Y. C. Lu, S. C. Porter, G. Kukla, X. H. Wu, and Y. M. Hua (1990), The long-term paleomonsoon variation recorded by the loess-paleosol sequence in central China, *Quat. Int.*, 7/8: 91–95.

Anderson & Hallett, 1996. Simulating Magnetic Susceptibility Profiles in Loess as an Aid in Quantifying Rates of Dust Deposition and Pedogenic Development. *Quaternary Research*, 45: 1–16.

Baiying Agriculture, n.d.. [online] URL: http://www.bynw.gov.cn/read.asp?NewsID=3730&BigClassID=24&SmallClassID=80&SpecialID=0 [Accessed 10/01/2007]

Barnosky C.W., 1984. Late Miocene Vegetational and Climatic Variations Inferred from a Pollen Record in Northwest Wyoming. *Science*, 223: 49-51.

Bartlein P.J., Prentice I.C. & Webb T.III, 1986. Climateic response surfaces from pollen data for some eastern North American taxa. *Journal of Biogeography*, 13:35-57.

Bausch & Lomb Nanolab Scanning Electron Microscope, n.d. [online], Earth Sciences Department, Simon Fraser University, Canada. URL: http://www.sfu.ca/~marshall/sem/mineral.htm [accessed 11/06/2008]

Beig M.S. and Luttge A., 2006. Albite dissolution kinetics as a function of distance from equilibrium: Implications for natural feldspar weathering. Geochimica et Cosmochimica Acta, 70 :1402–1420.

Betancourt J.L. and Devender T.R., 1981. Holocene Vegetation in Chaco Canyon, New Mexico. *Science*, 214: 656-658.

Bowers T.S., Jackson K.J., and Helgeson H.S., 1984. Equilibrium activity diagrams for coexisting minerals and aqueous solutions at pressures and temperatures to 5 kb and 600 °C, Springer-Verlag, Berlin.

Boyle J.F., 2000. Rapid elemental analysis of sediment samples by isotope source XRF. *Journal of Paleolimnology*, 23: 213-221.

Boyle J. F., 2001. Inorganic Geochemical Methods in Palaeolimnology. In Last W. M. & Smol J.P. (eds.) *Tracking Environmental Change Using Lake Sediments. Volume 2:*

Physical and Geochemical Methods. Kluwer Academic Publishers, Dordrecht, The Netherlands. Chapter 5, pp. 83-141.

Boyle J.F., 2007. Simulating long-term weathering loss of primary silicate minerals from soil using ALLOGEN: comparison with soil chronosequence, lake sediment, and river solution flux data. *Geomorphology*, 83: 121-135.

Boyle J.F., 2008. Climate and surface water acidity: development and application of generalized predictive model. *The Holocene*, 18(1): 69-81.

Bloemendal J. & Liu X., 2005. Rock magnetism and geochemistry of two plio-pleistocene Chinese loess-palaeosol sequences – implications for quantitative palaeoprecipitation reconstruction. *Palaeogeography, Palaeoclimatology, Palaeoecology*, 226 (1-2): 149-166.

Bronger A., Winter R., Sedov S., 1998. Weathering and clay mineral formation in two Holocene soils and in buried paleosols in Tadjikistan: towards a Quaternary paleoclimatic record in Central Asia. *Catena*, 34:19–34.

Burney D.A., 1987. Late Quaternary stratigraphic charcoal records from Madagascar. *Quaternary Research*, 28(2): 274-280.

Butzer K.W., 1963. Climate-geomorphologic interaction of Pleistocene sediment in the Eurafrican subtropics. In Bourliere F. and Howell C.F. (Eds.) *African Ecology and Human Evolution.*, Metbuen & Co. Ltd., London. Chapter 1, pp. 1-27.

Campbell, I.D., and Campbell C., 1994. Pollen preservation: experimental wet-dry cycles in saline and desalinated sediments. *Palynology*, 18:5-10.

Cao, J. X., Zhang, Y. T., Wang, J. M., 1997. Temporal and Spatial Characteristics of Loess Magnetic Susceptibility in the Yuanbao Loess Sect ion and the Climatic Change over the Past 150 000 Years. *Journal of Lanzhou University (Natural Sciences)*, 33 (1): 124-132 (in Chinese).

Catt J.A., 1990. Palaeopedology Manual. *Quaternary International*, 6: 1-95.

Chen F.H., Bloemendal J., Wang J.M., Li J.J., Oldfield F., 1997. High-resolution multi-proxy climate records from Chinese loess: evidence for rapid climatic changes over the last 75 kyr. *Palaeogeography, Palaeoclimatology, Palaeoecology*, 130: 323-335.

Chen J., An Z., Head J., 1999a. Variation of Rb/Sr Ratios in the Loess-Palaeosol Sequences of Central China during the Last 130,000 Years and Their Implications for Monsoon Palaeoclimatology. *Quaternary Research*, 51: 215–219.

Chen F.H., Bloemendal J., Feng Z.D., Wang J.M., Parker E., Guo Z.T., 1999b. East Asian monsoon variations during Oxygen Isotope Stage 5: evidence from the

northwestern margin of the Chinese loess plateau. *Quaternary Science Reviews*, 18: 1127-1135.

Chen J., Ji J., Balsam W., Chen Y., Liu L., An Z., 2002. Characterization of the Chinese loess-paleosol stratigraphy by whiteness measure. *Palaeogeography, Palaeoclimatology, Palaeoecology*, 183: 287-297.

Chen L., Zhang L., Wang H., Zhou L., Chen J. and Yuan B., 2005. Two different illites in Luochuan loess, Northern Shaanxi Province. *Chinese Science Bulletin,* 50(1): 82-87.

Clark J.S., 1988. Stratigraphic charcoal analysis on petrographic thin sections: Application to fire history in northwestern Minnesota. *Quaternary Research*, 30(1): 81-91.

Chen J.A., Wang G.J., Zhang F., Zhang D.D., Huang R.G., 2003. Reconstructing environmental changes from lake sediments under various timescales using grain size analysis. *Science in China (Series D)*, 33(6): 563-568 (in Chinese).

Chu K.C., 1973. A preliminary study on the climatic fluctuations during the last 5,000 years in China. *Scientia Sinica*, 16: 226–256.

Climate database for Chinese Loess Plateau, Scientific database website, Chinese Science Academy, n.d. [online]. URL: http://www.csdb.cn/viewdb.jsp?uri=cn.csdb.loess.clim [Accessed date: 13/03/2009] (in Chinese)

CSDB, n.d.. Climate database at the Chinese Loess Plateau. [online] In *Chinese Scientific Database.* URL: http://www.loess.csdb.cn/index.jsp?app=clim [Accessed on 12/03/2008]

Cushing, E.J. 1964. Redeposited pollen in late-Wisconsin pollen spectra from east-central Minnesota. *Amer. J. Sci.*, 262:1075-1088.

Davis J.C., 1973. *Statistics and data analysis in geology*. Wiley, USA.

Day, R., Fuller, M., Schmidt, V. A., 1977. Hysteresis properties of titanomagnetites: grain-size and compositional dependence. *Phys. Earth Planet. Inter.*, 13: 260–267.

Dearing J.A., Battarbee R.W., Dikau R., Larocque I., Oldfield F., 2006. Human–environment interactions: learning from the past. *Reg Environ Change*, 6: 1–16. DOI 10.1007/s10113-005-0011-8

Dearing, J.A., 1999. Holocene environmental change from magnetic proxies in lake sediments. In Maher B.A. and Thompson R. (Eds.) *Quaternary Climates, Environment and Magnetism*, Cambridge: Cambridge University Press.

Deer W.A., Howie R.A. & Zussman J., 1966. *An introduction to the Rock-forming Minerals*. John Wiley & Sons Inc., New York.

Delcourt, P.R. and Delcourt, H.R. 1980. Pollen preservation and Quaternary environmental history in the southeastern United States. *Palynology*, 4:215-231.

Deng C., Yuan B., Zhu R., 2000. Magnetic susceptibility of Holocene loess-black loam sequence from Jiaodao profile of china before and after Citrate-Bicarbonate-Dithionite extraction. *Chinese Journal of Geophysics*, 43(4): 505–514.

Deng C., Shaw J., Liu Q., Pan Y., Zhu R., 2006. Mineral magnetic variation of the Jingbian loess/paleosol sequence in the northern Loess Plateau of China: Implications for Quaternary development of Asian aridification and cooling. *Earth and Planetary Science Letters*, 241: 248–259.

Derbyshire E., Kemp R.A. and Meng X.M., 1995. Variations in loess and palaeosol properties as indicators of palaeoclimatic gradients across the Loess Plateau of North China. *Quaternary Science Reviews*, 14: 681-697.

Derbyshire E., Kemp R., 1997. Climate change, loess and palaeosols: proxy measures and resolution in North China. *Journal of the Geological Society*, London154: 793–805.

Dilks A. and Graham S.C., 1985. Quantitative Mineralogical Characterization of Sandstones by Back-Scattered Electron Image Analysis. *Journal of Sedimentary Research*, 55(3): 347-355.

Ding Z.L., Yang S.L., Sun J.M., Liu T.S., 1999. Pedostratigraphy and palaeomagnetism of a ~7.0 Ma aeolian loess–red clay sequence at Lingtai, Loess Plateau, north-central China and the implications for palaeomonsoon evolution. *Palaeogeography, Palaeoclimatology, Palaeoecology*, 152: 49–66.

Ding Z.L., Sun J.M., Yang S.L., Liu T.S., 2001. Geochemistry of the Pliocene red clay formation in the Chinese Loess Plateau and implications for its origin, source provenance and paleoclimate change. *Geochimica et Cosmochimica Acta*, 65(6): 901–913.

Ding Z. L., Derbyshire E., Yang S. L., Yu Z. W., Xiong S. F., and Liu T. S., 2002. Stacked 2.6-Ma grain size record from the Chinese loess based on five sections and correlation with the deep-sea $D^{18}O$ record. *Palaeoceanography*, 17(3): 5.1-5.21.

Ding Z.L. and Yang S.L., 2001. Iron geochemistry of loess and red clay deposits in the Chinese Loess Plateau and implications for long-term Asian monsoon evolution in the last 7.0 Ma. *Earth and Planetary Science Letters*, 185: 99-109.

Dixon, J.B., Weed, S.B., 1989. Minerals in soil environments. *Soil Science Society of America (SSSA)*, Book Series, vol. 1.

Dultz S., 2002. Effects of parent material and weathering on feldspar content in different particle size fractions from forest soils in NW Germany. *Geoderma,* 106: 63–81.

Dunne, T., 1978. Rates of chemical denudation of silicate rocks in tropical catchments. *Nature*, 274: 244-246.

Eberl D.D., 2003. User guide to RockJock-A program for determining quantitative mineralogy from powder X-ray Diffraction data, *US Geological Survey Open File Report* [online]. URL: http://www.ccp14.ac.uk/ccp/ccp14/ftp-mirror/mudmaster-galoper/pub/ddeberl/RockJock/RockMan4.pdf [Accessed on 11/06/2007]

Eberl D.D., 2006. RockJock model (version 5), [online]. *USGS*. URL: ftp://brrcrftp.cr.usgs.gov/pub/ddeberl/RockJock [accessed 01/06/2007]

Eberl D.D. and Smith D.B., 2009. Mineralogy of soils from two continental-scale transects across the United States and Canada and its relation to soil geochemistry and climate. *Applied Geochemistry*, 24(8): 1394-1404.

Elton N.J. and Smith D.K., 1999. Minerals and ceramics: Silica. In Chung F.H. and Smith D.K. (eds.), *Industrial applications of X-ray diffraction.* Marcel Dekker Inc., USA. Chapter 17.

Evans M.E. & Heller F., 2001. Magnetism of loess/palaeosol sequences: recent developments. *Earth-Science Reviews*, 54: 129–144.

Evans M.E. & Rokosh C.D., 2000. The last interglacial in the Chinese Loess Plateau: a petromagnetic investigation of samples from a north-south transect. *Quaternary International*, 68-71: 77-82.

FitzPatrick E.A., 1993. *Soil Microscopy and Micromorphology*. Wiley, Chichester.

Florindo F., Zhu R., Guo B., Yue L., 1999. Magnetic proxy climate results from the Duanjiapo loess section, southernmost extremity of the Chinese loess plateau. *Journal of Geophysical Research*, 104 (B1): 645-659.

Garrels R.M. & Mackenzie F. T., 1971. *Evolution of Sedimentary Rocks*, p.381-383. W. W. Norton & Company, Inc. New York.

Gu Z. Y., Lal D., Liu T. S., Guo Z. T., Southon J. and Caffee M. W., 1997. Weathering histories of Chinese loess deposits based on uranium and thorium series nuclides and cosmogenic ^{10}Be. *Geochimica et Cosmochimica Acta*, 61 (24): 5221-5231.

Guo Z.T., Liu T.S., Fedoroff N. and An, Z.S., 1993. Monsoon strength variations in the Loess Plateau before and after 0.85 Ma. *Chinese Science Bulletin*, 38: 143–146.

Guo Z.T., Fedoroff N., Liu D.S., 1996a. Micromorphology of the loess-paleosol sequence of the last 130 ka in China and paleoclimatic events. *Science in China (Series D)*, 39(5): 468-477 (in Chinese).

Guo, Z.T., Ding, Z.L. and Liu, T.S., 1996b. Pedosedimentary events in loess of China and Quaternary climate cycles. *Chinese Science Bulletin*, 41: 1189–1193.

Guo Z., Liu T., Fedoroff N., Wei L., Ding Z., Wu N., Lu H., Jiang W., An Z., 1998. Climate extremes in Loess of China coupled with the strength of deep-water formation in the North Atlantic. *Global and Planetary Change*, 18: 113–128.

Guo, Z., Biscaye P., Wei L., Chen X., Peng S., and Liu T., 1999. Summer monsoon variation over the last 1.2Ma from the weathering of loess-soil sequences in China. *Geophysical Research Letters*, 27 (12): 1751–1754.

Guo B. and Zhu R.X., 2001. Lack of correlation between paleoprecipitation and magnetic susceptibility of Chinese loess/paleosol sequences. *Geophysical Research Letters*, 28(22): 4259-4262.

Guo, Z.T., Ruddiman, W.F., Hao, Q.Z., Wu, H.B., Qiao, Y.S., Zhu, R.X., Peng, S.Z., Yuan, B.Y., & Liu, T.S., 2002. Onset of Asian desertification by 22 Myr ago inferred from loess deposits in China. *Nature*, 416: 159-163.

Gylesjų S. and Arnold E., 2006. Clay mineralogy of a red clay-loess sequence from Lingtai, the Chinese Loess Plateau. Global *and Planetary Change*, 51: 181–194

Han J., Lu H., Wu N., Guo Z.,, 1996. The magnetic susceptibility of modern soils in China and its use for palaeoclimate reconstruction. *Studia geoph. Geod*, 40: 262-275.

Han J., Fyfe W.S., Longstaffe F.J., 1998. Climatic Implications of the S5 Paleosol Complex on the Southernmost Chinese Loess Plateau. *Quaternary Research,* 50(1): 21-33.

Hao, Q., and Guo Z., 2005. Spatial variations of magnetic susceptibility of Chinese loess for the last 600 kyr: Implications for monsoon evolution, *Journal of Geophysidcal Research*, 110: B12101, doi:10.1029/2005JB003765.

Havinga A.J., 1974. An experimental investigation into the decay of pollen and spores in various soil types. In J. Brooks et al, (eds.), *SPOROPOLLENIN*, Academic Press. pp. 446-479

He H.C., Ding H.Y., Zhang Z.K., Shi X.D., Li S.H., Mao L.J., 2005. Grain-size Characteristics and Their Environmental Significance of Hongze Lake Sediments. *Scientia Geographica Sinica*. 25(5). (in Chinese)

Heller F. & Evans M.E., 1995. Loess magnetism. *Reviews of Geophysics,* 33: 211-240.

Heller F. & Liu T. S., 1982. Magnetostratigraphical dating of loess deposits in China. *Nature*, 300: 431–433.

Heller F. and Liu T.S., 1984. Magnetism of Chinese loess deposits. *Geophys. J. R. Astr. Soc.*, 77: 125–141.

Heslop D., Langereis C.G., Dekkers M.J., 2000. A new astronomical timescale for the loess deposits of Northern China. *Earth and Planetary Science Letters*, 184:125-139.

Heslop D., Dekkers M.J., Kruiver P.P., van Oorschot I.H.M., 2002a. Analysis of isothermal remanent magnetization acquisition curves using the expectation–maximization algorithm. *Geophys. J. Int.*, 148: 58–64.

Heslop D., Dekkers M.J., Langereis C.G., 2002b. Timing and structure of the mid-Pleistocene transition: records from the loess deposits of northern China. *Palaeogeography, Palaeoclimatology, Palaeoecology*, 185: 133-143.

Hill R.J., and Howard C.J., 1987, Quantitative phase analysis from neutron powder diffraction data using the Rietveld method. *Journal of Applied Crystallography*, 20: 467–474.

Huang C., Pang J., Chen S., Su H., Han J., Cao Y., Zhao W., Tan Z., 2006. Charcoal records of fire history in the Holocene loess-soil sequences over the southern Loess Plateau of China. *Palaeogeography, Palaeoclimatology, Palaeoecology*, 239 (1-2): 28-44. ISSN 0031-0182, DOI: 10.1016/j.palaeo.2006.01.004. (http://www.sciencedirect.com/science/article/B6V6R-4JF8JNC-2/2/82371e8cb70707a49c4bf0a4a35fc08b)

Huang, X., Chen, F., Xiao, S., Lv, Y., Chen, J., Zhou, A., 2008. Primary study on the environmental significances of grain-size changes of the Lake Bosten sediments. *Journal of Lake Sciences*, 20(3): 291-297.

Huntley B., 1992. Pollen-climate response surfaces and the study of climate change. In Gray J.M. (ed.) *Applications of Quaternary Research*, Quaternary Proceedings, 2, Quaternary Research Association, Cambridge, pp. 91-99.

Jahn B., Gallet S. and Han J., 2001. Geochemistry of the xining, Xifeng and Jixian sections, Loess Plateau of China: Aeolian dust provenance and paleosol evolution during the last 140 ka. *Chemical Geology*, 178(1-4): 71-94.

Jeong G.Y., Hillier S., Kemp R.A., 2008. Quantitative bulk and single-particle mineralogy of a thick Chinese loess-paleosol section: implications for loess provenance and weathering. *Quaternary Science Reviews*, 27(11-12): J 1271-1287.

Ji J., Chen J. and Lu H., 1999. Origin of illite in the loess from the Luochuan area, Loess Plateau, Central China. *Clay Minerals*, 34: 525-532.

Ji J., Balsam W., Chen J., 2001. Mineralogic and climatic interpretations of the Luochuan loess section (China) based on Diffuse Reflectance Spectrophotometry. *Quaternary Research*, 56: 23–30.

Jia, T.F., Dai X.R., Zhang W.G., Yu L.Z., 2006. Sediment records in Chaohu Lake and its significance on environmental change in Holocene. *Scientia Geographyica Sinica*, 26(6): 706-711. (in Chinese)

Jiang H. and Ding Z., 2005. Temporal and spatial changes of vegetation cover on the Chinese Loess Plateau through the last glacial cycle: evidence from spore-pollen records. *Review of Palaeobotany and Palynology*, 133: 23– 37.

Jones M.P., 1982. Designing an X-ray image analyser for measuring mineralogical data. *XIV Int.Min.Proc.Cong.*, Toronto, VIII-4.1 - 4.17.

Jorgensen P., 1977. Some properties of Norwegian tills. *Boreas*, 6: 149-157.

Kalm V.E., Rutter N.W., Rokosh C.D., 1996. Clay minerals and their paleoenvironmental interpretation in the Baoji loess section, Southern Loess Plateau, China. *Catena*, 27: 49-61.

Kemp R.A., 1985. Soil Micromorphology and the Quaternary. *Technical Guide No. 2*, Quaternary Research Association, Cmbridge.

Kemp R.A., 1996. Role of micromorphology in paleopedological research. *Quaternary International*. 51-52: 133-141.

Kemp R.A., 1999. Micromorphology of loess–paleosol sequences: a record of paleoenvironmental change. *Catena*, (35): 179–196.

Kemp R.A., 2001. Pedogenic modification of loess: significance for palaeoclimatic reconstructions. *Earth-Science Reviews*, 54: 145–156.

Kemp R.A., Derbyshire E., Meng X., 2001. A high-resolution micromorphological record of changing land scapes and climates on the western Loess Plateau of China during oxygen isotope stage 5. *Palaeogeography, Palaeoclimatology, Palaeoecology*, 170: 157-169.

Ketterings Q.M., Bigham J.M. and Laperche V., 2000. Changes in soil mineralogy and texture caused by slash-and-burn fires in Sumatra, Indonesia. *Soil Science Society of America Journal*, 64:1108-1117.

Krauskopf K.B. and Bird D. K., 1995. *Introduction to Geochemistry* (3rd ed.). McGraw-Hill, Inc., New York, pp 647.

Kretzschmar R., Robarge W.P., Amoozegar A., Vepraskas M.J., 1997. Biotite alteration to halloysite and kaolinite in soil-saprolite profiles developed from mica schist and granite gneiss. *Geoderma*, 75: 155-170.

Kukla G.J., Heller R., Liu X.M., Xu T.C., Liu T.S., and An Z.S., 1988. Pleistocene climates in China dated by magnetic susceptibility. *Geology*, 16: 811–814.

Kukla, G., and An Z. S., 1989. Loess stratigraphy in central China. *Palaeogeography, Palaeoclimatology, Palaeoecology*, 72: 203–225.

Leonard R.A. and Weed S.B., 1970. Mica weathering rates as related to mica type and composition. *Clay Miner.*, 18: 187-195.

Li G., Ji J., Zhao L., Mao C., Chen J., 2008. Response of silicate weathering to monsoon changes on the Chinese Loess Plateau. *Catena*, 72(3): 405-412. Available at : http://www.sciencedirect.com/science/article/B6VCG-4PMJB69-1/2/f906055d9a113dca2300efd877bee41a [accessed on 12/01/2009]

Li Y., Wang N., Morrill C., Cheng H., Long H., Zhao Q., 2009. Environmental change implied by the relationship between pollen assemblages and grain-size in N.W. Chinese lake sediments since the Late Glacial. *Review of Palaeobotany and Palynology*, 154(1-4): 54-64. URL: http://www.sciencedirect.com/science/article/B6V6W-4V74VG2-2/2/b9abe19009cdbd4a176a5d1d58dc8c1e [accessed on 11/10/2009]

Liu T.S., 1985. *Loess and Environment*. Science Press, Beijing (in Chinese).

Liu X.M., Bloemendal J., Rolph T., Pedogenesis and paleoclimate: Interpretation of the magnetic susceptibility record of Chinese loess-paleosol sequences: comments and reply. *Geology*, 22: 857–860.

Liu X.M., Hesse P., Rolph T., 1999. Origin of maghaemite in Chinese loess deposits: aeolian or pedogenic? *Physics of the Earth and Planetary Interiors*, 112: 191–201.

Liu Q., Banerjee S.K., Jackson M.J., 2003. Paleoclimatic significance of magnetic properties on the Red Clay underlying the loess and paleosols in China. *Palaeogeography, Palaeoclimatology, Palaeoecology*, 199: 153-166.

Liu Q., Banerjee S.K., Jackson M.J., Chen F., Pan Y., Zhu R., 2004a. Determining the climatic boundary between the Chinese loess and palaeosol: evidence from Aeolian coarse-grained magnetite. *Geophys. J. Int*, 156: 267-274.

Liu Q., Banerjee S.K., Jackson M.J., Deng C., Pan Y., Zhu R., 2004b.New insights into partial oxidation model of magnetites and thermal alteration of magnetic mineralogy of the Chinese loess in air. *Geophys. J. Int*, 158: 506-514.

Lowe J.J. & Walker M.J.C., 1997. *Reconstructing Quaternary Environments* (2nd Edition). Longman, Essex. p. 112-113

Lu H., Liu X., Zhang F., An Z. and Dodson J., 1999. Astronomical calibration of loess–paleosol deposits at Luochuan, central Chinese Loess Plateau. *Palaeogeography, Palaeoclimatology, Palaeoecology*, 154: 237–246.

Luo J.Y. & Chen Z.D., 1997. The mountain lake sediment in Taiwan as an indicator for the last 4000 yr climate and environmental changes. *Science in China (Series D)*, 27(4): 366 – 372. (in Chinese)

Lyon R.J.P., Tuddenhan W.M., Thompson C.S., 1959. Quantitative mineralogy in 30 minutes. *Economic Geology*, 54: 1047-1055.

Mack G. H. and Suttner L. J., 1977. Paleoclimate interpretation from a petrographic comparison of Holocene sands and the Fountain Formation (Pennsylvanian) in the Colorado Front Range. *Journal of Sedimentary Research*, 47(1): 89-100.

Maher B.A., 1998. Magnetic properties of modern soils and Quaternary loessic palaeosols: palaeoclimatic implications. Palaeogeography, *Palaeoclimatology, Palaeoecology*, 137: 25-54.

Maher B.A., Thompson R., Zhou L.P., 1994. Spatial and temporal reconstructions of changes in the Asian palaeomonsoon: A new mineral magnetic approach. *Earth and Planetary Science Letters*, 125: 461-471.

Maher B.A., Alekseev A., Alekseeva T., 2003. Magnetic mineralogy of soils across the Russian Steppe: climatic dependence of pedogenic magnetite formation. *Palaeogeography, Palaeoclimatology, Palaeoecology*, 201: 321-341.

Microanalytical Laboratory, Earth and Planetary Sciences [online], McGill University, Canada URL: http://www.eps.mcgill.ca/~lang/EDSSPEC/edshome.html [accessed on 11/06/2008]

Miller P.R., Reid A.F., Zuiderwyk M.A., 1982. QEM*SEM image analysis in the determination of modal assays, mineral association and mineral liberation, *XIV Int.Min.Proc.Cong.*, Toronto, VIII- 3.1 - 3.20.

Mullins, C.E., 1977. Magnetic susceptibility of the soil and its significance in soil science: a review. *J. Soil Sci.*, 28: 223–246.

Pal D. K., Srivastava P., Durge S. L., Bhattacharyya T., 2003. Role of microtopography in the formation of sodic soils in the semi-arid part of the Indo-Gangetic Plains, India, *Catena*, 51 (1): 3-31, ISSN 0341-8162, DOI: 10.1016/S0341-8162(02)00092-9. (http://www.sciencedirect.com/science/article/B6VCG-4700V23-1/2/fca86aa7fe9c6a8fdd607c22b190bd8f)

Parker E.J., 1999. *An assessment of environmental magnetics and particle size distribution analyses as proxies for variations in the intensity of the East Asian Monsoon*. Thesis Ph.D. Liverpool University.

Parker E.J., Bloemendal J., 2005. Aeolian process and pedogenesis under the influence of the East Asian monsoon: A statistical approach to particle-size distribution variability. *Sedimentary Geology*, 181: 195-206.

Patterson III W. A., Edwards K.J., Maguire D.J., 1987. Microscopic charcoal as a fossil indicator of fire. *Quaternary Science Reviews*, 6 (1): 3-23.

Petruk W., 1988. The capabilities of the microprobe Kontron image analysis system: application to mineral analysis. *Scanning Microscopy*, 2: 1247-1256.

Porter S.C., 2001. Chinese loess record of monsoon climate during the last glacial–interglacial cycle. *Earth-Science Reviews*, 54: 115–128.

Porter S.C. and Hallet B., 2001. Dependence of Near-Surface Magnetic Susceptibility on Dust Accumulation Rate and Precipitation on the Chinese Loess Plateau. *Quaternary Research*, 55: 271–283.

Pye K. & Croft D.J. (eds), 2004. *Forensic geoscience: principles, techniques and applications*. Geological Society, London, Special Publications, 103-122.

Rivière J.C., Myhra S. (eds), 1998. *Handbook of surface and interface analysis: methods for problem-solving*. Marcel Dekker Inc., New York. 643-667.

Rutter N., Ding Z., Evans M.E. and Wang Y., 1990. Magnetostratigraphy of the Baoji loess-palaeosoil section in the north central China loess plateau. *Quaternary International*, 7(8): 97–102.

Sima G., 1084. *Zizhi Tongjian* (Comprehensive Mirror to Aid in Government). In Chinese.

Sly P. G., 1978. Sedimentary processes in lakes. In Lerman A. (ed). *Lakes: Chemistry, Geology, Physics*. New York: Spring – Verlag. 65 - 90.

Srivastava P., 2001. Paleoclimatic implications of pedogenic carbonates in Holocene soils of the Gangetic Plains, India. *Palaeogeography, Palaeoclimatology, Palaeoecology*, 172: 207-222.

Suchet A. P. and Probst J.L., 1993. Modeling of Atmospheric CO_2 Consumption by Chemical Weathering of Rocks: Application to the Garonne, Congo, and Amazon Basins. *Chemical Geology*, 107: 205-210.

Sun W., Banerjee S.K., Hunt C.P., 1995. The role of maghemite in the enhancement of magnetic signal in the Chinsese loess-palaeosol sequence: an extensive rock magnetic study combined with citrate-bicarbonate-dithionite treatment. *Earth and Planetary Science Letters*, 133: 493-505.

Sun Y., An Z, Zhou J. and Lu X., 2000. Dry bulk density of loess samples measured by the oil-soaked method (in Chinese). *Geological Review*, 46(2): 220-224

Sverdrup H. and Warfvinge P., 1988. Weathering of primary silicate minerals in the natural soil environment in relation to a chemical weathering model. Water, Air, and Soil Pollution, 38: 387-408.

Sun, Y. B., Clemens S. C., An Z. S. and Yu Z. W., 2006. Astronomical timescale and palaeoclimatic implication of stacked 3.6-Myr monsoon records from the Chinese Loess Plateau. *Quat. Sci. Rev.*, 25, 33–48.

Sweatmean T.R. and Long J.V.P., 1969. Quantitative Electron-probe Microanalysis of Rock-forming Minerals. *Journal of Petrology*, 10(2): 332-79.

Syvitski, J.P.M., 1991. Principles, *methods and application of particle size analysis*. Cambridge University Press.

Talma, A. S. & Vogel, J. C., 1993. A Simplified Approach to Calibrating C14 Dates. *Radiocarbon*, 35(2): 317-322.

Taylor J.C., 1991. Computer programs for standardless quantitative analysis of minerals using the full powder diffraction profile. *Powder Diffraction*, 6: 2–9.

Taylor, J.C., and Matulis, C.E., 1991. Absorption contrast effects in the quantitative XRDanalysis of powders by full multiphase profile refinement. *Journal of Applied Crystallography*, 24: 14–17.

Tang et al., 2003. Records of magnetic properties in Quaternary loess and its paleoclimatic significance: a brief review. *Quaternary International*, 108: 33-50.

Thompson & Oldfield, 1986. *Environmental Magnetism*. Allen & Unwin, London, pp. 11–18

Tite, M., Linington, R.E., 1975. Effect of climate on the magnetic susceptibility of soils. *Nature* , 256: 565–566.

Torrent J., Barrón V., Liu Q.S., 2006. Magnetic enhancement is linked to and precedes hematite formation in aerobic soil, *Geophys. Res. Lett.*, 33, L02401.

Torrent J., Liu Q.S., Bloemendal J., Barrón V., 2007. Magnetic Enhancement and Iron Oxides in the Upper Luochuan Loess–Paleosol Sequence, Chinese Loess Plateau. *Soil Sci. Soc. Am. J.*, 71(5):1570–1578.

Tsatskin A., Heller F., Gendler T. S., Virina E. I., Spassov S., Du Pasquier J., Hus J., Hailwood E. A., Bagin V. I., Faustol S. S., 2001. A New Scheme of Terrestrial Paleoclimate Evolution During the Last 1.5 Ma in the Western Black Sea Region: Integration of Soil Studies and Loess Magmatism. *Phys. Chem. Earth (A)*, 26(11-12): 911-916.

Turc, L. 1954. Calcul du bilan de l'eau evaluation en fonction des precipitations et des temperatures. *IASH Rome Symposium*, 111 Publication no. 38, 188–202.

Uhlik P. and Eberl D.D., 2006. Evaluation of powder XRD data using the MUDMASTER and ROCKJOCK computer programs. *Acta Mineralogica Petrographica*, Abstract Series 5, Szeged.

Vidic N.J., Singer M.J., Verosub K.L., 2004. Duration dependence of magnetic susceptibility enhancement in the Chinese loess-palaeosols of the past 620 ky. *Palaeogeography, Palaeoclimatology, Palaeoecology*, 211: 271-288.

Wan G.J., Bai Z.G., Qing H., Mather J.D., Huang H.R., Tang D.G. and Xiao B.H., 2003. Geochemical records in recent sediments of Lake Erhai: implication for environmental changes in low latitude-high altitude lake in Southwest China. Journal of Asian Earth Sciences, 21(5): 489-502.

Wang X. Y., He H., Qian Y. C., 2005. An inference of ancient JUCHAO city based on environment archaeology. *J Anhui Norm Univ (Nat Sci)* (in Chinese), 28(1): 97-102

Wang Y., Yang J., Chen J., Zhang K., Rao W., 2007. The Sr and Nd isotopic variations of the Chinese Loess Plateau during the past 7 Ma: Implications for the East Asian winter monsoon and source areas of loess. *Palaeogeography, Palaeoclimatology, Palaeoecology,* 249 (3-4): 351-361.

Wang X.Y., Zhang G.S., Wu L., Zhang X.H., Zhang E.L., Xiao X.Y., Jiang Q., 2008. Environmental changes during early-middle Holocene from the sediment record of the Chaohu Lake, Anhui Province. *Chinese Science Bulletin*, 53 (Supp. I): 153-160.

Ward C.R., Taylor J.C., Cohen D.R., 1999. Quantitative mineralogy of sandstones by X-ray Diffractometry and normative analysis. *Journal of Sedimentary Research*, 69(5): 1050 – 1062.

Webb, T. III and Bryson, R., 1972. Late and postglacial climatic change in the northern Midwest USA: quantitative estimates derived from fossil pollen spectra by multivariate statistical analysis. *Quaternary Research*, 2: 70-115.

White A.F. and Blum A.E., 1995. Effects of climate on chemical_ weathering in watersheds. *Geochimica et Cosmochimica Acta*, 59(9): 1729-1747. URL: http://www.sciencedirect.com/science/article/B6V66-3YYTK9C-77/2/836b940ebfbc1afb7d8b63ffc88fcb4a [accessed on 01/11/2009]

White A.F., Blum A.E., Schulz M.S., Bullen T.D., Harden J.W., Peterson M.L., 1996. Chemical weathering rates of a soil chronosequence on granitic alluvium: I. Quantification of mineralogical and surface area changes and calculation of primary silicate reaction rates. *Geochimica et Cosmochimica Acta*, 60(14): 2533-2550. URL: http://www.sciencedirect.com/science/article/B6V66-3VW7RX2-1C/2/4dc7debbfbe3450ed079013d63c80b5f [accessed on 01/11/2009]

Wright Jr. H.E., Kutzbach J.E., Webb T.III, Ruddiman W.F., Street-Perrott A.F. & Bartlein P.J.(eds), 1993. *Global climates since the Last Glacial Maximum*. University of Minneapolics Press, Minnesota.

Xiao, J. L., and An Z. S., 1999. Three large shifts in East Asian monsoon circulation indicated by loess-paleosol sequences in China and late Cenozoic deposits in Japan, *Palaeogeogr. Palaeoclimatol. Palaeoecol.*, 154: 179–189

Xue et al., 2003. Susceptibility of the late Cenozoic red earth loess sequence in Xunyi, Shaanxi Province and environment variation. *Quaternary Sciences*, 23(1).

Yang & Ding, 2003. Color reflectance of Chinese loess and its implications for climate gradient changes during the last two glacial-interglacial cycles. *Geophysical Research Letters*, 30(20).

Yang J., Chen J., An Z., Shields G., Tao X., Zhu H., Ji J., Chen Y., 2000. Variations in 87Sr/86Sr ratios of calcites in Chinese loess: a proxy for chemical weathering associated with the East Asian summer monsoon. *Palaeogeography, Palaeoclimatology, Palaeoecology*, 157(1-2): 151-159.

Yang S.L., Ding F. and Ding Z.L., 2006. Pleistocene chemical weathering history of Asian arid and semi-arid regions recorded in loess deposits of China and Tajikistan, *Geochimica et Cosmochimica Acta*, 70: 1695–1709.

Yi S., Saito Y., Zhao Q., Wang P., 2003. Vegetation and climate changes in the Changjiang (Yangtze River) Delta, China, during the past 13,000 years inferred from pollen records, *Quaternary Science Reviews*, 22 (14): 1501-1519.

Young S.B. and Schofield E.K., 1973. Pollen Evidence for Late Quaternary Climate Changes on Kerguelen Islands. *Letter to Nature*, 245: 311-312.

Yu S., Zhu C., Song J., Qu W., Role of climate in the rise and fall of Neolithic cultures on the Yangtze Delta, *Boreas*, 29: 157–165.

Zhai, Q.M., Li, R.Q., Guo, Z.Y., 2002. Annual Laminations of Grain Size in Angulinuo Lake and the Environmental Changes in Bashang Plateau. *Scientia Geographica Sinica/Dili Kexue [Scientia Geographica Sinica/Dili Kexue]*. 22(3): 331-335.

Zheng et al., 1991. The magnetic properties of particle-sized samples from the Luochuan loess section: evident for pedogenesis. *Physics of the Earth and Planetary Interiors*, 68: 250-258.

Zhong M., Fan W., Liu T., Wei X., Li P., 2006. Trends analysis of fire accidents in the history of China: B.C.221-A.D.1949. *Journal of Loss Prevention in the Process Industries*, 19(4): 367-370.

Zhu R., Deng C., and Jackson M.J., 2001a. A Magnetic Investigation Along a NW-SE Transect of the Chinese Loess Plateau and its Implications. *Phys. Chm. Eurih (A)*, 26(11-12): 867-872.

Zhu, R.X., Shi, C.D., Suchy, V., 2001b. Magnetic properties and paleoclimatic implications of loess–paleosol sequences of Czech Republic. *Science in China (Series D)*, 44 (5): 385–394.

Appendix I Pretreatment methods for radiocarbon dating

Standard Pretreatment Protocols at Beta Analytic

Unless otherwise requested by a submitter or discussed in a final date report, the following procedures apply to pretreatment of samples submitted for analysis. This glossary defines the pretreatment methods applied to each result listed on the date report form (e.g. you will see the designation "acid/alkali/acid" listed along with the result for a charcoal sample receiving such pretreatment).

Pretreatment of submitted materials is required to eliminate secondary carbon components. These components, if not eliminated, could result in a radiocarbon date which is too young or too old. Pretreatment does not ensure that the radiocarbon date will represent the time event of interest. This is determined by the sample integrity. Effects such as the old wood effect, burned intrusive roots, bioturbation, secondary deposition, secondary biogenic activity incorporating recent carbon (bacteria) and the analysis of multiple components of differing age are just some examples of potential problems. The pretreatment philosophy is to reduce the sample to a single component, where possible, to minimize the added subjectivity associated with these types of problems. If you suspect your sample requires special pretreatment considerations be sure to tell the laboratory prior to analysis.

Acid wash

Surface area was increased as much a possible. Solid chunks were crushed, fibrous materials were shredded, and sediments were dispersed. Acid (HCl) was applied repeatedly to ensure the absence of carbonates. Chemical concentrations, temperatures, exposure times, and number of repetitions, were applied accordingly with the uniqueness of each sample. The sample was not be subjected to alkali washes to ensure the absence of secondary organic acids for intentional reasons. The most common reason is that the primary carbon is soluble in the alkali. Dating results reflect the total organic content of the analyzed material. Their accuracy depends on the researcher's ability to subjectively eliminate potential contaminants based on contextual facts.

Typically applied to: organic sediments, some peats, small wood or charcoal, and special cases.

Acid etch

The calcareous material was first washed in de-ionized water, removing associated organic sediments and debris (where present). The material was then crushed/dispersed and repeatedly subjected to HCI etches to eliminate secondary carbonate components. In the case of thick shells, the surfaces were physically abraded prior to etching down to a hard, primary core remained. In the case of porous carbonate nodules and caliche, very long exposure times were applied to allow infiltration of the acid. Acid exposure times,

concentrations, and number of repetitions, were applied accordingly with the uniqueness of the sample.

Typically applied to: shells, caliche, calcareous nodules

From: http://www.radiocarbon.com/pretreatment.htm Beta Analytic Inc. [accessed on 12/12/2009]

Appendix II Organic Carbon Extraction (Walkley-Black Method)

Reagents

Potassium dichromate solution, M/6: Pure (Analar) potassium dichromate is dried in an oven at 105°C and cooled in a desiccator. 49.04g are accurately weighted, dissolved in water and the solution diluted to 1 dm^3.

Concentrated sulphuric acid.

Concentrated *o*-phosphoric acid.

Barium diphenylamine sulphonate: 0.16% w/v, aqueous.

Ammonium iron (II) sulphate solution, 0.5 M (approx.): 196 g ammonium iron (II) sulphate are dissolved in water. Filter if necessary, add 5 cm3 conc. H2SO4 and dilute to 1 dm3. In practice it will be found convenient to prepare this reagent in 5-dm3 amounts.

Procedure

Weigh a quantity of 0.15 mm soil containing up to about 25mg C (usually about 0.5g to 1.0g) into a 500 cm3 conical flask. Add 10 cm3 of potassium dichromate solution, using a safety pipette, and gently swirl the flask to mix the reagent with the soil. Rapidly add 20 cm3 of concentrated sulphuric acid from a measuring cylinder and again swirl the flask for about 30 seconds. Allow the flask to stand on an asbestos pad for 30 minutes. Add about 200 cm3 of water and 10 cm3 of phosphoric acid and allow solution to cool (the end-point of the titration is more easily determined with cold mixture). Add 0.5 cm3 of barium diphenylamine sulphonate solution and titrate the excess dichromate with ammonium iron (II) sulphate solution. Near the end-point the colour becomes deep violet-blue and at this stage add the iron (II) solution dropwise with shaking. At the end-point the colour changes sharply to green. If the end-point is overshot add 0.5 cm3 of dichromate solution and continue the titration dropwise.

If more that 8 cm3 of the dichromate solution has been used the experiment should be repeated using less soil, unless as little as 0.5 g had been originally taken, when the experiment should be repeated using more dichromate solution.

A blank determination made exactly as above but without soil serves to standardize the iron (II) solution.

Calculations

Per cent oxidisable, organic carbon (uncorrected)

$$= \frac{(blank\ titre - actual\ titre) \times 0.3 \times M}{weight\ of\ oven-dry\ soil\ in\ g}$$

where M is the concentration of the ammonium iron (II) sulphate solution.

The result can be expressed as per cent organic carbon (Walkley-Black, uncorrected) or converted to total organic carbon by multiplying by 1.33 (or by an experimentally found, more applicable factor), or as per cent organic matter by multiplying by 2. The factor 2 is an approximation of 2.29 and incorporates the two assumed factors of 1.33 and 1.724.

Appendix III Chemical analysis of reference minerals for normative mineral estimation.

Conc moles/mole	formula	SiO_2	$AlO_{1.5}$	CaO	MgO	$NaO_{0.5}$	$KO_{0.5}$	TiO_2	$FeO_{1.5T}$	BaO	$RbO_{0.5}$	SrO
Quartz	SiO2	1	0	0	0	0	0	0	0			
K spar	KAlSi3O8	2.9425	1.0423	0.0025	0.0033	0.2385	0.7138	0.0028	0.024	0.0283*	0.0014*	
Na-Ca plagioclase		3.4	1.4	0.2								
Kaolinite	Al4Si4O10(OH)8	3.94	4.01	0.04	0.02	0	0	0	0.05			
Illite	$K_{0.6}(H_3O)_{0.4}Al_{1.3}Mg_{0.3}Fe^{2+}{}_{0.1}Si_{3.5}O_{10}(OH)_2{\cdot}(H_2O)$	3.5	1.3	0	0.3	0	0.7*	0	0.067*			
Chlorite	(Mg,Al, Fe)12[(Si, Al)8O20](OH)16	5.747	4.678	0.097	3.681	0.071	0.047	0	4.645*			0
Biotite		5.545	3.28	0.025	1.7	0.126	1.787	0.272	2.95		0.0247*	0.0125
Rutile	TiO2	0	0	0	0	0	0	1	0			
Conc moles/mole	**formula**	**SiO_2**	**$AlO_{1.5}$**	**CaO**	**MgO**	**$NaO_{0.5}$**	**$KO_{0.5}$**	**TiO_2**	**$FeO_{1.5T}$**	**ZrO2**	**CO_2**	**$PO_{2.5}$**
Calcite	CaCO3	0	0	1	0	0	0	0	0	0	1	
Apatite	Ca5(PO4)3(OH)			5								3
Zircon	$ZrSiO_4$	1	0	0	0	0	0	0	0	1		

Note: The concentration of oxides in each mineral is in moles/mole. Numbers with * are experimentally set up.